AD-A068 337 NAVAL RESEARCH LAB WASHINGTON D C F/G 8/3
REMOTE SENSING OF OCEAN SIGNIFICANT WAVE HEIGHT BY FORWARD SCAT--ETC(U)
APR 79 C I BEARD

UNCLASSIFIED NRL-MR-3968 NL

| OF |
AD
A068837

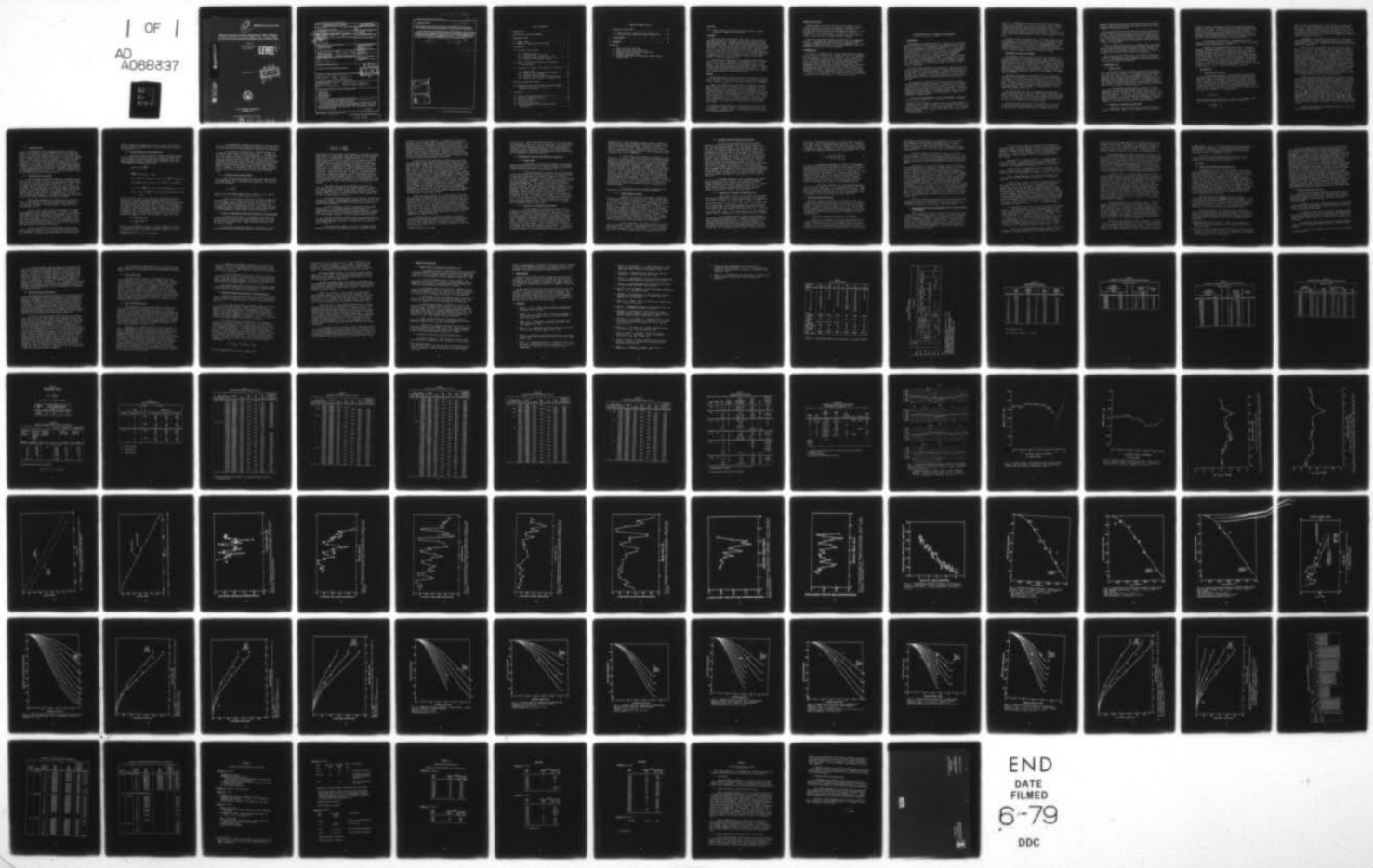

END
DATE
FILMED
6-79
DDC

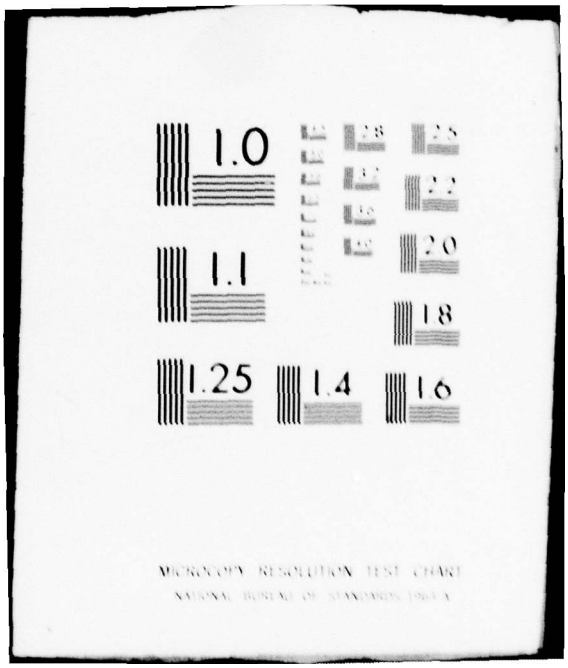
1.0
1.1
1.25
1.4
2.0
1.8
1.6
MICROCOPY RESOLUTION TEST CHART
NATIONAL BUREAU OF STANDARDS 1963-A

NRL Memorandum Report 3968

Remote Sensing of Ocean Significant Wave Height by Forward Scattering: Examples from L-Band Data

C. I. BEARD

Airborne Radar Branch
Radar Division

LEVEL II

April 18, 1979

NAVAL RESEARCH LABORATORY
Washington, D.C.

SECURITY CLASSIFICATION OF THIS PAGE (When Data Entered)

REPORT DOCUMENTATION PAGE

READ INSTRUCTIONS BEFORE COMPLETING FORM

1. REPORT NUMBER: NRL Memorandum Report 3968
2. GOVT ACCESSION NO.
3. RECIPIENT'S CATALOG NUMBER (9)
4. TITLE (and Subtitle) (6): REMOTE SENSING OF OCEAN SIGNIFICANT WAVE HEIGHT BY FORWARD SCATTERING: EXAMPLES FROM L-BAND DATA
5. TYPE OF REPORT & PERIOD COVERED: Final Report
6. PERFORMING ORG. REPORT NUMBER
7. AUTHOR(s) (10): C. I. Beard
8. CONTRACT OR GRANT NUMBER(s)
9. PERFORMING ORGANIZATION NAME AND ADDRESS: Naval Research Laboratory, Washington, DC 20375
10. PROGRAM ELEMENT, PROJECT, TASK AREA & WORK UNIT NUMBERS: 61153N-31; RR031-03; RR031-03-43; NRL Problem R07-40.102
11. CONTROLLING OFFICE NAME AND ADDRESS: Department of the Navy, Office of Naval Research, Arlington, Virginia 22217
12. REPORT DATE (11): 18 Apr 79 — April 18, 1979
13. NUMBER OF PAGES: 90
14. MONITORING AGENCY NAME & ADDRESS (if different from Controlling Office) (12): 91 p.
15. SECURITY CLASS. (of this report): UNCLASSIFIED
15a. DECLASSIFICATION/DOWNGRADING SCHEDULE
16. DISTRIBUTION STATEMENT (of this Report): Approved for public release; distribution unlimited.

17. DISTRIBUTION STATEMENT (of the abstract entered in Block 20, if different from Report) (14): NRL-MR-3968
18. SUPPLEMENTARY NOTES (16): RR031 03 (17): RR031 0343
19. KEY WORDS (Continue on reverse side if necessary and identify by block number)

Forward scattering
Remote sensing
Reflection coefficient
Surface scattering

20. ABSTRACT (Continue on reverse side if necessary and identify by block number)

This is the final report of a series of three on measurements of 1.3-GHz (L-band) electromagnetic wave, forward reflection coefficients of the ocean.

The L-band line-of-sight path was chosen between a transmitter in an aircraft flying at constant altitude towards receiving horns mounted on the stabilized platform of a destroyer. Six days of data were obtained by flights off the Atlantic Coast in 1974. Wave heights were measured by an airborne laser profilometer.

(Continues)

251 950

20. Abstract (Continued)

The measured L-band forward reflection coefficients followed Ament's theoretical curve as a function of apparent surface roughness $(\sigma_w \sin\psi)/\lambda$ for the small roughnesses encountered (≤ 0.1).

A remote sensing method for significant wave height emerges from recasting Ament's theoretical expression into a series of curves vs grazing angle (ψ), with wave height (σ_w) as a parameter. Plotting the measured reflection coefficients on this graph then yields significant wave height $(4\sigma_w)$ directly. The average spread in the values of σ_w predicted by this method is + 0.12 ft for values of σ_w from 0.4 to 0.9 ft. An FM-sweep system is proposed which should improve this accuracy.

TABLE OF CONTENTS

TABLE OF CONTENTS (Cont'd)

APPENDICES

MEMORANDUM

Subj: Remote sensing of ocean significant wave height by forward scattering: Examples from L-band data

BACKGROUND

Forward scattered electromagnetic (EM) energy from the ocean is generally detrimental to low-angle tracking radars, guidance systems, and communication links, although positive use is made of it in some height-finding systems. In both cases, a thorough understanding of the interaction of the EM waves with water waves is needed to analyze their performance. Because Navy applications often include conditions beyond those of previous data, the original purpose of this program was to extend the range of microwave frequency to 1.3 GHz (L-band) where there is a scarcity of data. In the course of the data analysis, however, a different application of the data emerged, namely, that of remote sensing of ocean wave characteristics.

A first series of measurements in 1973 provided forward-scattered data from the slightly rough waters of Chesapeake Bay [1]. A second series in 1974 involved reflection from the rougher waters off the Atlantic Coast using the same airborne transmitter flying at constant altitude toward receiving antennas mounted on a destroyer [2]. This is the third and final report on the analysis of the L-band data and the remote sensing methods which have been developed.

FINDINGS

The measured forward reflection coefficients from the radar-tracked runs follow Ament's [1953] theoretical curve as a function of apparent surface roughness $[(\sigma_w \sin\psi)/\lambda]$ for the small values (≤ 0.1) encountered.

A remote sensing methodology using forward scattering to measure wave heights (for values of roughness below 0.1) emerges by recasting Ament's expression into a series of curves vs grazing angle (ψ), with standard deviation of the wave height (σ_w) as a parameter. Plotting the measured reflection coefficients on this graph then determines wave height (σ_w) directly. The average spread in the values of σ_w predicted by this method is $\pm$ 0.12 ft for values of σ_w from 0.4 to 0.9 ft. The overall average error in σ_w for six runs, compared to the laser profilometer wave heights, is $\pm$ 5%, an indication of the possible accuracy of the method. An FM-sweep method is proposed which should improve this accuracy.

Procedures have been developed for possible remote sensing of the two-dimensional correlation lengths of the ocean surface. These will be presented in a separate report. A brief summary, however, is given in an internal memorandum [22].

RESEARCH IMPLICATIONS

Remote sensing of the ocean "significant wave height" ($4\sigma_w$) by forward reflection is shown to be possible with reasonable accuracy for many applications, at values of roughnesses less than 0.1. Improved accuracy should result from increasing the frequency to 10 GHz and changing to the FM-sweep method. The remotely sensed σ_w is primarily that of the peak spectral component of the power spectral curve; in the ocean, this is commonly the swell component.

There is no established forward scattering theory for roughnesses above 0.1. The implications are that the two-dimensional surface correlation lengths are involved at the higher roughnesses [22]. It is necessary to resolve these basic questions experimentally. Such an experiment is discussed in the next paragraph.

RECOMMENDATIONS

As there is no adequate theory for the forward-scattered coherent field (reflection coefficient) for roughnesses above 0.1, an experiment has been proposed to find the basic mechanisms. The different functional dependencies of shadowing [20, 18] and spherical wave theories [17, 5, 15] and hypotheses involving the two-dimensional correlation lengths [22] would be exploited in establishing the mechanisms. Measurements would be made under controlled two-dimensional water-wave conditions, with adjustable wave directions, heights, lengths, and two-dimensional surface correlation functions. To satisfy these two-dimensional conditions, a wave basin is required (e.g., David Taylor Model Basin). To achieve roughnesses above 0.1, a short EM wavelength of 3.3 mm (90 GHz) is required. This frequency will also be advantageous in extending the wavelength region of forward scattering data.

Remote Sensing of Ocean Significant Wave Height by Forward Scattering: Examples from L-Band Data

1. INTRODUCTION

The measurements described previously [1, 2] and in this report were originally carried out to obtain data on the forward reflection coefficient of the ocean at an electromagnetic wavelength of 23.1 cm (L-band). Years ago, measurements of forward scattering of 5.7- to 35-GHz microwave radiation from the surface of the ocean led to the establishment of a scattering model [3, 4, 5] for both the coherent and incoherent scattered fields as a function of "apparent surface roughness."* Although this model exists, Navy applications often include conditions beyond those of the data forming the model. For example, valid L-band data (with ocean wave measurements) at low grazing angles are scarce [6]. One purpose of this program was to extend the range of parameters to a lower frequency (1.3 GHz) so that the model could serve a wider range of applications.

Such data provide information for analysis of a radar being used for height finding of aircraft, for design of low-angle tracking radars, for use in simulators of low-angle tracking of aircraft and cruise missiles, for analysis of over-ocean communication circuits, IFF, and missile guidance, and, in general, for any Navy application in which an antenna beam is directed over water such that some water-scattered energy is received.

A new application emerged from the analysis of the data, namely, remote sensing of ocean wave parameters. Determination of the "significant wave height" is demonstrated in this report with the L-band data. The measured L-band forward reflection coefficients, when plotted on a graph, yield the "significant wave height" ($4\sigma_w$) directly. In addition, procedures are being worked out for possible remote sensing of the two-dimensional correlation lengths of the ocean surface. These will be presented in a future report.

A first series of measurements in 1973 provided data of reflection from the slightly rough waters of Chesapeake Bay as well as a system

---

* Apparent surface roughness is defined here as the "phase roughness" of the surface, i.e., $(\sigma_w \sin\psi)/\lambda$, where σ_w is the standard deviation of the surface height variations, ψ is the grazing angle, and λ is the electromagnetic wavelength. This quantity can be converted to phase in radians by multiplying by 2π.

Note: Manuscript submitted January 19, 1979.

test []. A fixed receiver on a cliff overlooking the Bay received energy from a transmitter in an aircraft flying at constant altitudes. A second series involved reflection from the rougher waters off the Atlantic Coast using the same airborne transmitter but with the receiving antennas mounted on a stabilized platform of a destroyer. Six days of data were obtained during the period February to April 1974, and a preliminary report was written [2]. This is the final report on these data.

The report covers two principal topics, (a) remote sensing of ocean wave parameters, and (b) detailed analysis of the L-band data. Those readers who may be interested only in the remote sensing aspects should see Sections 5.2, 6.1, 6.2, 6.3, and 6.6. In reading Section 5.2, concentrate principally on the results from radar-tracked Missions 17 and 18; in Missions 13, 14, and 15 the ship's radar was not working, and optical tracking presumably produced wild swings in the data.

2. DESCRIPTION OF TESTS AND EQUIPMENT

The measurement system was relatively simple and consisted of a CW, airborne transmitter and a shipboard receiver. Both the direct ray from the transmitter and the surface-reflected signal entered the wide-beam receiving horns. As the aircraft approached the ship, the received signal traced out the usual interference (or lobe) pattern formed by the direct and reflected signals, which combine at a continuously increasing phase angle corresponding to the increasing path length difference between direct and specularly reflected rays. As details of the equipment and experiment are given in [2], only a brief summary is included here for continuity.

The L-band CW transmitter was mounted within an oval shaped pod suspended from the outboard port bomb rack of the NRL S-2D aircraft. The antenna, a 15.5-dB standard gain rectangular horn, had its central axis depressed 8° below the horizontal to improve illumination of the water. Although preflight selection of either horizontal or vertical polarization was possible, only horizontal polarization was used in these measurements. Antenna beamwidth was approximately 32° in both planes with patterns shown in [2].

Two receiving horns (15.5 dB, 32° beamwidth), one horizontally polarized and one vertically polarized, were mounted 50 feet above the water on the antenna yoke of the Mark 25 fire control radar/gun director on each of two destroyers, the USS JOHNSTON (DD-821) and the USS LAFFEY (DD-724). This mounting point was cross-level stabilized to minimize the effect of roll and pitch on the received signal.

Ship motion was recorded aboard the USS JOHNSTON. The outputs of the ship's gyro system were digitally recorded on a separate time-synchronized tape. The ship motion data were needed for receiver

antenna orientation corrections for interpretation of the interference patterns. Wind speed and direction were obtained aboard ship from an anemometer 113 feet above sea level.

Data were taken as the S-2D aircraft flew directly toward the ship. Either the Mark 25 radar or an optical tracker tracked the incoming aircraft to point the receiving horns and to provide range data. Only two flight altitudes were used (1000 and 2500 feet) to enable repeat runs at the same altitude in an attempt to obtain a better statistical sample. The pilot estimated that he maintained the altitude to within $\pm$ 20 feet of these values.

Ocean wave heights were obtained by an airborne laser profilometer [7]. For the series of tests with the USS JOHNSTON, a separate Piper Navaho aircraft (provided by NOVA University) carried the laser. In the later test with USS LAFFEY, the laser profilometer was mounted in the same NRL S-2D aircraft which carried the transmitter.

Aerial photographs were also taken at an altitude of 1000 feet by a camera in the transmitter pod for analysis by the Stilwell method [8, 9]. The wide-angle photographs needed for density normalization in this analysis were taken from shipboard.

3. EXPERIMENTAL DATA

3.1 Summary Tables

Data were collected at different locations off the Atlantic Coast from Florida to Virginia on six different days during February to April 1974, as listed in Table I. All transmitter aircraft altitudes were 1000 feet, excpet for those runs marked by an asterisk. The headings of the transmitter aircraft relative to the wind direction are given for each run, where known, in Table II. The transmitting horn was oriented for horizontal polarization in level flight for these six days of data. All data in this report are for horizontal polarization, except for Fig. 12 from an earlier report [1].

In the shipboard receiving system, a coaxial diode switch alternately connected the single channel receiver input to the two orthogonally polarized (horizontal and vertical) receiving horns. The switch was driven at a 100-Hz rate. This situation is denoted by the symbol HV in Table I. In the remaining runs (denoted by H) only horizontal polarization was recorded. The data were digitally recorded on magnetic tape at a sampling rate of 100 Hz, synchronized to the r-f switching. The times of the data runs are given in Appendix A.

3.2 Examples of Interference Pattern Data

Analog strip chart recordings were also made to monitor the signals in real time. Figure 1 is an example of the analog charts

showing a continuous interference pattern for an aircraft-transmitter altitude of 1000 feet. A dB-scale of relative signal strength has been placed on the ordinate. On the abscissa, elapsed time increases to the right as the aircraft carries the transmitter toward the receiver. A time scale and approximate ranges in kiloyards are marked on the chart. At ranges less than three kiloyards, the record is unusable because the specular ray is "sliding down the side" of the antenna beam.

In comparison, the regularity of an interference pattern measured over the calmer waters of Chesapeake Bay [1, Fig. 7] is striking compared to the over-ocean results of Fig. 1.

Instead of the condensed analog trace of Fig. 1, sections of expanded, calibrated-computer plots are given in Fig. 2. These are different sections of one run, i.e., during one incoming aircraft pass. The signal-strength scale is in dB below an arbitrary level. The elapsed-time scale is one second for one inch on the original computer plot for the several minute runs. All the small spikes and the sporadic large spikes in Fig. 2 are noise and should be ignored. Various types of interference minima are encountered, as illustrated by the samples in Fig. 2. These include the sharp, clean, deep type in Fig. 2a, the broad type in Fig. 2b, and smaller apparent minima on the slopes of larger minima in Figs. 2c and 2d. These are discussed in Section 4.

4. DATA REDUCTION

4.1 Calculated Lobe positions

The calculated positions of the interference pattern minima are used to select the proper minima and reject spurious minima which arise from causes to be discussed. The simplest procedure will be used to calculate the positions of the maxima and minima by assuming a flat, smooth surface, no atmosphere (or, a homogeneous one) and that Z_1^2, $Z_2^2 \ll R^2$, where Z_1 and Z_2 are the receiver and transmitter heights, respectively, and R is the range. Then the difference between the direct ray path length, $[R^2 + (Z_2-Z_1)^2]^{1/2}$, and the specularly reflected ray path, $[R^2 + (Z_2+Z_1)^2]^{1/2}$, is approximately:

$$\Delta L \cong 2Z_1Z_2/R.$$

Maxima and minima occur when $\Delta L = n\lambda/2$, where n is an integer. Then the locations of maxima and minima are given approximately by:

$$R \cong \frac{(4Z_1Z_2)}{\lambda} \cdot \frac{1}{n}$$

Table III lists calculated values of R for various n to compare with Fig. 1. The values are alternately maxima and minima, but without designation. Normally, maxima would occur for odd values of n because the reflection coefficient for horizontal polarization is near -1. As these simplified calculations do not include an atmosphere, antenna differential phase shifts, etc., the calculated values can be shifted as a group to obtain the best match.

Refinements to these simple calculations could incorporate a standard atmosphere, (4/3 radius earth approximation), and spherical earth geometry, if warranted. Programs for these calculations have been worked out by Blake [10].

Two of the best fits between calculated and actual minima positions are for Run 2 of Mission 14, given in Table IV, and Run 5 of Mission 15 in Table V. Last in Table VI is an example of an inferior fit. The best match to the even-integer calculated ranges (the ones matching the other two runs so well) is obtained when n = 6 at the most distant observed minimum of 15.34 kyds. The match to the odd set of integers, beginning with n = 7, is just as good, but with the added point that the differences between calculated and observed positions are constant at ~ 2 kyds (after the first minimum). How such a difference could have arisen is not clear. Could a bias have existed in the optical tracker, in reading ranges from the TACAN system, etc., during the first run of the day? The correspondences to the sets beginning with n = 5 or n = 8 are worse than those shown for n = 6 and n = 7. When the fit of the absolute positions is poor, as in Table VI, then first differences are used to help select the proper minima and reject the extraneous minima (the latter are discussed below).

Radar tracking ranges became available for reducing the data when the Mk 25 radar first became operational in Mission 16. Problems are encountered, however, with calculated lobe positions and with the specular ray "sliding off the beam" at an unlikely value of the grazing angle. It is found that the radar ranges in Missions 16 and 17 are greater than the optical tracker ranges by 10,000 ft and 11,000 ft, respectively. Figure 3 shows this discrepancy for one run of Mission 17. In Mission 18 on a different ship, and hence with a different radar, the radar and optical ranges agree (Fig. 4). The trouble could have been either in the radar (which had to be repaired) or in the range conversion unit which converted time delay into digital range. In Mission 18, the fact that the radar and optical ranges agree tends to exonerate the range conversion unit. Hence, the interference pattern data of Missions 13 through 17 are computed using optical tracker ranges, while radar ranges are used in Mission 18, as they are recorded directly on tape.

Some possible causes for disagreement between the computed and actual patterns, are as follows.

4.1.1 Incoherent Field

The incoherent field (of random magnitude and phase) is produced by scattering of the electromagnetic waves at the rough sea surface. This incoherent field adds to all parts of the interference pattern, but produces the greatest visible effect at the pattern minima, where the signal is weak, being the difference of the direct and coherent fields. Thus, although the airborne transmitter in constant altitude flight has to "fly through" each interference minimum, there is the possibility that a correct minimum may not be the deepest of the nearby spurious (or real) minima. The reason is that the incoherent field may be additive at the particular instant when the aircraft "flies through" it, thus raising the depth of the minimum. Background information on the incoherent field is available [3, 4, 5], and some preliminary results for the Chesapeake Bay data have been given [1].

4.1.2 Vertical Motion of Aircraft

The calculated lobe patterns assume that the aircraft transmitter flies at a constant altitude. If it does not, the positions of the lobes will be altered. Table VII tabulates values of height changes, ΔZ_2, which will produce phase changes of 180°, 90°, 45°, and 30°. At the longer range of 75,000 feet, all values of ΔZ_2 are too large to be of concern. At the shorter range of 10,000 feet, however, the required values of ΔZ_2 for phase changes of 90° or less are within the $\pm$ 25-foot altitude tolerance of the aircraft. As an example, if the aircraft passes through a minimum and is 45° in phase away from it, a drop, ΔZ_2, of 9 ft would return the signal to the minimum; the recorded signal would show an extra minimum riding on the shoulder of a minimum.

Rapid height changes are not necessary for all the effects. If the aircraft descends at the proper constant angle (a multiple of $\lambda/2Z_1$, as seen from a point on the water under the receiving horn), it can "ride down" a minimum. This behavior might be the cause of the broad minimum in Fig. 2b.

Also, a ΔZ_2 of a size to shift from a maximum to a minimum is not necessary to cause good-sized minima. Table VIII lists signal level changes for various phase angles from a minimum. For a 30°-phase change from the minimum, the signal will change 14 dB; this is for a ΔZ_2 of only 6 ft at the shortest range of 10,000 ft, instead of 37 feet for the full 180° change. In Fig. 2c, from 54 to 56 seconds, the aircraft may be bobbing up and down one or two feet, possibly from turbulence, to produce the signal fluctuations. A drop of six feet is then sufficient to reach the minimum of 58 seconds.

In Fig. 2d, there are three approximately constant-signal regions, below the signal levels of the maxima, where the aircraft may be flying slightly downward at the proper angle (as described for Fig. 2b) to remain at a constant signal level position in the interference

pattern.* (These three regions are from 6 to 7 secs, 8 to 8 1/2 secs, and 9 to 10 secs.) A six-foot drop in altitude would then account for the minimum at 11 secs.

4.1.3 Vertical Motion of First Fresnel Zone

Even if the aircraft flies at a constant altitude, the swell moves sizeable areas of water up and down. Usually the Fresnel zones are long enough to extend over several swell wavelengths, but at the shortest ranges this may no longer be true. Estimates of this effect can be made by the following calculations:

$$\text{Again, } \Delta L/\lambda \cong \frac{2Z_1Z_2}{\lambda R}$$

$$\frac{d(\Delta L/\lambda)}{dZ} \cong \frac{2}{\lambda R}\,[Z_1 dZ_2 + Z_2 dZ_1].$$

For a water level change, $dZ = dZ_1 = dZ_2$, $\frac{d(\Delta L/\lambda)}{dZ} \cong \frac{2}{\lambda R}\,(Z_1+Z_2)$.

As an example, for $Z_1 = 50$ ft, $Z_2 = 1000$ ft, $R = 20{,}000$ ft

$f = 1.3$ GHZ, $\frac{d(\Delta L/\lambda)}{dZ} \cong 0.139 \cong 50°$ phase change per foot of dZ.

For $Z_2 = 2500$ ft, $\frac{d(\Delta L/\lambda)}{dZ} \cong 0.336 \cong 120°$ phase change per foot of dZ.

Thus, if the swell could lift the entire 1st Fresnel zone up and down only one foot, the signal would move through a good fraction of the interference minimum. Some example dimensions of the 1st and 10th Fresnel zones, calculated by the equations in Kerr [11], are given in Table IX for aircraft altitudes of 1000 and 2500 ft. Where X_o is the distance of the center of the 1st Fresnel zone from the receiver, ξ is the length of the semi-major axis of the ellipse (along the line between receiver and transmitter), and y is the semi-minor axis. Thus for $Z_2 = 2500$ ft and $R = 20{,}000$ ft, the 1st Fresnel zone is centered at 422 ft (from the receiver) and extends $\pm$ 137 ft from this point, or from 285 to 559 ft.

For deep-water waves,

$$\lambda_w = \frac{g}{2\pi f^2} \cong \left(\frac{g}{2\pi}\right) T^2,$$

where λ_w is the wavelength in feet if g is the acceleration of gravity in feet/second^2, and T is the period in seconds. Example: T = 7 secs., λ_w = 250 ft, T = 8 secs., λ_w = 328 ft, and T = 9 secs., λ_w = 415 ft.

* Removing the 1/R factor from the discussion.

If the transmitter aircraft flies parallel to the wave crests, the narrow 1st Fresnel zone fits between the crests and could rise and fall as an entity; short-crested waves would break this up to some extent.

If the aircraft flies either up- or downwind courses, only the smallest Fresnel zones in Table IX might qualify. For example, at Z_2 = 2500 ft and R = 20,000 ft, the 1st Fresnel zone of 274-foot length barely fits between the crests of the 8-second wave, and obviously a crest could lift only part of this zone. The 9-second wave of 415 ft wavelength, lifting and dropping a significant portion of the 1st Fresnel zone, could cause at least a partial, or small interference minimum. It appears that this phenomenon would only be operative at the shortest ranges (< 20,000 ft) for an aircraft height of 2500 ft when the course is up- or downwind. The lifting and lowering of the Fresnel zone would occur at the slow swell period, and thus could account for several minima.

4.1.4 Shipboard Antenna Height Changes

The receiving horns, mounted 50 ft above the water, are subject to changes in height as the ship rolls and pitches. The effect of this height change, ΔZ_1, is calculated as in Section 4.1.2 for vertical motion of the aircraft.

$$\Delta Z_1 \cong \frac{\lambda}{2Z_2} \frac{R}{n}$$

Let n = 2, or a 180° phase change, and R = 10,000 ft; if Z_2 = 2500 ft then $\Delta Z_1 \cong 0.75$ ft; if Z_2 = 1000 ft, then $\Delta Z_1 \cong 1.9$ ft.

Thus, for an altitude of 2500 ft at the shortest ranges, the required change in ΔZ_1 is easily achieved with ship rolls of less than 10°. The maximum change of height occurs four times during a roll period, or with typical destroyer roll periods of 9 seconds, every 2 1/4 seconds. Hence, this mechanism could be a likely cause of several additional minima at the shorter ranges. Roll and pitch were recorded on the USS JOHNSTON, but these records have not been reduced.

4.2 Plots of "Instantaneous Reflection Coefficient" vs Grazing Angle

If the reflecting surface were a perfectly smooth plane, the interference pattern would be smooth, because there would be no fluctuating incoherent scattered field. Signal maxima occur when the direct and coherent reflected rays add in phase, and minima occur when they are 180° out of phase.

The value of the amplitude reflection coefficient, r, is then calculated from adjacent maxima and minima by the usual expression

$$r = \frac{E_M - E_m}{E_M + E_m} = \frac{1 - E_m/E_M}{1 + E_m/E_M} , \qquad (1)$$

where E_M and E_m are the electric field strengths at the maxima and minima, respectively. At longer ranges where the spherical earth becomes important, r has to be multiplied by a divergence factor [11, 12]. These spherical earth effects are not important at the ranges and altitudes used in these tests. When the surface is not smooth, this simple expression is no longer correct because of the addition of the random incoherent field; a statistical treatment then has to be used. Nevertheless, eq. (1) is applied to the successive maxima and minima of several runs to form what might be called an "instantaneous reflection coefficient." The purpose is to show the scatter of the data points--the results, however, are startling. Instead of a random scatter of points about a gradually decreasing curve of "instantaneous reflection coefficient" as the grazing angle increases, the data points depict a series of oscillations, as shown in Fig. 5 for Run 9 of Mission 13. The two large circle points are for smoothing over 1° grazing angle intervals, as described later. Table X lists the data points from which Fig. 5 is plotted.

The theoretical curve of the coherent field reflection coefficient versus the apparent surface roughness parameter $(\sigma_w \sin\psi)/\lambda$ is a Gaussian shape, as derived by Ament [13]. (See plot later in Fig. 13.) Assuming that σ_w is constant during one data run (an inbound aircraft flight), and with λ fixed, the abscissa variable becomes $\sin\psi$, or just ψ for small angles as in Fig. 5.

The angular separation between the four peaks of "instantaneous coefficient" in Fig. 5 is approximately a constant of $0.40° \pm 0.05°$. The time intervals between the successive peaks continually decrease as the aircraft comes in (Table X).

A plot for another run (Run 12) on Mission 13 shows similar behavior (Fig. 6). The angular separation between peaks of the "instantaneous reflection coefficient" is again approximately a constant, being $\sim 0.6° \pm 0.1°$, and the time intervals between peaks also decrease as the grazing angle increases. Table XI contains the data for Fig. 6.

The plot for Run 8 of Mission 15 shows a remarkable series of six peaks, the last five of which have a regular spacing of $0.87° \pm 0.08°$ and decreasing spacing in time (Fig. 7 and Table XII), as do the two runs of Mission 13.

On these two days (Missions 13 and 15), only manual optical tracking of the aircraft was used because the Mk 25 automatic tracking

radar had a fault and was inoperative. The suggestion was made* that the manual optical tracking might be responsible for the sequential oscillations in the "instantaneous reflection coefficient" plots. The assumed mechanism would be that as the receiver antenna pointing overshot and pointed above the aircraft, the reflected specular "ray" would slide down the side of the antenna beam, resulting in too small an "instantaneous reflection coefficient." Conversely, as the receiver antenna pointing overshot in the other direction and pointed below the aircraft, the direct ray would slide down the side of the beam to cause too large an"instantaneous reflection coefficient."

Figures 8 and 9 (and Tables XIII and XIV) made to test this hypothesis show one run on each of the last two days (Missions 17 and 18) when automatic radar tracking of the aircraft is used to point the receiving horns. Indeed, Fig. 8 looks like a marked departure from Figs. 5, 6, and 7 in that the oscillations are "suppressed" and do not begin until 5°. Figure 9 (Run 3 of Mission 18) also looks similar to Fig. 8 in that the oscilllations are "suppressed" until 3 3/4°. Thus, surprisingly, both Figs. 8 and 9 with automatic radar tracking show some oscillatory behavior (albeit at higher grazing angles, or shorter ranges) similar to the manual optical tracking data in Figs. 5 to 7. As the oscillations are apparently reduced at the longer aircraft ranges (lower grazing angles) by the radar tracking, it could be inferred that perhaps the tracking loop or stabilization system is not adequate. For example, is it possible, as the angular tracking rates increase at the shorter aircraft ranges, that the ship's roll and pitch are not adequately compensated? If so, this would be true for both the two different destroyers used in Missions 17 and 18. Ship motion data were recorded for Missions 13 and 17, but not for Mission 18. There has not been sufficient time to reduce these records.

What can be done, however, is to compare results of aircraft data runs made over Chesapeake Bay, with the receiver horn fixed on a building atop the cliff at the edge of the Bay. Thus, there will be no ship motion involved, but only the motion of the aircraft. The next three Figs., 10, 11, and 12, are data from the Chesapeake Bay report [1] with the addition of connecting lines between the points for easier comparison to Figs. 5 to 9. Whether any regularity still remains in Figs. 10 and 11 is doubtful; there does not appear to be any regularity in Fig. 12. In any case, the elimination of the ship with its tracking system as a receiving terminal has at least greatly reduced, if not eliminated, any apparent regularity.

Whatever the cause, the large "instantaneous reflection coefficient" swings and their regularity cast doubt on the validity of the data, unless properly handled. In this vein, it is reassuring to see how well the points using 1° grazing angle interval smoothing (described later) appear visually to describe the average of the swings

---

* David L. Drake, Code 5363, NRL.

in Figs. 5 to 9. (Grazing angle smoothing intervals of 1/2° are found to be inadequate; Figs. 5 to 7 show one reason why.) Thus, data results which use smoothing intervals, such as the coherent field reflection coefficient, can be obtained from Missions 13 to 18 with shipboard receiving terminals; a meaningful incoherent field cannot be obtained, however, because its computation uses instantaneous signal values, which may be contaminated by ship motion effects.

4.3 Calculation of Coherent Field Reflection Coefficient

4.3.1 Signal Model

To calculate the reflection coefficient of the coherent field from total field data, it is necessary to extract the incoherent scattered field from the total field. Use can be made of a statistical forward scattering model based upon experimental data [3, 4].

A brief recapitulation is included here for completeness. Let the instantaneous total received field be E_T. The temporal envelope of this field, fluctuating at the doppler frequencies, is what is detected and measured; for simplicity of notation, it will be denoted as T. This total field is composed of a direct field D, a coherent reflected field (of magnitude C and phase Θ, and a random incoherent field of instantaneous magnitude I. The strength of the direct field varies inversely with slant range from receiver to aircraft transmitter. If both the transmitter and receiver were fixed instead of moving, then the magnitude C and phase Θ would be constant in a time-average sense. The incoherent field I is usually assumed to arise from a large number of independent, random, surface scatterers and thus to be Rayleigh distributed with equiprobable phase. For deviations from the Rayleigh distribution, see [5]. A combined "signal" phasor S is introduced as $S = |\hat{D} + \hat{C}|$, the phasor sum of D and C. The "signal plus noise" statistics of S.O. Rice [14] are used to analyze the received total field (for a Rayleigh incoherent field), using $S = |\hat{D} + \hat{C}|$ as the "signal" and the incoherent field I as the "ncise."

4.3.2 Effects of the Changing Aircraft Range

In the experiments establishing the model, both the transmitter and receiver positions were fixed during a data run, and a recording of the received field was made over a time interval (e.g., 10 minutes) to obtain the fluctuating signal time average and variance. In the measurements of this report, however, the transmitter position moves continuously, consequently rotating the phase angle (Θ) between C and D continuously, and giving rise to the maxima and minima of the signal. There are five factors (at least) affecting the amplitude of the field as the range changes. First, the magnitude of C changes in a functional relationship with apparent ocean roughness, $\Phi \equiv (\sigma_w \sin\psi)/\lambda$, as $C(\text{rough}) = \exp - 2(2\pi\Phi)^2$, as derived by Ament [13]. As the airborne transmitter approaches at constant altitude, the grazing angle (ψ)

increases, and C(rough) decreases according to Ament's expression. Second, the smooth surface reflection coefficient, C(smooth), varies with grazing angle (and polarization), as given by the curves in Figs. 5.3 to 5.6 of Kerr [11]. (Other influencing factors such as salinity, temperature, surface contamination, etc., have to be assumed to be constant over the propagation path.) Third, the spherical earth divergence factor will be neglected.

A fourth factor arises because of differences in illumination of the surface. Ament's [13] expression was derived assuming plane waves, whereas spherical waves modified by various antenna beam patterns are used experimentally. This effect cannot be expressed by a simple multiplication of an antenna beam illumination factor times C(rough), as has been done in the past. For example, a narrow beam, pointed horizontally, will illuminate the Fresnel zones on the distant side of the specular point almost uniformly, whereas the Fresnel zones on the near side of the specular point can be illuminated very non-uniformly. This illumination changes as the aircraft approaches and the grazing angle changes. Thus, an integration of the illumination over the rough surface is necessary. For example, Beckmann [15] used isotropic spherical wave illumination to derive an expression for the coherent field, which is a confluent hypergeometric function. Additional observations are in Section 6.3. Further work on this theoretical problem would be useful in experimental work and for application to practical systems.

A fifth factor is that the one-way transmitted field strength has to be corrected for the 1/R geometrical behavior.

4.3.3 Limited Number of Minima

Because of the relatively small number of maxima and minima in each aircraft run (at L-band with a 50-foot receiver height), it is difficult to obtain an adequate statistical sample at any one set of conditions (grazing angle, sea state, σ_w, angle between the electromagnetic wave propagation path and the ocean wave propagation direction(s)). Conceivably, some large number (e.g., > 100) of aircraft flights could be made in succession and treat the > 100 interference patterns as an ensemble to obtain the coherent field and the incoherent field using the statistical signal model [4]. There must not, however, be the large ship-induced oscillations in the data, described in Sec. 4.2, if the incoherent field is to be obtained. Even so, these > 100 flights would have to be repeated for the number of wave heights desired (σ_w) and for a number of different path angles relative to ocean wave directions--an obviously impractical total number.

In future experiments, the number of maxima and minima could be increased as follows. As the angular spacing of the lobes is approximately $\lambda/2Z_1$, either the terminal height (Z_1) can be increased (e.g., from the present 50 feet to 100 feet), or a shorter wavelength can be used. Or, for an alternate form of processing, see Sec. 6.6.

4.3.4 Smoothed "Apparent Reflection Coefficient"

In order to do the smoothing of the interference patterns to calculate the coherent field, the runs are divided into equal intervals of grazing angle. A 0.5° grazing angle interval contains only one minimum or maximum at the lower grazing angles. As a compromise, a 1° smoothing angle interval is adopted; a larger interval is undesirable because the coherent field changes over the grazing angle interval with $(\sigma_w \sin\psi)/\lambda$, by the C(smooth) vs ψ relation, and as the result of illumination varying with ψ. As C makes up only part of the mean field at a minimum or a maximum, corrections for these variations of C with ψ are difficult. On the other hand, the 1° interval would often contain only two minima or maxima. To obtain a better statistical sample, given the experimental setup at L-band as described, those values of reflection coefficient in the same grazing angle interval can be averaged from different runs, if the ocean roughness and the propagation path angle with respect to the ocean wave directions remain constant. This restriction is not always satisfied from one run to the next, however, because either σ_w or the path azimuth changes. Internal consistency was helpful in some cases as an aid, as will be seen later.

The signal amplitudes in the 1° intervals are corrected for the 1/R factor before averaging. From the smoothed minima and maxima (averaged over the 1° grazing angle intervals), smoothed "apparent reflection coefficients" are calculated from eq. (1). These are the points denoted by the large symbols in Figs. 5 to 9; they appear visually to follow the mean trend of the "instantaneous reflection coefficient" in spite of its large swings.

4.3.5 Correction for Presence of Incoherent Field

These are not, however, the true values of the coherent field reflection coefficient, because a correction for the incoherent field has yet to be made. At an interference minimum, for example, the signal power measured is $\overline{T_m^2} = (D-C)^2 + \overline{I^2}$, where $\overline{I^2}$ = incoherent power and $\overline{T^2}$ = total power. Because $\overline{T_m^2}$ is larger than it would be without the incoherent power, the calculated apparent reflection coefficient will be smaller than the true reflection coefficient (C/D). A correction at a maximum, $\overline{T_M^2} = (D+C)^2 + \overline{I^2}$, is also required, but its percentage change is small in comparison to the percentage correction at a minimum.

It is necessary to know, or assume, the statistical distribution of the incoherent field. Rayleigh statistics may be adequate for approximate calculations [4]. Where the sphericities of the illuminating and receiving wave fronts are important, however, the incoherent field statistics depart from a Rayleigh distribution [5]. The procedure is as follows for the Rayleigh distribution: Calculate the mean $(\overline{T_m})$ and the standard deviation $(T_{sd})_m$ of the minima signal

levels in a 1° grazing angle interval. From their ratio, $(T_{sd})_m/\overline{T_m}$, enter tables of Rice "signal-plus noise" statistics [16] to obtain the ratio $S/\overline{T_m}$. Multiply this ratio by $\overline{T_m}$ to obtain the "signal" phasor at a minimum, i.e., $S_m = (S/\overline{T_m})\overline{T_m} = D-C$. Perform the similar calculation to obtain the "signal" at a maximum, which is $S_M = (S/\overline{T_M})\overline{T_M} = D+C$. The coherent field reflection coefficient (C/D) is then:

$$r = C/D \cong \frac{S_M - S_m}{S_M + S_m} \cong \frac{\overline{T_M} - S_m}{\overline{T_M} + S_m} \qquad (2)$$

Although this procedure is applied to the Chesapeake Bay data [1] (fixed-point-to-airplane data), it can not be applied to the present ship-to-airplane data (Missions 13-15) because of the non-random (probably ship motion) behavior of the data (Figs. 5 to 7). Such calculations are made anyhow as a test; in a large number of cases, the ratio $(T_{sd})/\overline{T}$ of the minima in a 1° grazing angle interval is greater than 0.5227, which is the largest value allowable for Rice statistics (corresponding to zero coherent field plus a Rayleigh incoherent field). This result is consistent with the observed non-random effects in the data (Figs. 5 to 7) and confirms that this correction procedure cannot be used for the shipboard missions.

This result forces the use of the smoothed "apparent reflection coefficients" (Sec. 4.3.4) as approximations to the coherent field reflection coefficients for the remainder of this report. These are still adequate, nonetheless, for even if proper corrections (for the incoherent field) could be made, they would usually amount to only a few percent in the coherent field reflection coefficient.

5. REFLECTION COEFFICIENT RESULTS

This section contains the main data results of the report, the coherent field reflection coefficient, as approximated by the smoothed "apparent reflection coefficient" whose calculation is described in Section 4.3. Some data will be shown first as a function of apparent surface roughness to compare with Ament's theory [13]. Most of the data will be displayed as a function of grazing angle with wave heights as parameters to find how well wave height is determined for remote sensing purposes.

5.1 Reflection Coefficient vs Apparent Surface Roughness

Figure 13 is a comparison of the reflection coefficient data of Run 8 of Mission 15 (on 3/4/74) with Ament's theory [13] of the coherent field reflection coefficient vs apparent surface roughness, $(\sigma_w \sin\psi)/\lambda$. For the open square symbols, the values of $(\sigma_w \sin\psi)/\lambda$ are calculated using a σ_w of 0.64 feet, as determined by the airborne laser

profilometer, and the values of ψ at the midpoints of the 1° grazing angle intervals. The open squares obviously result in values of abscissa which are too high; the solid squares using σ_w = 0.55 ft result in a good fit to the theoretical curve. In this and all other curves, increments of 0.05 ft in σ_w are used as the smallest warranted by the data.

In Run 11 of Mission 17 (3/8/74), a value of σ_w of 0.45 ft provides a good fit to the theoretical curve, as shown in Fig. 14. For Run 12 of Mission 17 in Fig. 15, the abscissa values are calculated with σ_w = 0.5 ft. In Fig. 15, the aircraft altitude is 2500 ft; in all other figures, unless specifically stated otherwise, the aircraft altitude is 1000 ft.

At the times of the runs in both Figs. 14 and 15 there are no laser profilometer runs to provide σ_w. Estimated values of σ_w, however, can be derived from laser profilometer runs earlier in the day as follows. The available values of σ_w end about one hour before Runs 11 and 12 on 3/8/74, as shown in Fig. 16. Wind speed data exhibit a linear decrease over the 2 1/2-hour span of Mission 17 (Fig. 16). It therefore seems reasonable to extrapolate the σ_w data in a linear trend parallel to that of the wind speed, as done in the figure. Some justification for this extrapolation is found in the visual sea state observations made from shipboard (Appendix C). The waves are estimated to have dropped from "2 to 3 ft" at 1437 GMT to "1 to 2 ft" at 1705 GMT, or from an average of 2.5 ft to an average of 1.5 ft. This 40% drop is consistent with the extrapolation of σ_w shown in Fig. 16. The extrapolated values are $\sigma_w \approx 0.45$ ft at the time of Run 11 and $\sigma_w \approx 0.40$ ft at the time of Run 12 (to the nearest 0.05 ft); these are to be compared to the values used for the abscissa in Figs. 14 and 15 of 0.45 ft and 0.50 ft, respectively. The correspondence is within the inaccuracies involved in the extrapolation.

Within the tolerances shown, Figs. 13 to 15 indicate that these particular data runs are following Ament's theoretical curve [13] for roughnesses $(\sigma_w \sin\psi)/\lambda$ of less than 0.1. This is reassuring in view of the possible ship-caused data excursions illustrated in Fig. 7.

5.2 Reflection Coefficient vs Grazing Angle Plots for Remote Sensing of Wave Height

When the measured reflection coefficients are plotted on graphs of Ament's [13] theoretical curves as a function of grazing angle with wave height (σ_w) as a parameter (Fig. 17), the values of σ_w to secure a fit are automatically displayed. This results in an easy graphical method of finding wave heights for remote sensing. A series of these curves (with λ corresponding to a frequency of 1.3 GHz) follows to test how well the wave heights determined by this method agree with wave heights given by the laser profilometer. Table XV will summarize the results of this series of figures.

The data of Figs. 13 and 15 are replotted in this format for comparison. Figure 18 (Run 8, Mission 15) is one of the best data runs in terms of length of run and the small scatter of points using optical tracking. The predicted wave height (σ_w) is easily determined by the points as $\sigma_w = 0.55 \pm 0.05$ ft, compared to 0.64 ft from the laser profilometer. (Again, increments of 0.05 ft are the smallest which will be used.)

Similarly, Fig. 19 (Run 11, Mission 17) is another example of a good run in which σ_w can be determined by cursory inspection as $\sigma_w = 0.45 \pm 0.05$ ft. (The point at a grazing angle of 1° is obviously in error.) The extrapolated profilometer σ_w is 0.45 ft (Sec. 5.1).

In Fig. 20 (Run 12, Mission 17) with only four points, the scatter is wider, but σ_w is determined as $\sigma_w \approx 0.5$ ft within the tolerance of $\pm$ 0.05. The extrapolated profilometer σ_w is 0.40 ft (Sec. 5.1).

Thus, in these three runs, the reflection coefficient data determined the wave height standard deviation (σ_w) to a tolerance of $\pm$ 0.1 ft.

Figure 21 (Run 5, Mission 15) shows considerable scatter, but two points closely follow the $\sigma_w = 0.6$-ft curve and two points fall around the $\sigma_w = 1.0$- to 1.1-ft curves. A possible cause of this behavior might be how the large data excursions (such as those which appear in the data obtained by optical tracking in Mission 15) happen to straddle the 1° smoothing intervals. In Run 8 of Mission 15 (Figs. 7 and 18), apparently the excursions meshed with the 1° intervals in such a way as to almost average them out. In general, a bias upward in some 1° intervals and downward in others might be expected, given the large, regular excursions of the optical tracking data (Fig. 7). The average σ_w of the five points in Fig. 21 is 0.8 $\pm$ 0.3 ft, compared to an interpolated laser profilometer σ_w of 0.8 ft. The exact agreement is fortuitious, of course.

The next three Figures (22, 23, and 24) are data from Mission 16 on 3/6/74. Although there are no laser profilometer data on this day, visual sea state observations made from shipboard (Appendix C) are "swells approximately 3 ft, occasionally 5 ft." Assuming that the 3-ft value corresponds to the significant wave height, $H_{1/3}$, then $\sigma_w = (H_{1/3})/4 \sim 0.75$ ft. Similarly, assuming that $H_{1/10} = 5$ ft, then $\sigma_w = (H_{1/10})/5.1 \sim 1$ ft. Thus, visual observations give a range for σ_w of approximagely 0.75 to 1 ft. In Fig. 22, the points of Run 2 indicate an average value of σ_w of 0.65 $\pm$ 0.15 ft, or 0.1 ft below the side of the visual ranges of values. In Fig. 23, Run 5 yields a σ_w of 0.9 $\pm$ 0.1 ft, which falls within the visual range of values.

In Fig. 24 are the remaining two Mission 16 data runs which do not have any internal consistency and are widely scattered. The values of σ_w indicated for the Run 3 and 4 points are 1.0 and 0.6 ft,

respectively (about the same spread given by the other Mission 16 runs in Figs. 22 and 23), and the average for all the points in Fig. 24 is $\sigma_w \cong 0.8 \pm 0.2$ ft. Thus, the average σ_w derived from all the Mission 16 points is 0.8 ± 0.2 ft, which is at least consistent with the visually estimated values of 0.75 to 1.0 ft. If the actual value happened to be 0.8 ft, the error of $\pm$ 0.2 ft would correspond to $\pm$ 25%.

The tracking radar was repaired and placed into operation for the first time during Mission 16. Run 2 used optical tracking to point the receiving horns, but radar tracking pointed the horns for Run 3 and thereafter. It is interesting to note the very wide scatter of points in Run 3, medium scatter in Run 4, and the low scatter in Run 5. Is this a result of improvement in radar performance, after just being turned on at 1243 GMT, from the beginning of Run 3 at 1252 GMT to the end of Run 5 at 1317 GMT? Or just happenstance? At least in Mission 18, with a different radar on a different ship, these problems of wide scatter are relatively minor. This mission will be discussed next.

In contrast to Fig. 24, the much reduced scatter of points with good radar tracking is shown in Fig. 25 (Runs 1 and 3, Mission 18). In Run 1, one of the four points departs considerably from the trend of the other three; it is very similar in appearance to the radar tracking run in Fig. 20. In Run 3 (Fig. 25), only one point (at $\psi = 1.5°$) of the five is obviously in error; this run is similar to the radar tracking run in Fig. 19, which also contains a low point at the same angle. Thus, the radar tracking runs may have perhaps one point clearly in error, but the remainder of the points form a consistent trend with relatively small scatter. The points of Run 1 give an average $\sigma_w \cong 0.06 \pm 0.15$ ft; the points of Run 3 (excluding the point at $\psi = 1.5°$) yield $\sigma_w \cong 0.65 \pm 0.1$ ft. The average value of the four laser profilometer σ_w values (0.65, 0.72, 0.59, and 0.62 ft) taken during the period of Runs 1 to 4 is $\sigma_w = 0.65 \pm 0.07$ ft, which agrees within the error tolerances.

The roughest two days are for Missions 14 and 13. There is not much to say about Mission 14 in Fig. 26 except that it is a bad example. Although there are six runs, the number of points per run ranges from only 1 to 3, not enough to use internal consistency as an aid. Even the averages of the points at each grazing angle do not have the correct trend. This is an optical tracking day, and the large scatter is presumed to be a result of the large pointing excursions, as previously explained. The average σ_w given by all of the points in Fig. 26 is $\approx 0.8 \pm 0.5$ ft, compared to the average laser profilometer value of 1.15 ± 0.12 ft, or 30% low, a large error.

The data for the roughest day, 2/25/74 (Mission 13), are given in Fig. 27. The wide scatter follows from the optical-tracking behavior of the instantaneous values shown in Figs. 5 and 6. There are only two points in two runs and three points in the third run; a run is not long enough to use internal consistency as a help. The indicated values of

σ_w range from 0.7 to 1.2 ft, but with no proportional correspondence to the profilometer values, i.e., a behavior more consistent with just random errors. The average of the σ_w values from all the points in Fig. 27 is 0.9 $\pm$ 0.3 ft, compared to an average of 1.33 ft for the profilometer values, or a large error of 32%.

The results of the comparisons made in Figs. 18 to 27 are listed in detail in Table XV, including the dubious runs. This comparison will be discussed next in Section 6.

6. DISCUSSION

6.1 Errors in the Remotely Sensed Values of σ_w

In assessing the validity of using reflection coefficients as a remote sensing indicator of σ_w, it is necessary to use data runs in which there is most confidence. These "qualified" runs have 4 or more points with some internal consistency; they are summarized in the shorter Table XVI for ease in comparison. The average percent error for all runs with 4 or more points per run just happens to balance out to zero, but could have been $\pm$ 5%.* In Mission 16 when only visual estimates of wave heights were available, an error estimate of less than $\pm$ 25% was made; this value was not included in the averages because neither the magnitude nor the sign of the error was known. If, however, the Mission 16 error were the maximum of +25%, the average error for the runs would increase from 0% to +3%; if the Mission 16 error were -25%, the average error for the runs would change from 0% to -4%, neither change being very significant.

The error limits on the deduced values of σ_w (third column, Table XVI) encompass the maximum spread of the points. For the five radar-tracked runs, these are $\pm$ 0.15 ft for one run and $\pm \leq$ 0.1 ft for the remaining four runs. Even these moderate tolerances result in a 25% error at the lowest wave height of 0.4 ft (Run 12 of Mission 17), whereas, at the largest σ_w of 0.9 ft for radar-tracked runs (Run 5, Mission 16), the $\pm$ 0.1-ft tolerance causes only an 11% error.

Thus, the comparison of σ_w obtained from the "qualified" reflection coefficient runs to the laser profilometer σ_w's is favorable. Even if the optically-tracked runs of Missions 13 and 14, which are short and of doubtful validity, are thrown in for a worst cast estimate, the average error for all runs is still -14% (right-hand column of Table XVI.**

---

* Taking the worst cases in Column 5 of Table XVI and assuming that either only the +25% error existed for the 6 runs, or that only the -22% error existed.

** This is the result of assuming that the total of 21 points in Missions 13 and 14 is the equivalent of 5 runs of 4 points each. These five runs with an error of -31% per run are then weighted with the remainder of the runs in Table XVI to obtain -14%.

On the two roughest days, Missions 13 and 14, the reflection coefficient data indicate values of σ_w which are approximately 31% low, i.e., the reflection coefficients are higher than they should be for correspondence. Is this the result of a trend at higher surface roughnesses, or a result of the large, regular data excursions resulting (presumably) from optical tracking? The highest profilometer value of σ_w on any other day (for which reflection coefficients exist) is 0.8 ft from Run 5 of Mission 15 (an optical tracking day); the reflection coefficient data yield $\sigma_w = 0.8$ ft, to agree with the profilometer value. On Mission 16, another day of comparable roughness, visual wave observations give σ_w as 0.75 to 1 ft; the average of all σ_w values from the Mission 16 reflection coefficients is 0.8 ± 0.2 ft, a consistent value. Thus, any trend, if one exists, would have to begin for values of σ_w above 0.8 ft and would have to be 30% low by a σ_w of 1.14 ft (Mission 14). Such a trend seems doubtful; the values of roughness $(\sigma_w \sin\psi)/\lambda$ reached in the data in this report are generally ≤ 0.1, and the earlier data taken between fixed points [4] (where ship and airplane motions are not involved) show an experimental trend of reflection coefficient breaking away above Ament's [13] theoretical curve only for $(\sigma_w \sin\psi)/\lambda > 0.1$. Thus it seems more likely that the 30% low values of σ_w given by Missions 13 and 14 are the result of the large, optical tracking-induced excursions. Moreover, it would be expected that the most difficulty with optical tracking would occur on the roughest days.

6.2 Methods of Reducing Error in σ_w

There are several feasible methods of reducing the error in the individual runs of the method so as to approach the low average error that is realized for all the runs. The major error source is an insufficient number of minima and maxima within the grazing angle smoothing interval.

a. Operate at a shorter wavelength, such as 3 cm. This would produce seven times as many minima in the same grazing angle interval as the 1.3 GHz used in these tests. (A new set of Ament's curves has to be drawn for the new wavelength.)

b. Increase the size of the grazing angle smoothing interval to, say, 2° instead of the 1° used in this report. This change makes the corrections listed in Section 4.3.2 more difficult. A new set of Ament's curves vs grazing angle, but averaged over 2° intervals, also is required.

c. Raising the lower terminal height (the shipboard antenna herein) will also increase the number of minima in the grazing angle interval.

d. Use wide antenna beamwidths in any case to avoid problems of pointing errors.

e. For best accuracy, choose a range of grazing angles such that there is a wide spacing between the different σ_w curves over the range of wave heights to be covered (such as 4° to 5° in Fig. 17 for 1.3 GHz), but such that the minimum reflection coefficient is greater than 0.4. The reason for the latter stipulation is that Ament's [13] theoretical curves hold for $(\sigma_w \sin\psi)/\lambda \leq 0.1$, but the experimental data "curve" [4] breaks away and becomes larger than Ament's theoretical curve for $(\sigma_w \sin\psi)/\lambda > 0.1$. This value of roughness corresponds to a coherent field reflection coefficient of 0.4. As there are conflicting theories for the coherent field behavior above roughnesses of 0.1, it is necessary at the moment for remote sensing applications to restrict the measured reflection coefficients to ≥ 0.4 so that Ament's [13] theoretical curves can be used.

6.3 Non-Uniform Illumination Errors

The receiving horn elevation beamwidths of 32° were sufficiently wide when the beams were pointed horizontally as in the Chesapeake Bay tests [1]. On shipboard, the horns were mounted on top of the MK 25 tracking radar antenna to obtain a mounting point that was cross-level stabilized. In tracking the aircraft, the radar pointed the horns at the aircraft, but also elevated the beams and reduced the illumination of the water at the higher grazing angles. There is no simple way to correct for this effect (Sec. 4.3.2). Some authors have made a multiplying "correction" factor from relative strengths of the direct ray and the specularly reflected ray directions as they emerge from the antenna patterns, but this procedure is not necessarily correct [4].

In Fig. 28, the points denoted by open squares are the same as given before in Fig. 18. These points, after being multiplied by the ratio of direct to specular ray antenna beam amplitudes, for both transmitting and receiving beams, become the asterisks. The two asterisks at the two highest grazing angles appear to be "overcorrected," and the average σ_w indicated by the asterisks is 0.45 ft, compared to 0.55 ft for the uncorrected points and 0.64 ft for the laser profilometer. In Fig. 29, the "overcorrections" are obvious, with the asterisks indicating a σ_w of 0.25 ft, compared to the σ_w of 0.45 ft given by both the uncorrected points and the laser profilometer. Thus, the uncorrected points agree with the profilometer far better than the so-called "corrected" points. There is a possible reason for part of this behavior. Since these receiving horns were aligned visually, there is at least the possibility that they were pointed a few degrees downward instead of at zero, as reported, when the radar dish was pointed at zero degrees elevation. This would mean that the illumination was greater than thought, and that any "corrections" would be too much, as Figs. 28 and 29 indicate. Thus, the reflection coefficients in all the figures prior to Fig. 28 are uncorrected ones, as measured.

This problem of the quantitative effect of non-uniform illumination on the rough surface coherent field is one requiring theoretical work. Meanwhile, the experimenter needs to use wide beams to avoid the effect.

6.4 Directional Effect

There are insufficient data to find whether there is any directional effect, i.e., of the microwave propagation path relative to the ocean wave propagation direction(s). Of the runs of 4 or more points in Table XVI, in only two is the aircraft heading relative to the wind known: Run 8, Mission 15, is upwind at 75° to the wind (UW/75°), and Run 11, Mission 17, is downwind at 30° to the wind (DW/30°). In both of these runs, the predicted values of σ_w agreed with the laser profilometer values within $\pm$ 0.1 ft. The other short runs of Missions 13, 14, and 15 (listed in Table XV) give contradictory results, i.e., there are more errors in these short, optically-tracked runs than whatever directional effect might exist. Thus, a large number of flights would be necessary to establish and measure a directional effect by this method.

6.5 Laser Profilometer Errors

The information on the laser profilometer performance is as follows. Two Missions (14 and 18) provided a good test of repeatability in that in each of the Missions, the values of σ_w from the different runs were tightly clustered and showed no trend (Appendix B). The entries of profilometer σ_w in Tables XV and XVI for Missions 14 and 18 are the means, plus or minus the spread of all the values about the mean for all of the runs (on each day). If the profilometer is assumed (for discussion) to have no error, the small spread shows the constancy of the waves; conversely, if the sea is assumed constant, the spread gives the repeatability of the laser profilometer measurements. For both days the repeatability spread is $\pm$ 10%.

Information on the absolute accuracy of the profilometer is scanty. Measurements by a laser profilometer have been compared with those of a wave staff by other organizations with satisfactory results. Although photographs of the ocean taken from the airborne L-band transmitter pod were submitted to the appropriate group for spectral analysis, the report received was that no wave spectra could be obtained for a variety of reasons, such as sun glitter, too great an angle between wind and wave directions, not enough waves in the photograph, etc. In these tests, the course of the S-2D aircraft carrying the transmitter-camera pod was constrained by the ship's course, and, consequently, photographs may not have been taken under ideal conditions. At least in these tests, the requirements for taking photographs for analysis by the Stilwell method were too constraining and restrictive to allow results to be obtained.

A comparison of profilometer results to visual observations (Appendix C) shows the profilometer values being about half as large (Mission 13) to twice as large (Mission 18) with reasonable agreement in between (Mission 17). This is probably consistent with the accuracy of the visual observations.

A circuitous reasoning provides some confidence in the laser profilometer data, however. As the reflection coefficients agree with Ament's curve when the profilometer σ_w's are used to calculate apparent surface roughness, and because Ament's curve has been confirmed in the past, then the profilometer values of σ_w should be correct.

Laser profilometer spectra could not be used, however, because of aliasing inherent in making a line measurement of a two-dimensional surface spectrum.* This does not affect the values of σ_w.

6.6 Proposed FM-Sweep Method and Remote Sensing Application

In the data processing used herein, a statistically significant number of maxima and minima can not be obtained in the 1°-grazing-angle intervals without an inordinate number of aircraft flights (Secs. 4.3.3 and 4.3.4).

To avoid these difficulties, an FM-sweep technique is proposed, in which the microwave frequency is swept at a rapid rate, thus presenting (on an oscilloscope, e.g.) an essentially "instantaneous" section of the interference pattern. The FM-sweep rate is set high enough so that signal changes do not occur within one sweep period, and thus the waves can be considered to be "frozen." Then a sufficient number of such sweeps, depending upon geometry and velocity, is recorded to obtain an adequate ensemble for statistical treatment.

The signal processing is straightforward. The frequency deviation of the FM can be adjusted to sweep through one maximum and one minimum of the interference pattern on each sweep. One could imagine many sweeps being integrated by a long-persistence oscilloscope screen, with photographs being taken of the averaged interference pattern traces, but this is an unwieldy method. A possible analog processing method would be to use two envelope detectors, back-to-back, the bias of one set for detection of the signal maxima, and the bias of the reverse detector set for detection of the signal minima. For remote sensing, a simple procedure is to pass the two detector outputs through long-time constant filters to obtain $\overline{T}_{Max}$ and $\overline{T}_{min}$. Then, C/D is calculated from the approximation:

$$C/D \cong (\overline{T}_{Max} - \overline{T}_{min}) \Big/ (\overline{T}_{Max} + \overline{T}_{min}).$$

---

* Private communication from Donald L. Hammond, NRL.

Plotting C/D on a set of curves like Fig. 17 (but calculated for the value of λ being used) determines σ_w of the waves. A given value of grazing angle (and λ) determines a vertical slice through the curves in Fig. 17. An equation can be determined for this slice, so that the value of C/D could yield σ_w directly without plotting, if desired.

The antenna beamwidth needs to be constant over the frequency sweep (e.g., 10 to 12 GHz). The system gain should preferably also be constant over this frequency band, although a calibration curve correction could be inserted in the computations.

This FM-sweep method trades some complexity of equipment and data handling for a prohibitive number of aircraft flights. Even though this trade would usually be desirable, the FM method in addition has the unique feature of presenting "instantaneous" sections of interference patterns for "frozen" seas.

Would it be suitable for remote sensing by forward scatter from satellites, however? There are two obvious drawbacks. One is poor resolution because the Fresnel zones cover a large area at grazing angles of 4° to 6°. Because it has been shown that 20 Fresnel zones provide all but a few percent of the scattered energy, the "resolution area" could be considered as the area inside the 20th Fresnel zone.

The second point is that although forward scattering requires two satellites, one each for transmitter and receiver, this is not the devastating requirement that it once was. A system which meets the geometry needed for the remote sensing methods in this report is being proposed by the Applied Physics Laboratory of Johns Hopkins University [21] to measure surface pressure for weather forecasting. It consists of two satellites which make use of both the direct (line-of-sight path) between them and also the specularly reflected path from the earth's surface at a grazing angle of 4° to 6°. It is conceivable that such satellites might be designed to also carry the equipment for the sea surface remote sensing as proposed in this report and thus serve a dual application.

On the positive side, the accuracy in wave height obtained with the method used herein (1°-slices in grazing angle) compares very favorably with the preflight specifications of the altimeter in SEASAT-A, and the proposed FM-sweep method should increase this accuracy. In addition, procedures for possible remote sensing of the two-dimensional correlation lengths of the ocean surface will be described in another report.

7. SUMMARY AND CONCLUSIONS

7.1 Remote Sensing of Significant Wave Height ($4\sigma_w$)

1. The measured reflection coefficients from the six qualified* runs follow Ament's [13] theoretical curve of reflection coefficient as a function of apparent surface roughness $(\sigma_w \sin\psi)/\lambda$. Only small roughnesses of ≤ 0.1 are encountered at this microwave frequency of 1.3 GHz.

2. As a remote sensing method, a series of Ament's [13] theoretical curves is recast as a function of grazing angle, with wave height (σ_w) as a parameter. A measured reflection coefficient value plotted at a given grazing angle then gives σ_w directly.

3. The average spread in the values of σ_w predicted by this remote sensing method is $\pm$ 0.12 ft in the six runs. This is equivalent to errors in individual runs of from $\pm$ 30% at the lowest wave height (0.4 ft) to $\pm$ 13% at the highest wave height (0.9 ft) encountered.

4. The accuracy of this remote sensing method is indicated by the fact that the average (over the six runs) percentage error of the predicted σ_w compared to the laser profilometer σ_w is only $\pm$ 5%.

5. Several feasible methods of reducing the error in the individual runs of the method so as to approach a low overall average error are listed. The major error source is an insufficient number of minima and maxima within the 1°-grazing angle-smoothing interval. The best remedy is to operate at a shorter wavelength, such as 3 cm. This would produce seven times as many minima in the same grazing angle interval as at the 1.3-GHz frequency used in these tests.

6. There are insufficient data to determine whether any directional effect exists, i.e., angle of electromagnetic wave propagation path relative to the ocean wave direction(s).

7. There is not an adequate statistical data base for calculating the incoherent field because of the large, regular excursions in the optically-tracked data, and because of an inadequate number of minima in the grazing angle-smoothing interval at L-band.

7.2 Proposed FM Sweep Method for Remote Sensing of σ_w

A system is proposed for remote sensing of σ_w which repetitively sweeps (FM) the microwave carrier frequency at a rapid rate to

* The "qualified" runs are six runs with four or more points and with internal consistency. These are primarily only the radar-tracked runs, but include two optically-tracked runs which have internal consistency.

present an "instantaneous" interference pattern that "freezes" the waves as far as signal changes are concerned. An ensemble average is then performed to calculate the reflection coefficients and σ_w with only a relatively few aircraft flights for different azimuths.

8. ACKNOWLEDGMENT

Appreciation is due many persons and organizations who helped in this project. Thanks are given to W. Loescher who carried the full programming load, to B. Kremer for working out the digital circuitry, to J. Kirkwood for maintaining the transmitter and aerial camera pod, and to others who assisted in the field work, G. Hermann, A. Long, and F. Sollner.

The NRL Operations Services pilots of the S-2D aircraft were very cooperative. The laser profilometer was secured through the good services of NAVOCEANO and operated by R. Sheil of NAVOCEANO. NOVA University provided a separate aircraft for the laser profilometer in the first at-sea tests. The officers and crew of the USS JOHNSTON (DD-821) and of the USS LAFFEY (DD-724) afforded our personnel space and time during the tests off the Atlantic Coast.

9. REFERENCES

1. Beard, C. I., D. L. Drake, and C. M. Morrow, Measurements of microwave forward scattering from the ocean at L-Band, NRL Memo Report 2794, June 1974.

2. Beard, C. I., D. L. Drake, and C. M. Morrow, Measurements of L-Band forward reflection from the sea surface, NRL Memo Report 3048, April 1975.

3. Beard, C. I., I. Katz, and L. M. Spetner, Phenomenological vector model of microwave reflection from the ocean IRE Trans. AP-4 162-167, 1956.

4. Beard, C. I., Coherent and incoherent scattering of microwaves from the ocean, IRE Trans. AP-9, 470-483, 1961.

5. Beard, C. I., Behavior of non-Rayleigh statistics of microwave forward scatter from a random water surface, IEEE Trans. AP-15, 649-657, 1967.

6. Rider, G. C., Fading amplitude due to interference from forward sea scatter, NATO/AGARD Conference Proceedings No. 37, Scatter Propagation of Radar Waves, Part I, Sandefjord, Norway, August 1968.

7. Ross, D. B., and Cardone, V. J., Laser observations of wave growth and foam density for fetch-limited 17-25 m/s winds, IEEE Trans. Geosci. Electron, GE-8, 326-336, 1970.

8. Stilwell, D., Directional energy spectra of the sea from photographs, J. Geophys. Res. 74, 1974, 1969.

9. Pilon, R. O., Determination of ocean surface descriptors using sea photo analysis techniques, NRL Report 7574, July 1973.

10. Blake, L. V., Machine plotting of radio/radar vertical-plane coverage diagrams, NRL Report 7098, June 1970.

11. Kerr, D. E., ed., Propagation of Short Radio Waves, McGraw-Hill Book Co., Inc., New York, NY, 1951.

12. Beckmann, P. and Spizzichino, A., The Scattering of Electromagnetic Waves from Rough Surfaces, Pergamon Press, The Macmillan Co., NY, NY, 1963.

13. Ament, W. S., Toward a theory of reflection by a rough surface, Proc. IRE, 41, 142-146, 1953.

14. Rice, S. O., Mathematical analysis of random noise, Bell. Sys. Tech. J., 23, 282-332, 1944; 24, 46-156, 1945.

15. Beckmann, P., Scattering from rough surfaces for finite distances between transmitter and receiver, Boeing Scientific Research Laboratory Report, DI-82-0657, Oct 1967.

16. Norton, K. A., L. E. Vogler, W. V. Mansfield, and P. J. Short, The probability distribution of the amplitude of a constant vector plus a Rayleigh-distributed vector, Proc. IRE, 43, 1354-1361, 1955.

17. Beard, C. I., T. H. Kays, and V. Twersky, Mid-field forward scattering, J. Appl. Phys. 33, 2851-2867, 1962.

18. Boyd, M. L. and R. L. Deavenport, Forward and specular scattering from a rough surface: theory and experiment, J. Acoustical Soc. Am., 53, 791-800, 1973.

19. Brown, R. M. and A. R. Miller, Geometric-optics theory for coherent scattering of microwaves from the ocean surface, NRL Report 7705, June 1974.

20. Wagner, R. J., Shadowing of randomly rough surfaces, J. Acoustical Soc. of Am., 41, 138-147, 1967.

21. Surface pressure measurements from space platforms: A feasibility study, Report FS-75-211, 1 Nov 75, Applied Physics Laboratory, The Johns Hopkins University, Johns Hopkins Road, Laurel, MD 20810.

22. Beard, C. I., unpublished internal memorandum: Forward-scatter remote sensing, 15 April 1978. This is reproduced in Appendix E.

Table I
List of 1974 Data Runs

Mission No. / Date	13 2/25	14 2/27	15 3/4	16 3/6	17 3/8	18 4/8
Run 1	H	H	H	NG	H	H
2	H	H	HV	H	H	H
3	H	H	HV	H	HV	H
4	H	H	HV	HV	HV	H
5	H	H	HV	HV	HV	H*
6	HV	HV	HV	HV	H	H
7	HV		HV	H	HV	
8	HV		HV	H	HV	
9	HV		HV	H*	HV	
10	H		HV	HV*	H*	
11	H			HV*	HV	
12	HV			HV*	HV*	
13					HV*	
Sig. Gen. Calibration	Not too stable	Normal	Normal	Jogs	Shifts	Normal
Optical tracking	Yes	Yes	Yes	Yes	Yes	Yes
Radar tracking	MK25-NG	MK25-NG	MK25-NG	Yes	Yes	Yes
Laser profil	Yes	Yes	Yes	Yes	Yes	Yes
Stilwell photos	Yes	Yes	Yes	Yes	Yes	Yes
Ship motion recording	Yes	Yes	Yes	Yes	Yes	No
Ship	DD-821	DD-821	DD-821	DD-821	DD-821	DD-724
Xmtr. polariz.	Horiz.	H	H	H	H	H

Transmitter — aircraft altitude 1000 ft., except runs marked by an asterisk are 2500 ft.

Table II
Transmitter-Aircraft Headings

Date	Mission No.	Run Numbers												
		1	2	3	4	5	6	7	8	9	10	11	12	13
2/25/74	13	NG	DW 23 kt	UW/53° 23 kt No range	DW/60° 25 kt No range	UW/55°	DW/54° 25 kt No range	UW/43° 21 kt	DW/57° 20 kt	UW/71° 19 kt short run	DW/71°	UW/66° (average	XW (average)	—
2/27/74	14	UW/5° 14 kt	UW/55°	UW/(?)	DW 13 kt	UW/27° 13 kt	UW/(?)	—	—	—	—	—	—	—
3/4/74	15	UW/14° 3 kt	UW/26°	UW/13° 3 kt	NG	NG	short run	NG	UW/75°	NG short run	No range	—	—	—
3/6/74	16	NG	8 kt		8 kt	8 kt				*	*	*	* 4 kt	—
3/8/74	17	17 kt		UW 20°-50°		UW/55° 10 kt	NG	NG			UW/44° *	DW/30°	*	DW/44° *
4/8/74	18		UW/(?)	UW/(?)	UW/(?)	NG *	NG	—	—	—	—	—	—	—

Notes:

1. UW/53° = flying upwind at 53° to wind. DW = downwind, XW = crosswind.
   UW(?) = flying upwind but angle is unknown.
2. All aircraft altitudes are 1000 ft, except runs marked by asterisks are 2500 ft.
3. In Mission 13, Runs 3, 4, and 6 with no range marks are unusable.
   Where no aircraft heading appears, it is unknown.
4. Data runs were made except where a dash appears in the box.

Table III
Calculated Lobe Positions
(Plane earth and no atmosphere)

n	Range kyds	Range difference kyds	n	Range kyds	Range difference kyds
4	22.01	—	3	29.35	—
6	14.68	7.33	5	17.61	11.74
8	11.01	3.67	7	12.58	5.03
10	8.81	2.20	9	9.78	2.80
12	7.34	1.47	11	8.01	1.77
14	6.29	1.05	13	6.77	1.24
16	5.50	0.79	15	5.87	0.90
18	4.89	0.61	17	5.18	0.69
20	4.40	0.49	19	4.63	0.55
22	4.00	0.40	21	4.19	0.44
24	3.67	0.33	23	3.83	0.36
26	3.39	0.28	25	3.52	0.31
28	3.14	0.25	27	3.26	0.26
30	2.93	0.21	29	3.04	0.22
32	2.75	0.18	31	2.84	0.20
34	2.59	0.16	33	2.67	0.17

$R \cong (4Z_1 Z_2/\lambda)/(1/n)$

Z_1 = 50 ft., Z_2 = 1000 ft., f = 1.3 GHz

Table IV
Comparison of Measured and Calculated Minima Positions

Mission 14, Run 2					
Measured Minima Positions Range			Calculated Positions		Difference kyds
ft	kyds		n	Range kyds	
42232	14.08		6	14.68	0.6
33541	11.18		8	11.01	-0.2
26485	8.83		10	8.81	0.0
22835	7.61		12	7.34	-0.3
18018	6.00		14	6.29	0.3
15946	5.32		16	5.50	-0.2
14463	4.82		18	4.89	0.1

Table V
Comparison of Measured and Calculated Minima Positions

Mission 15, Run 5					
Measured Minima Positions Range			Calculated Positions		Difference kyds
ft	kyds		n	Range kyds	
40625	13.542		6	14.68	1.1
32002	10.667		8	11.01	0.3
25928	8.643		10	8.81	0.2
22729	7.576		12	7.34	-0.3
19141	6.380		14	6.29	-0.1
17130	5.710		16	5.50	-0.2
15270	5.090		18	4.98	-0.2
13299	4.433		20	4.40	0.0
11910	3.970		22	4.00	0.0
10772	3.591		24	3.67	0.1
9812	3.271		26	3.39	0.1
8911	2.970		28	3.14	0.2
8231	2.744		30	2.93	0.2
7474	2.491		32	2.75	0.3
6709	2.236		34	2.59	0.4

Table VI
Comparison of Measured and Calculated Minima Positions

Mission 15, Run 1							
Measured Minima Positions		Calculated Positions					
ft.	kyds	n	Range kyds	Diff. kyds	n	Range kyds	Diff. kyds
46025	15.34	6	14.68	-0.6	7	12.58	-2.7
35615	11.87	8	11.01	-0.8	9	9.78	-2.0
30408	10.14	10	8.81	-1.3	11	8.01	-2.1
26518	8.84	12	7.34	-1.5	13	6.77	-2.0
23290	7.76	14	6.29	-1.5	15	5.87	-1.9
21097	7.03	16	5.50	-1.5	17	5.18	-1.8
19383	6.46	18	4.89	-1.5	19	4.63	-1.9
18040	6.01	20	4.40	-1.6	21	4.19	-1.8
17187	5.73	22	4.00	-1.7	23	3.83	-1.9
16406	5.47	24	3.67	-1.7	25	3.25	-1.9
15623	5.21	26	3.39	-1.9	27	3.26	-1.9
15116	5.04	28	3.14	-1.9	29	3.04	-2.0
14339	4.78	30	2.93	-1.9	31	2.84	-1.9

Table VII
Phase Changes Produced by
Aircraft-Height Variations

$$\Delta Z_2 \cong \frac{\lambda}{2 Z_1 N} R$$

Z_1 = 51 ft. λ = 0.757 ft. (1.3 GHz)

Range R ft.	Altitude Variations ΔZ_2 (ft.) to cause phase changes of			
	180°	90°	45°	30°
10,000	37	19	9	6
75,000	278	139	70	46

Table VIII
Signal-Level Changes vs. Phase Angle from a Minimum

δ	α	ρ	E_T/E_D	Signal Level	Signal Level
Phase angle from a minimum	Phase angle between direct and reflected signals	Reflection Coefficient (assumed)		relative to direct signal	relative to a maximum
(deg)	(deg)			dB	dB
0	180	0.9	0.100	−20	−25.6
15	165		0.26	−11.7	−17.3
30	150		0.500	−6.0	−11.6
45	135		0.735	−2.7	−8.3
66	114		1.000	0.0	−5.6
90	90		1.345	+2.6	−3.0
180	0		1.900	+5.6	0.0

Calculations assume a smooth, plane surface.

$$E_T/E_D = [1 + \rho^2 + 2\rho \cos \alpha]^{1/2}.$$

Table IX
Fresnel Zone Dimensions

	f = 1.3 GHz		z_1 = 51 ft.		
	Zone	Z_2	dimension (ft.)		
Number	Description*	(ft.)	r=10,000 ft.	r=20,000 ft	r=75,000 ft.
1	χ_0	1000	516	1093	5295
	ξ	"	180	514	3930
	y	"	19	27	57
	χ_0	2500	206	422	1810
	ξ	"	48	137	1024
	y	"	12	17	35
10	χ_0	1000	755	2059	15136
	ξ	"	627	1847	14844
	y	"	68	104	256
	χ_0	2500	257	618	4388
	ξ	"	160	475	4147
	y	"	41	61	147

* χ_0 = center of ellipse

ξ = semi-major axis

y = semi-minor axis

Table X
Interference Pattern Data, Mission 13, Run 9

Time – GMT			Range	ψ	Max.	Min.	Diff.	"Instantaneous Reflection Coefficient"
hr	min	sec	ft	deg	dB	dB	dB	
18	23	20.10	37807	1.60	–	–82.0	–	–
		29.40	35609	1.69	–43.3	–	38.7	0.976
		34.40	34426	1.75	–	–67.6	24.3	0.884
		39.10	33315	1.81	–43.0	–	24.6	0.888
		43.40	32298	1.86	–	–64.4	21.4	0.842
		44.50	32038	1.88	–40.8	–	23.6	0.876
		49.20	30927	1.95	–	–61.7	20.9	0.832
		50.70	30572	1.97	–47.0	–	14.7	0.690
		51.60	30359	1.98	–	–72.8	25.8	0.902
		53.10	30005	2.00	–41.0	–	31.8	0.949
		56.70	29154	2.06	–	–66.7	25.7	0.901
		59.40	28515	2.11	–41.2	–	25.5	0.900
18	24	02.10	27877	2.16	–	–60.0	18.8	0.792
		02.80	27711	2.18	–43.8	–	16.2	0.732
		04.40	27333	2.21	–	–62.5	18.7	0.790
		05.60	27049	2.23	–45.0	–	17.5	0.775
		07.60	26576	2.27	–	–50.4	5.4	
		07.80	26529	2.27	–45.7	–	4.7	
		09.90	26033	2.32	–	–63.3	17.6	0.776
		10.60	25867	2.33	–44.7	–	19.1	0.800
		12.20	25489	2.36	–	–67.5	23.3	0.872
		15.20	24779	2.43	–40.5	–	27.0	0.913
		15.70	24661	2.44	–	–73.3	32.8	0.954
		17.20	24306	2.48	–47.0	–	26.3	0.907
		18.80	23928	2.52	–	–63.0	16.0	0.728
		20.10	23621	2.55	–45.2	–	17.8	0.770
		20.60	23503	2.56	–	–62.5	17.3	0.760
		22.90	22959	2.62	–42.5	–	20.0	0.817
		23.10	22911	2.63	–	–55.8	13.3	0.650
		23.95	22710	2.65	–42.9*	–	12.--	0.60
		24.80	22510	2.68	–	–61.4	18.5	0.786
		25.20	22415	2.69	–43.3	–	18.1	0.777
		26.30	22155	2.71	–	–65.3	22.0	0.852
		27.10	21966	2.73	–43.6	–	21.7	0.847
		28.00	21753	2.77	–	–67.5	23.9	0.880
		29.00	21516	2.80	–42.8	–	24.7	0.890
		29.40	21422	2.81	–	–66.6*	24.--	0.88
		29.80	21327	2.83	–42.3	–	24.--	0.88
		30.60	21138	2.85	–	–65.8	23.5	0.875
		31.30	20973	2.86	–40.8	–	25.0	0.893
		32.40	20713	2.90	–	–64.2	23.4	0.873

* = Missing values "faked" as the average of the two surrounding values to make the computer program run.

Table XI
Interference Pattern Data, Mission 13, Run 12

Time — GMT			Range	ψ	Max.	Min.	Diff.	"Instantaneous Reflection Coefficient"
hr	min	sec	ft	deg	dB	dB	dB	
18	46	19.70	59315	1.01	—	?		
		58.50	49205	1.22	−43.3	—	—	—
	47	15.40	44801	1.34	—	−72.5	29.2	0.931
		33.60	40059	1.50	−45.8	—	26.7	0.910
		44.00	37349	1.61	—	−78.3	32.5	0.952
		50.20	35733	1.68	−52.5	—	25.8	0.902
	48	07.00	31355	1.92	—	−93.3	40.8	0.981
		14.80	29323	2.05	−50.2	—	43.1	0.986
		19.50	28098	2.14	—	−75.2	25.0	0.893
		20.30	27890	2.16	−48.3	—	26.9	0.913
		29.00	25623	2.35	—	−66.7	18.4	0.783
		33.30	24502	2.46	−43.3	—	23.4	0.874
		36.50	23669	2.54	—	−70.0	26.7	0.911
		38.30	23200	2.59	−41.7	—	28.3	0.924
		41.50	22366	2.69	—	−60.0	18.3	0.783
		44.90	21480	2.80	−40.8	—	19.2	0.802
		47.20	20880	2.88	—	−55.6	14.8	0.695
		48.50	20542	2.93	−43.3	—	12.3	0.608
		50.20	20099	2.99	—	−58.8	15.5	0.715
		53.90	19135	3.14	−35.9	—	22.9	0.867
		55.40	18744	3.21	—	−63.3	27.4	0.917
		56.20	18535	3.25	−36.2	—	27.1	0.914
		56.90	18353	3.28	—	−57.5	21.3	0.840
		58.80	17858	3.37	−38.2	—	19.3	0.803
	49	00.30	17467	3.44	—	−57.5	19.3	0.802
		01.10	17259	3.49	−37.2	—	20.3	0.822
		01.50	17154	3.51	—	−52.5	15.3	0.710
		04.30	16425	3.66	−37.8	—	14.7	0.690
		05.20	16190	3.72	—	−55.0	17.2	0.756
		06.60	15825	3.80	−40.3	—	14.7	0.690
		07.20	15669	3.84	—	−54.6	14.3	0.678
		08.80	15252	3.94	−38.8	—	15.8	0.725
		09.60	15044	4.00	—	−50.1	11.3	0.572
		10.70	14757	4.08	−39.8	—	10.3	0.532

Table XII
Interference Pattern Data, Mission 15, Run 8

Time – GMT			Range	ψ	Max.	Min.	Diff.	"Instantaneous Reflection Coefficient"
hr	min	sec	ft	deg	dB	dB	dB	
17	08	08.60	26843	2.24	−39.3	–	–	–
		12.02	26034	2.31	–	−64.3	25.0	0.893
		19.21	24334	2.47	−38.3	–	26.0	0.904
		22.92	23457	2.57	–	−61.6	23.3	0.871
		29.25	21960	2.74	−37.8	–	23.8	0.878
		33.84	20875	2.82	–	−71.8	34.0	0.960
		39.53	19530	3.08	−37.0	–	34.8	0.960
		42.84	18747	3.21	–	−51.7	14.7	0.690
		45.46	18128	3.32	−35.3	–	16.4	0.737
		48.63	17378	3.46	–	−64.2	28.9	0.930
		53.03	16338	3.68	−36.3	–	27.9	0.923
		54.79	15922	3.78	–	−50.8	14.5	0.685
		56.88	15427	3.90	−32.7	–	18.1	0.775
		58.72	14992	4.01	–	−49.2	16.5	0.740
	09	01.81	14262	4.22	−35.4	–	13.8	0.665
		04.09	13723	4.38	–	−57.7	22.3	0.857
		05.52	13385	4.50	−34.1	–	23.6	0.875
		08.30	12727	4.73	–	−50.7	16.6	0.740
		09.38	12472	4.82	−35.2	–	15.5	0.715
		10.53	12200	4.93	–	−46.1	10.9	0.556
		12.50	11734	5.13	−32.2	–	13.9	0.667
		13.77	11434	5.26	–	−56.9	24.7	0.890
		14.58	11242	5.35	−33.1	–	23.8	0.879
		15.35	11060	5.44	–	−49.2	16.1	0.730
		16.16	10869	5.54	−31.0	–	18.2	0.780
		17.50	10552	5.70	–	−40.0	9.0	0.476
		18.57	10299	5.84	−35.3	–	4.7	0.256
		19.79	10011	6.01	–	−45.7	10.4	0.536
		20.23	9907	6.07	−33.0	–	12.7	0.62
		21.08	9706	6.20	–	−59.4	26.4	0.908
		22.07	9471	6.35	−30.5	–	28.9	0.930
		22.47	9377	6.42	–	−38.2	7.7	0.424
		22.97	9259	6.50	−31.4	–	6.8	0.373
		23.63	9103	6.61	–	−42.7	11.3	0.572
		23.95	9027	6.67	−34.2	–	8.5	0.453
		24.31	8942	6.73	–	−43.0	8.8	0.467
		25.30	8708	6.91	−32.1	–	10.9	0.556
		25.73	8606	6.99	–	−57.2	25.1	0.894
		26.13	8511	7.07	−33.3	–	23.9	0.880
		26.50	8424	7.14	–	−43.7	10.4	0.536
		27.40	8211	7.33	−32.0	–	11.7	0.587
		27.89	8095	7.43	–	−42.0	10.0	0.520
		28.40	7975	7.55	−31.0	–	11.0	0.560
		28.81	7878	7.64	–	−40.1	9.1	0.480
		29.55	7703	7.81	−31.4	–	8.7	0.462
		30.00	7596	7.92	–	−39.5	8.1	0.435
		30.27	7533	7.99	−30.7	–	8.8	0.467

Table XIII
Interference Pattern Data, Mission 17, Run 11

Time – GMT			Range	ψ	Max.	Min.	Diff.	"Instantaneous Reflection Coefficient"
hr	min	sec	ft	deg	dB	dB	dB	
16	34	05.00	80000	0.75	−52.0	–	–	–
		41.80	70500	0.85	–	−83.0	31.0	0.943
	35	13.00	62750	0.96	−50.0	–	33.0	0.955
		49.30	53500	1.12	–	−76.0	26.0	0.904
	36	19.50	46300	1.30	−46.5	–	29.5	0.934
		44.00	49500	1.52	–	−71.5	25.0	0.892
		59.50	36000	1.67	−44.0	–	27.5	0.918
	37	16.75	31800	1.89	–	−66.5	22.5	0.860
		26.25	29300	2.05	−36.2	–	30.3	0.940
		39.40	26600	2.26	–	−65.0	28.8	0.928
		46.60	24400	2.47	−41.5	–	23.5	0.875
		51.85	23000	2.62	–	−70.0	28.5	0.925
		57.40	21600	2.79	−33.5	–	36.5	0.970
	38	01.55	20600	2.92	–	−60.0	26.5	0.909
		09.50	18500	3.25	−37.0	–	23.0	0.867
		21.75	15750	3.82	–	−56.0	19.0	0.800
		24.50	15000	4.01	−36.0	–	20.0	0.816
		28.87	14000	4.30	–	−59.5	23.5	0.875
		30.20	13500	4.46	−37.7	–	21.8	0.850
		32.00	13000	4.63	–	−61.0	23.3	0.872
		36.25	12000	5.01	−36.5	–	24.5	0.887
		36.92	11750	5.12	–	−52.0	15.5	0.715
		38.30	11500	5.23	−31.0	–	21.0	0.836
		39.65	11200	5.37	–	−53.0	22.0	0.852
		41.10	10900	5.52	−32.0	–	21.0	0.836
		41.90	10600	5.68	–	−45.0	13.0	0.635
		42.60	10500	5.73	−28.5	–	16.5	0.740
		43.50	10250	5.87	–	−45.8	17.3	0.760
		44.90	9800	6.14	−35.8	–	10.0	0.520
		45.40	9750	6.17	–	−48.0	12.2	0.600
		46.75	9500	6.33	−30.0	–	18.0	0.775
		47.35	9250	6.50	–	−47.0	17.0	0.752
		48.30	8900	6.76	−29.5	–	17.5	0.763

Table XIV
Interference Pattern Data, Mission 18, Run 3

Time – GMT			Range	ψ	Max.	Min.	Diff.	"Instantaneous Reflection Coefficient"
hr	min	sec	ft	deg	dB	dB	dB	
16	02	35.75	53318	1.13	−53.5	–	–	–
	03	01.80	46114	1.31	–	−69.2	15.7	0.720
		27.00	39240	1.53	−48.0	–	21.2	0.840
		37.30	36429	1.65	–	−66.5	18.5	0.786
		45.50	34215	1.76	−46.2	–	20.3	0.823
		59.75	30465	1.98	–	−72.5	26.3	0.907
	04	11.50	27295	2.20	−45.0	–	27.5	0.918
		19.12	25236	2.38	–	−67.7	22.7	0.865
		27.70	22921	2.63	−40.2	–	27.5	0.918
		34.90	20858	2.88	–	−63.2	23.0	0.868
		41.50	18980	3.17	−40.5	–	22.7	0.865
		44.30	18196	3.31	–	−60.0	19.5	0.807
		47.70	17244	3.49	−39.2	–	20.8	0.832
		51.20	16276	3.70	–	−53.7	14.5	0.685
		54.30	15433	3.90	−39.7	–	14.0	0.671
		55.90	15000	4.01	–	−62.6	22.9	0.867
		58.50	14291	4.21	−37.0	–	25.6	0.900
		59.90	13927	4.32	–	−54.5	17.5	0.764
	05	02.16	13224	4.55	−36.5	–	18.0	0.775
		03.40	13016	4.62	–	−47.0	10.5	0.540
		05.02	12594	4.78	−36.2	–	10.8	0.552
		06.96	12090	4.98	–	−66.5	30.3	0.940
		08.35	11729	5.13	−34.5	–	32.0	0.950
		09.15	11521	5.22	–	−55.2	20.7	0.830
		09.90	11326	5.31	−36.5	–	18.7	0.790
		11.40	10923	5.51	–	−48.7	12.2	0.600
		12.30	10702	5.62	−34.5	–	14.2	0.677
		13.10	10494	5.73	–	-45.3	10.8	0.552
		14.40	10156	5.92	−36.5	–	8.8	0.467

Table XV
Tabulated Results of All Runs

Date 1974	Mission No.	Run No.	No. of points in graph	σ_w-ft. predicted from reflection coefficient	σ_w-ft laser profil-ometer	error %	Wind-kts A/C course relative to wind
4/8	18	1	4	0.60 ± 0.15	0.65	−8	UW
		3	5	0.65 ± 0.1	±0.07	0	UW
3/8	17	9	2	≈ 1.2 (?)	~0.5*	+140	8/
		10	2	~0.6	~0.5*	+20	7.5/UW44°
		11	6	0.45 ± 0.05	~0.45*	0	7/DW30°
		12	4	0.50 ± 0.1	~0.40*	+25	6/
3/6	16	2	5	0.65 ± 0.15	—	—	8/
		3	4	~1.0	—	—	8/
		4	3	≈0.6	—	—	8/
		5	4	0.90 ± 0.1	—	—	7/
		Avg.		0.8 ± 0.2	(0.75 to 1.0)**	(±<25)	
3/4	15	1	3	≈0.8	0.52	+54	3/UW14°
		2	2	≈0.65	0.55	+18	3/UW26°
		5	5	0.8 ± 0.3	~0.8	0	
		8	6	0.55 ± 0.05	0.64	−14	/UW75°
2/27	14	1	2		1.08		14/UW5°
		2	3		1.18		14/UW55°
		3	2		1.18		14/UW
		4	1		1.18		13/DW
		5	3				13/UW27°
		6	3				13/UW
		Avg.		0.8 ± 0.5	1.15 ±0.12	≈−30	
2/25	13	2	2	≈0.7	1.58	−50	23/DW
		9	2	≈1.2	1.28	−6	19/UW71°
		12	3	~0.8	1.13	−29	/XW
		Avg.		~0.9 ± 0.3	1.33	−32	

*Extrapolated with the same slope as the wind speed (Fig. 16).
**Visual estimates — see text

UW = up wind, DW = down wind, XW = cross wind.

Table XVI
Comparison of Remotely Sensed and Measured
Wave Heights for the Qualified‡ Runs

Mission No.	Run Nos.	σ_w from reflection coeff. ft.	Laser profil. σ_w ft.	% error (for runs ≥ 4 points)	Ship	Tracking	% error (all days)
13	2, 9, 12	0.9±0.3*	1.33*	—	DD821	Optical	−32
14	1 to 6	0.8±0.5*	1.15±0.12	—	"	"	−30
15	5	0.8±0.3	0.8	0	"	"	0
"	8	0.55±0.05	0.64	−14	"	"	−14
16	2	0.65±0.15	(0.75	—	"	"	—
"	5	0.9±0.1	to 1.0)**	—	"	Radar	—
17	11	0.45±0.05	~0.45*	~0	"	"	~0
"	12	0.5±0.1	~0.4*	~+25	"	"	~+25
18	1	0.60±0.15	0.65±0.07	−8	DD724	"	−8
"	3	0.65±0.1		0	"	"	0
Average (Exclud-Mission 16		±0.12		±5			−14

‡ = "Qualified" means those runs with 4 or more points with internal consistency.
* = Average of the runs
** = From visual estimates
• = Extrapolated with same slope as wind speed.

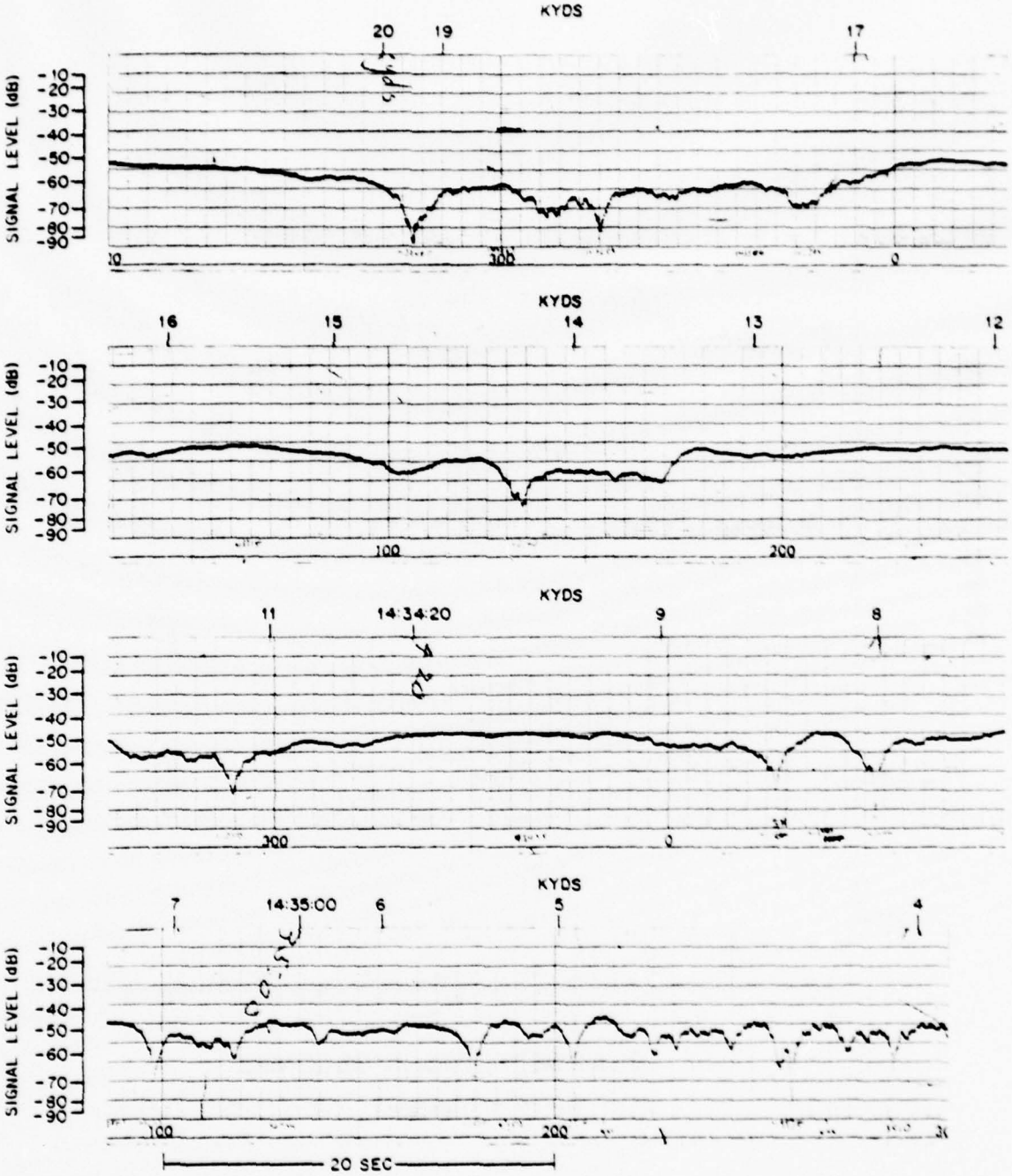

Fig. 1 - Continuous interference pattern on analog chart recorder Data of 8 March 1974, 14:31:40 GMT, Mission 17, Run 2. σ_w(standard deviation of water surface height) = 0.65 ft. Common conditions for all the 1974 data:

Transmitter-aircraft altitude = 1000 ft. unless otherwise specified. Shipboard-receiver height = 50 ft. Frequency = 1.3 GHz. Polarization = horizontal. Taken from (2, Fig. 5).

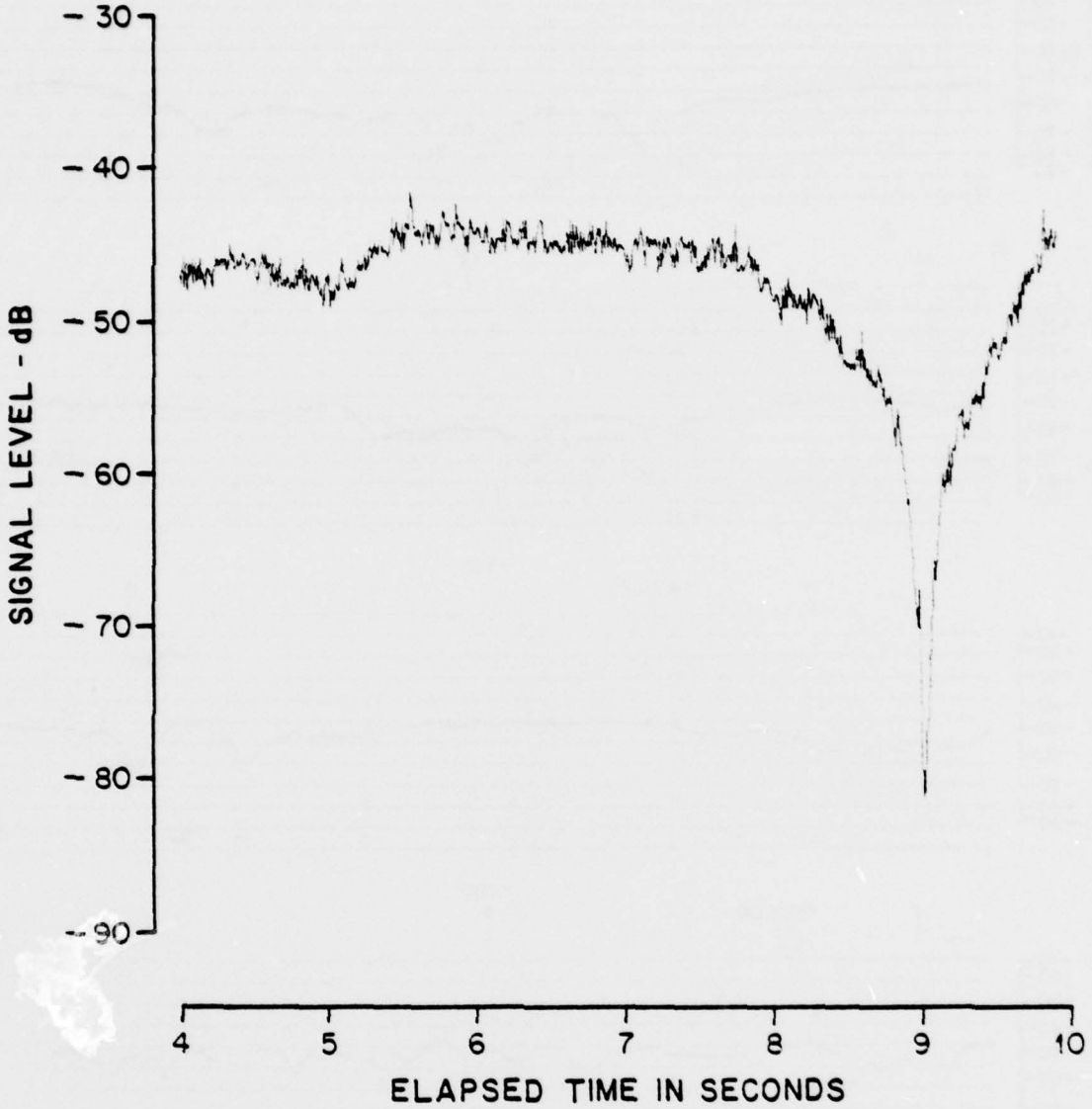

(a) Sharp minimum

Fig. 2 - Different types of interference minima, digital-computer plotted. Data of 8 March 1974, Mission 17, Run 2, starting at 14:32:48 GMT. σ_w = 0.65 ft. Taken from (2, Fig. 9).

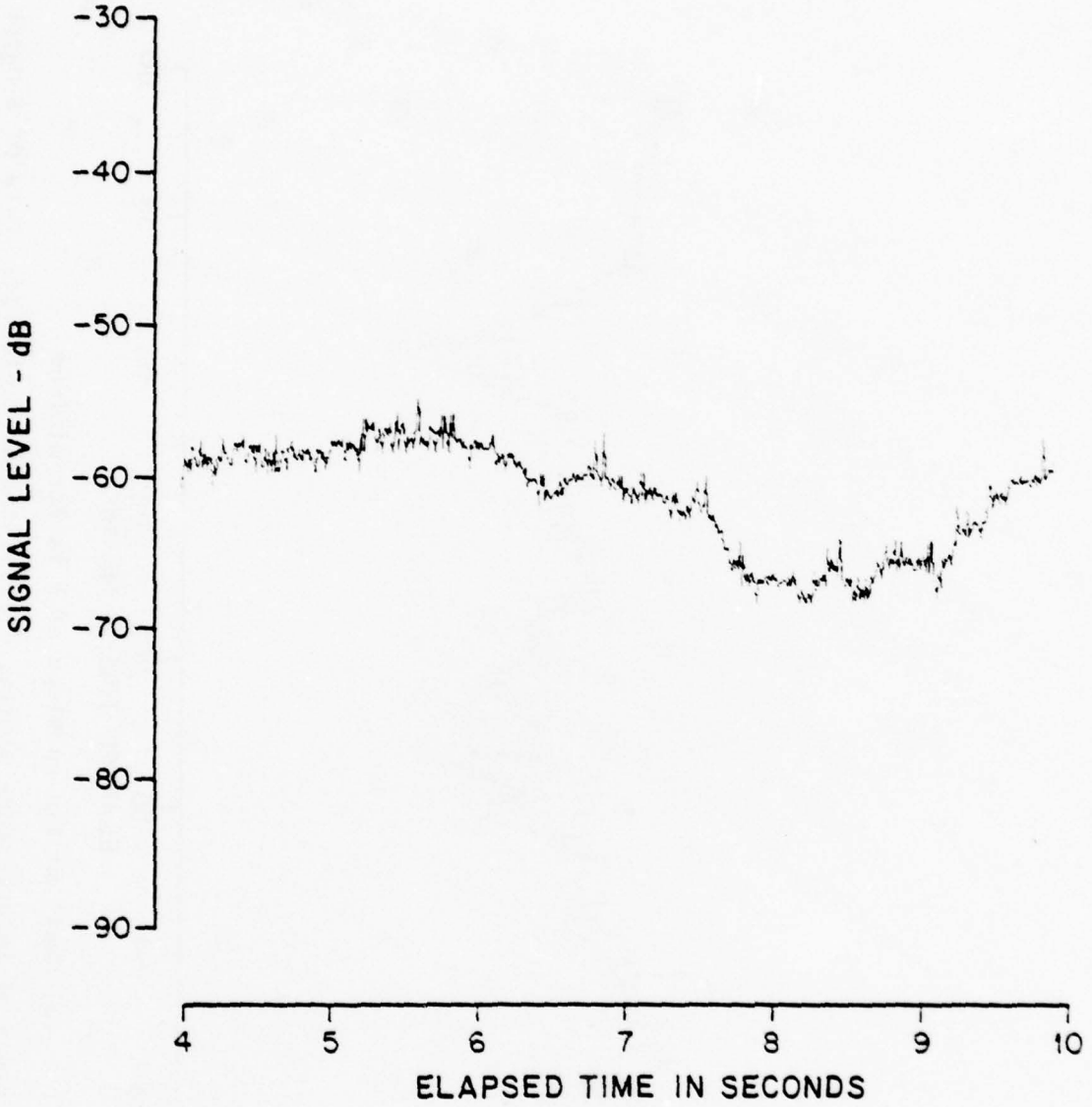

(b) Broad minimum

Fig. 2 - Different types of interference minima, digital-computer plotted. Data of 8 March 1974, Mission 17, Run 2, starting at 14:32:48 GMT. σ_w = 0.65 ft. Taken from (2, Fig. 9).

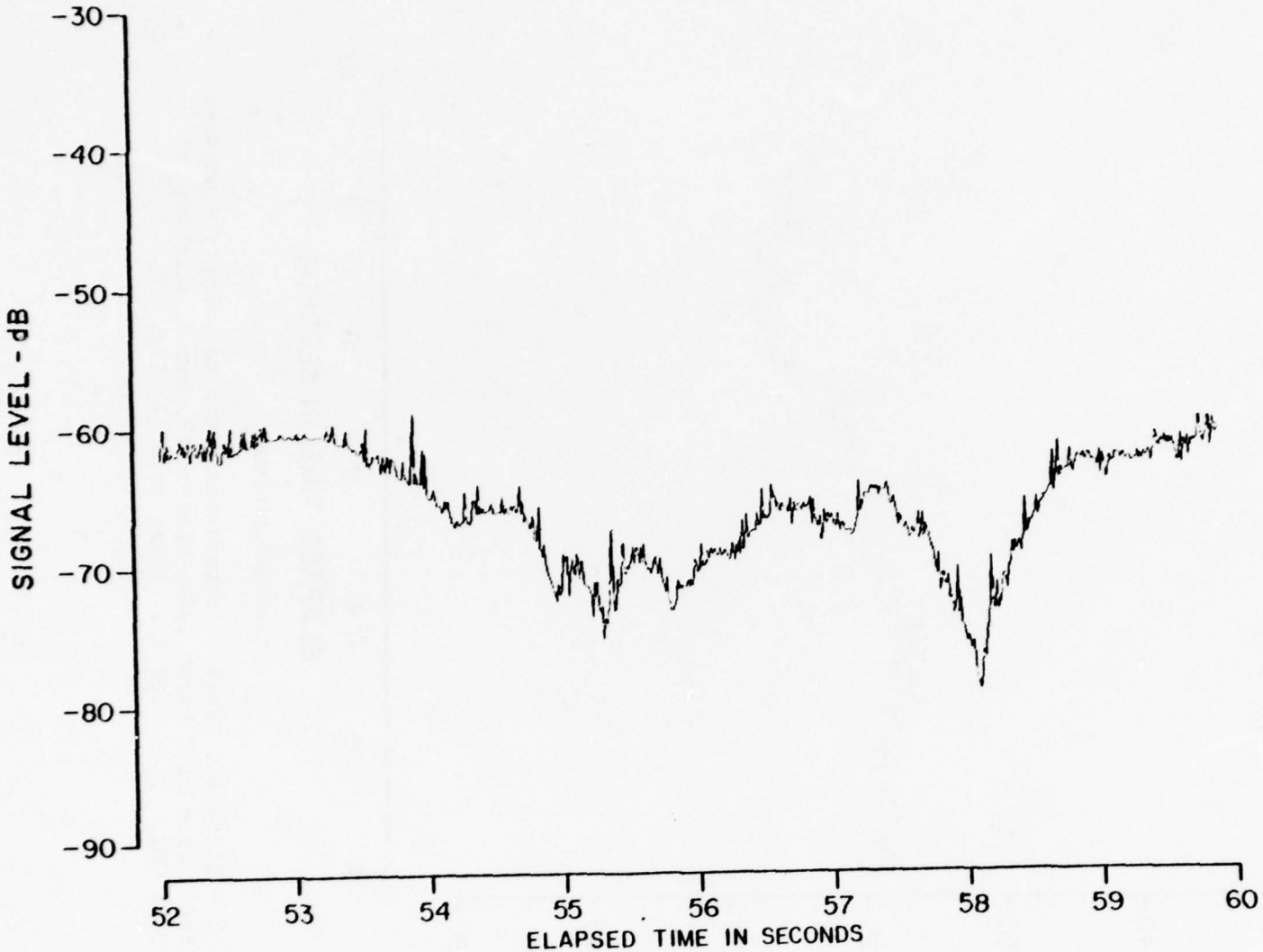

(c) Small minima on slope of a larger minimum

Fig. 2 - Different types of interference minima, digital-computer plotted. Data of 8 March 1974 Mission 17, Run 2, starting at 14:32:48 GMT. σ_w = 0.65 ft. Taken from (2, Fig. 9)

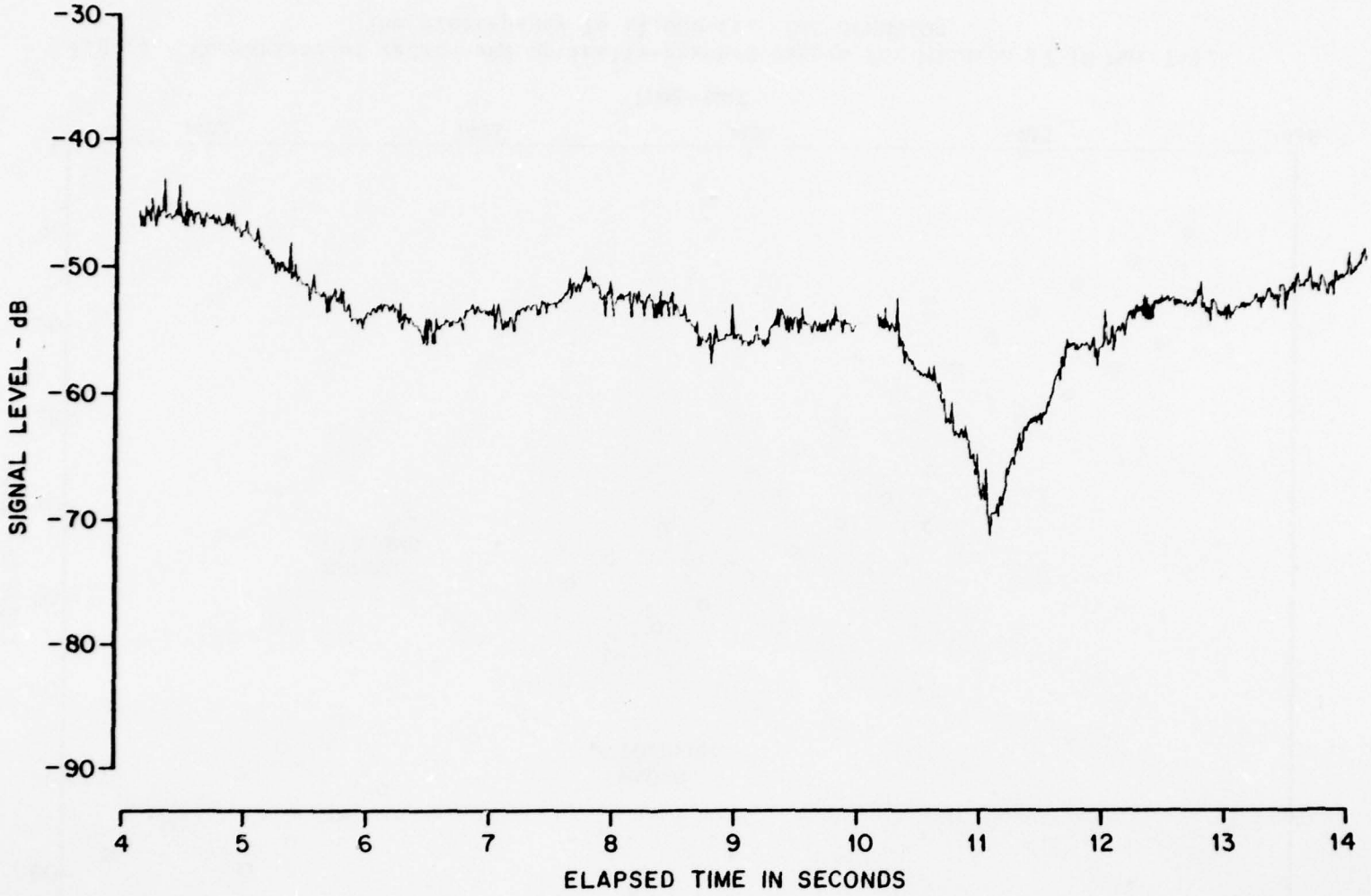

(d) Small minima on slope of a larger minimum

Fig. 2 - Different types of interference minima, digital-computer plotted. Data of 8 March 1974 Mission 17, Run 2, starting at 14:32:48 GMT. σ_w = 0.65 ft. Taken from (2, Fig. 9)

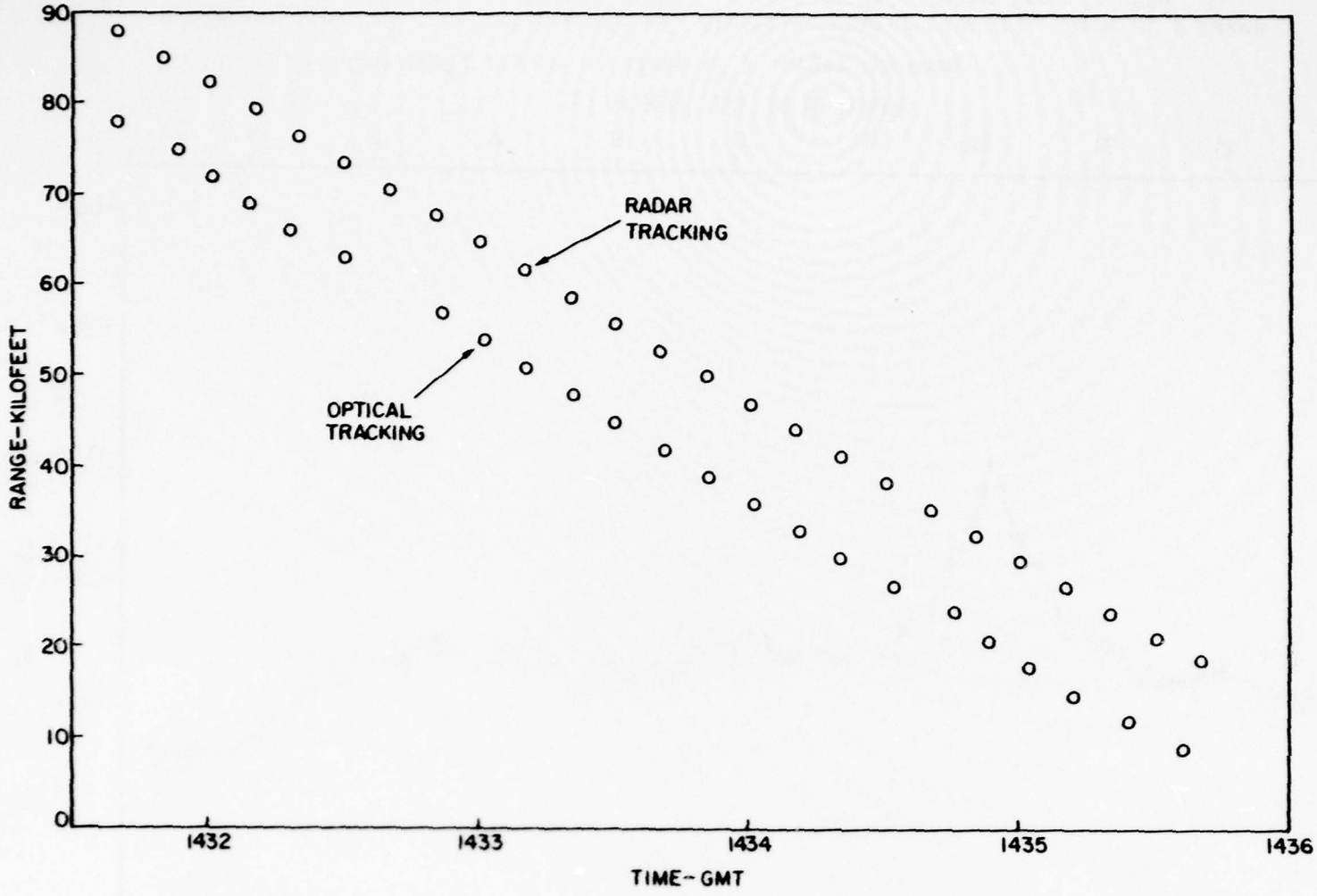

Fig. 3 - Comparison of radar- and optically-tracked ranges for Mission 17 (8 Mar 74). The discrepancy is 11,000 ft. USS JOHNSTON.

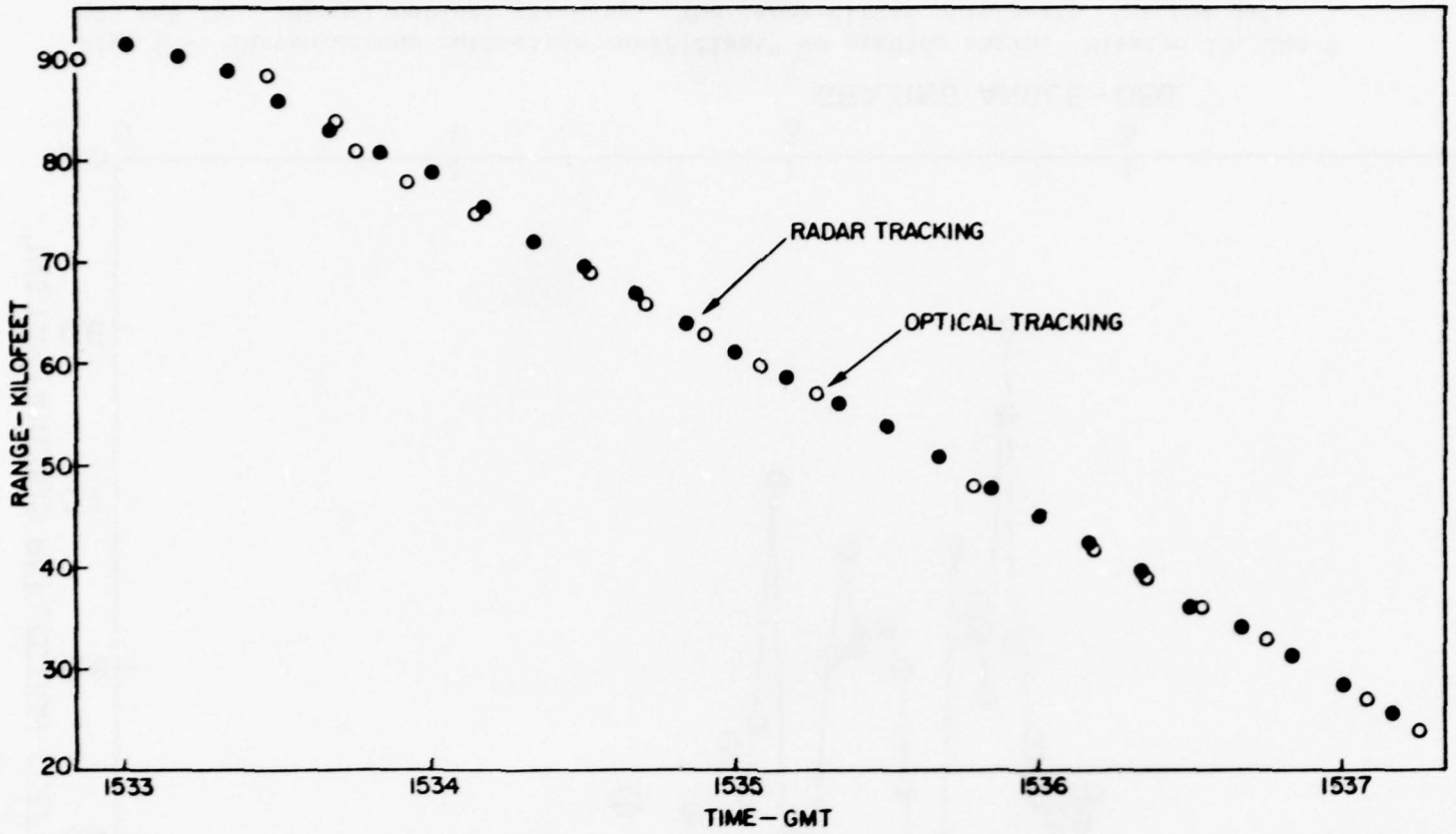

Fig. 4 - Comparison of radar- and optically-tracked ranges for Mission 18 (8 Apr 74). USS LAFFEY.

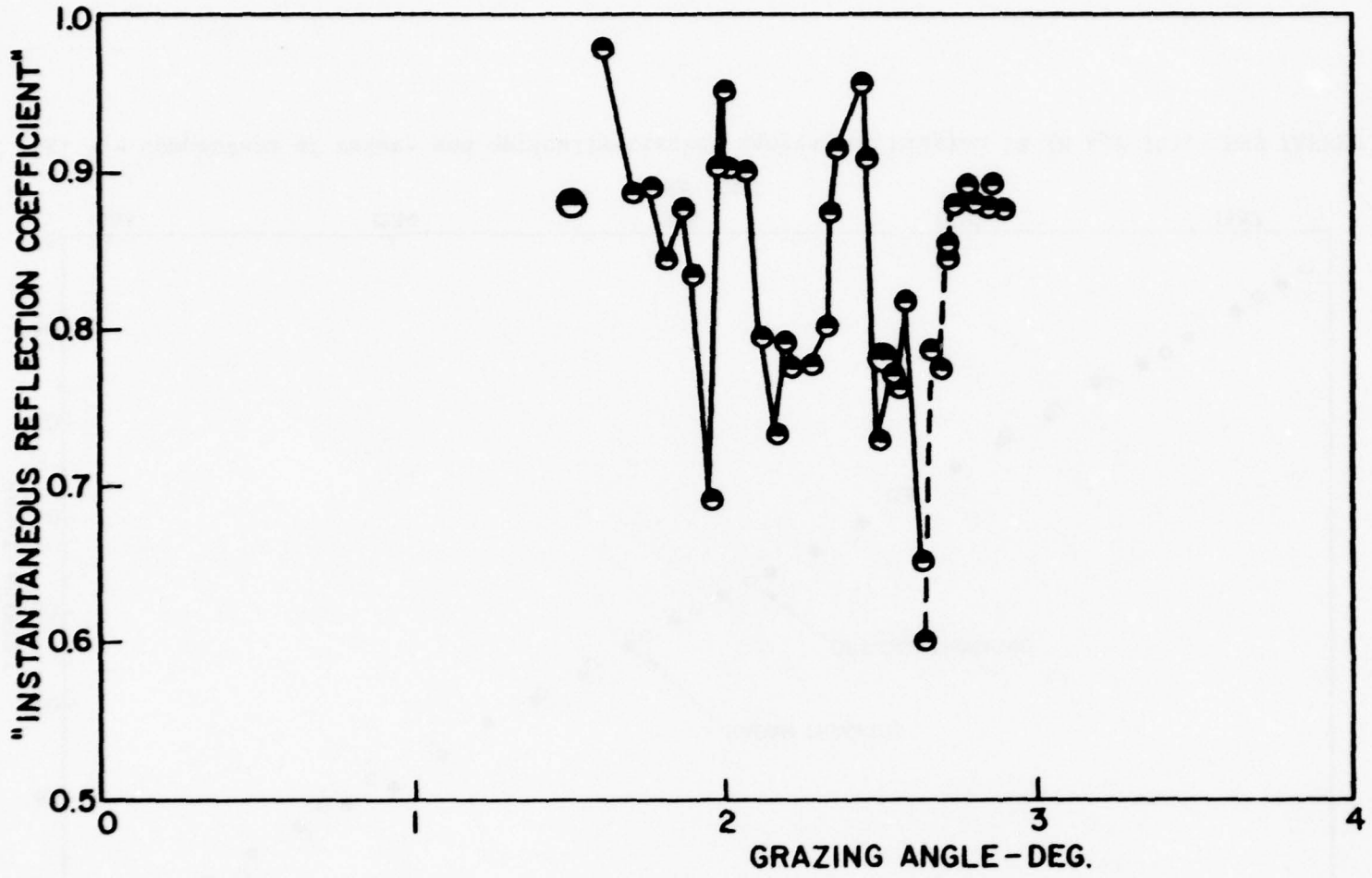

Fig. 5 - "Instantaneous reflection coefficient" vs grazing angle. Mission 13, Run 9 (25 Feb 74). Manual optical tracking. The large-circle points are for the data smoothed over 1^{o} grazing-angle intervals.

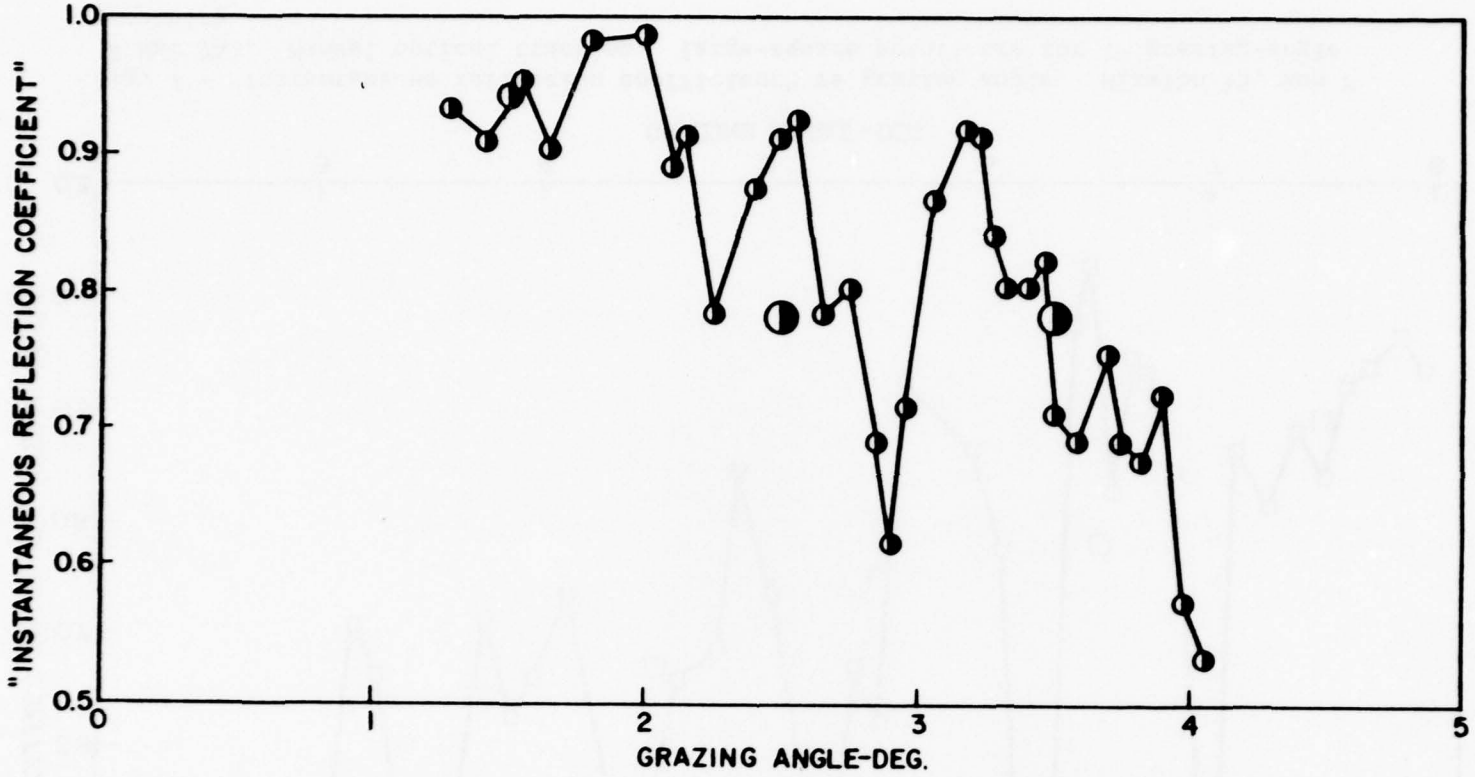

Fig. 6 - "Instantaneous reflection coefficient" vs grazing angle. Mission 13, Run 12 (25 Feb 74). Manual optical tracking. Large-circle points are for 1^{o} grazing-angle smoothing.

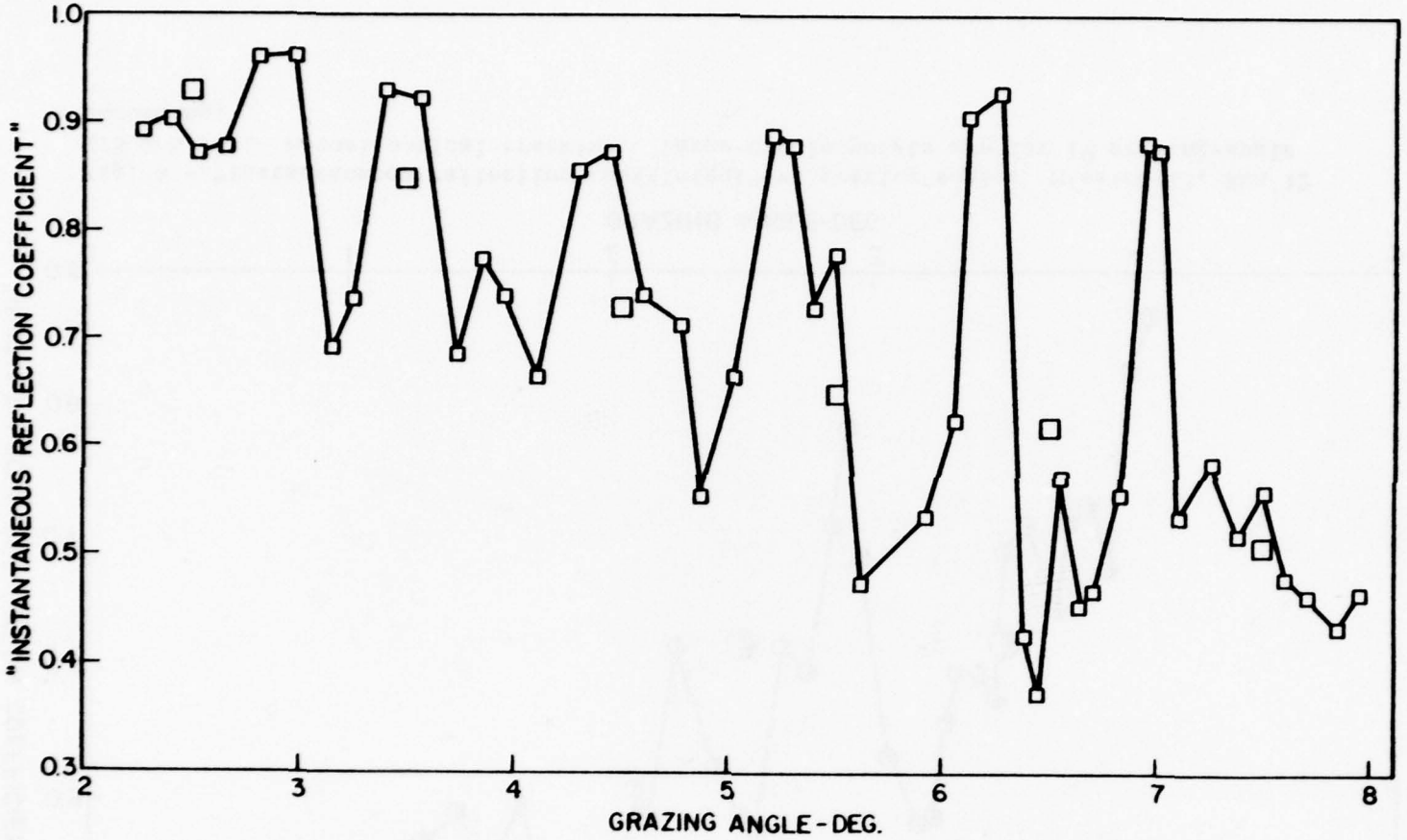

Fig. 7 - "Instantaneous reflection coefficient" vs grazing angle. Mission 15, Run 8 (4 Mar 74). Manual optical tracking. Large-square points are for 1° grazing-angle smoothing.

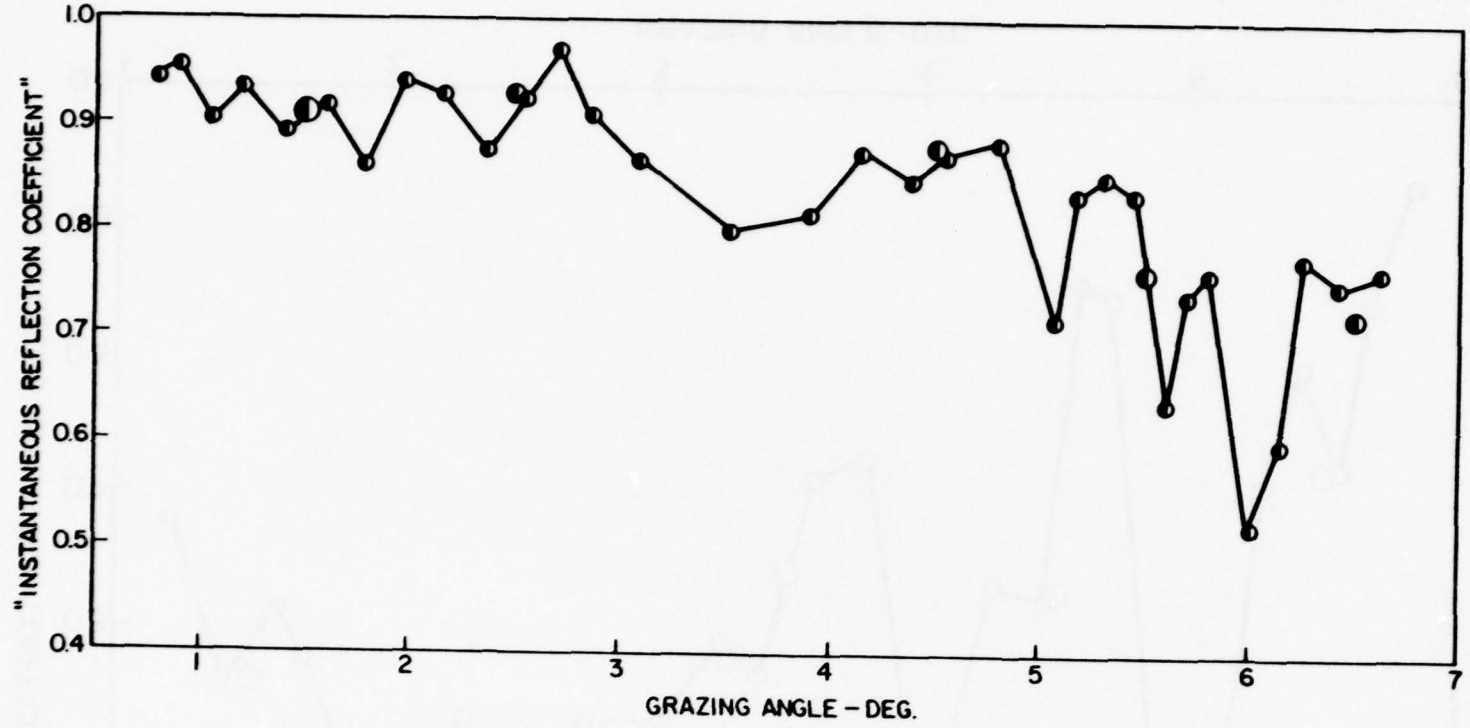

Fig. 8 - "Instantaneous reflection coefficient" vs grazing angle. Mission 17, Run 11 (8 Mar 74). Automatic radar tracking. Large-circle points are for 1^{o} grazing-angle smoothing.

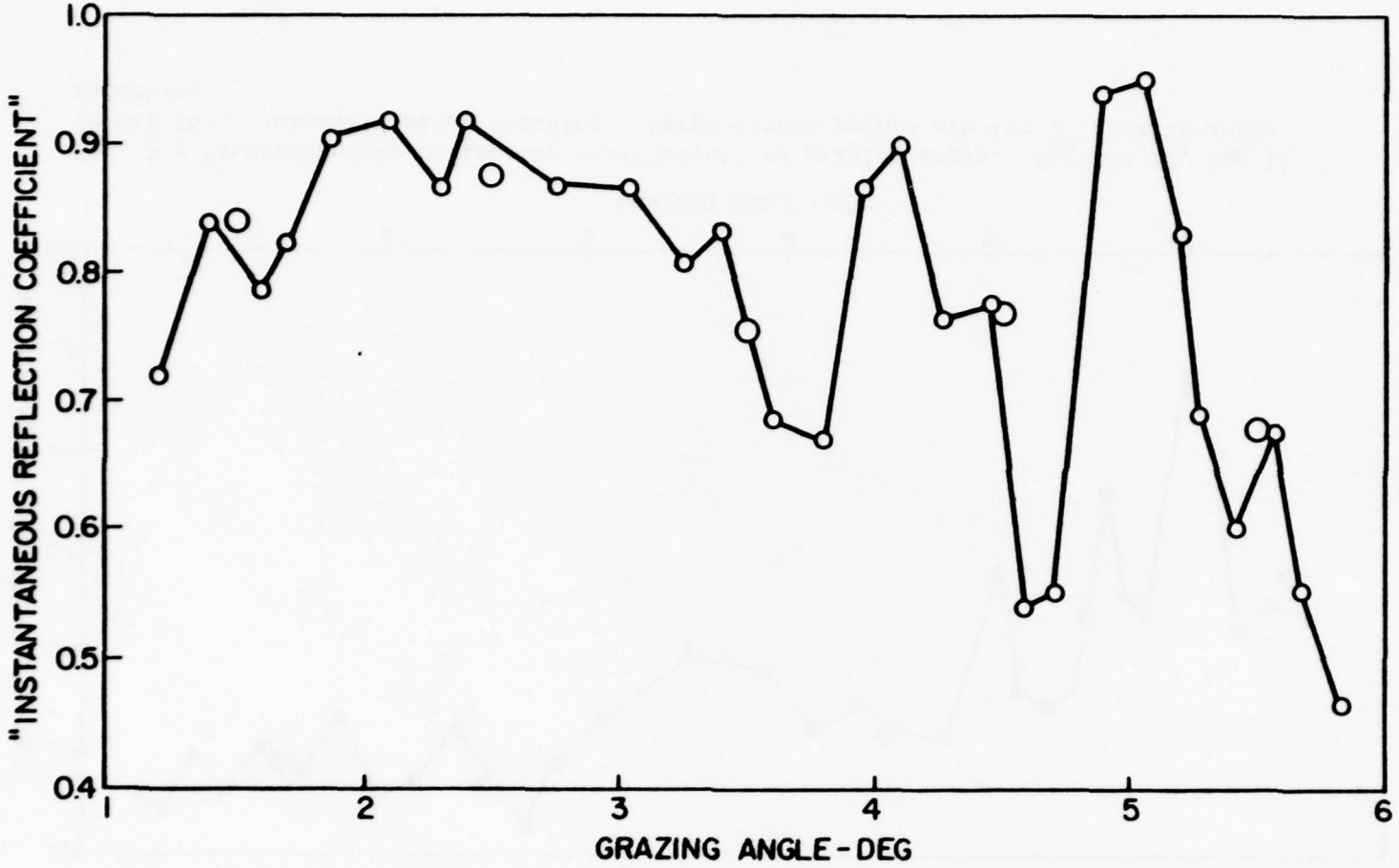

Fig. 9 - "Instantaneous reflection coefficient' vs grazing angle. Mission 18, Run 3 (8 Apr 74). Automatic radar tracking. Large-circle points are for 1^{o} grazing-angle intervals.

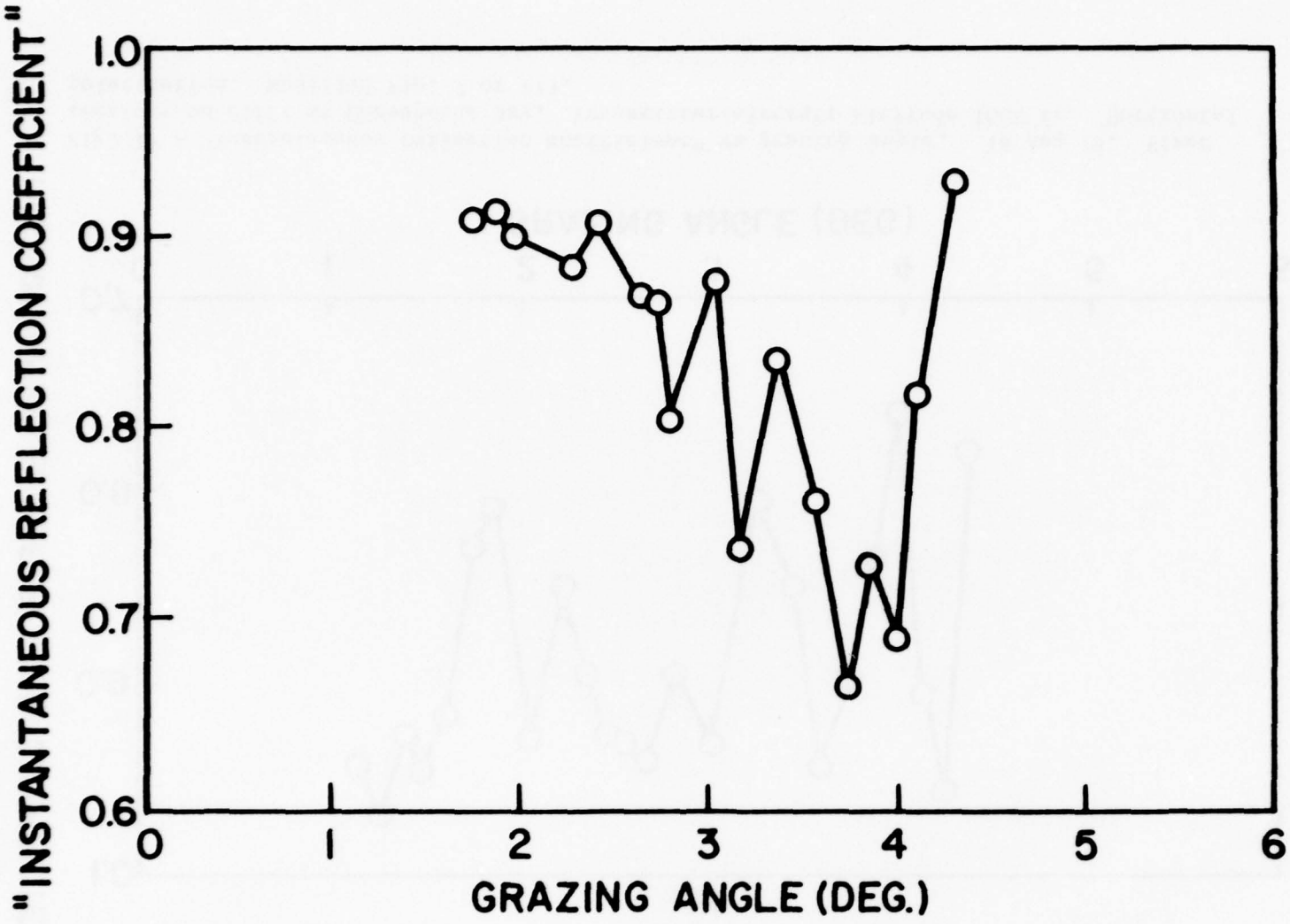

Fig. 10 - "Instantaneous reflection coefficient" vs grazing angle. 2 Jul 73. Fixed receiver on cliff at Chesapeake Bay. Transmitter-aircraft altitude 2500 ft. Horizontal Polarization. Modified Fig. 6 of (1).

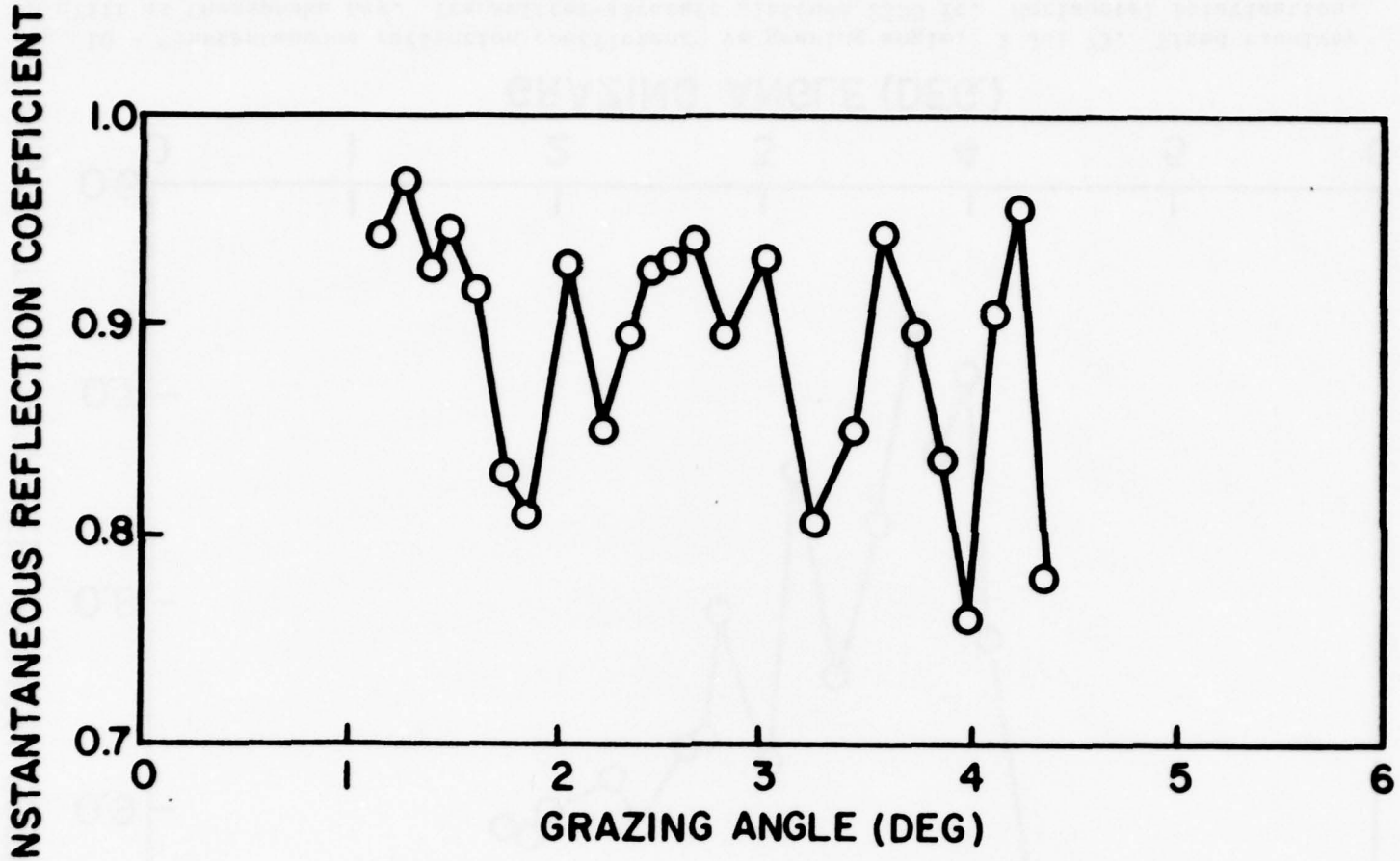

Fig. 11 - "Instantaneous reflection coefficient" vs grazing angle. 16 Aug 73. Fixed receiver on cliff at Chesapeake Bay. Transmitter-aircraft altitude 1000 ft. Horizontal polarization. Modified Fig. 7 or (1).

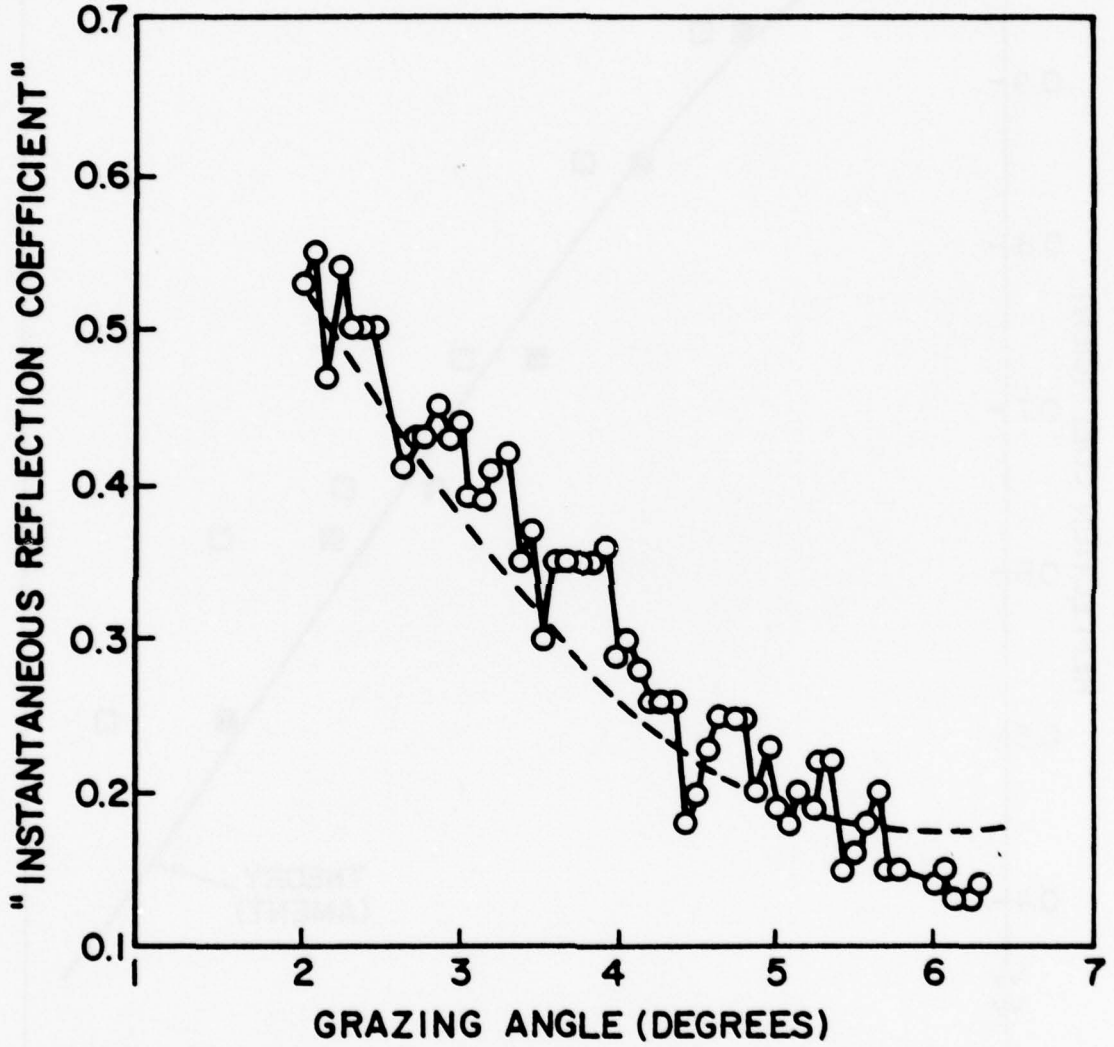

Fig. 12 - "Instantaneous reflection coefficient" vs grazing angle. 13 Sep 73. Fixed receiver on cliff at Chesapeake Bay. Transmitter-aircraft altitude 2000 ft. Vertical polarization. Modified Fig. 8 of (1).

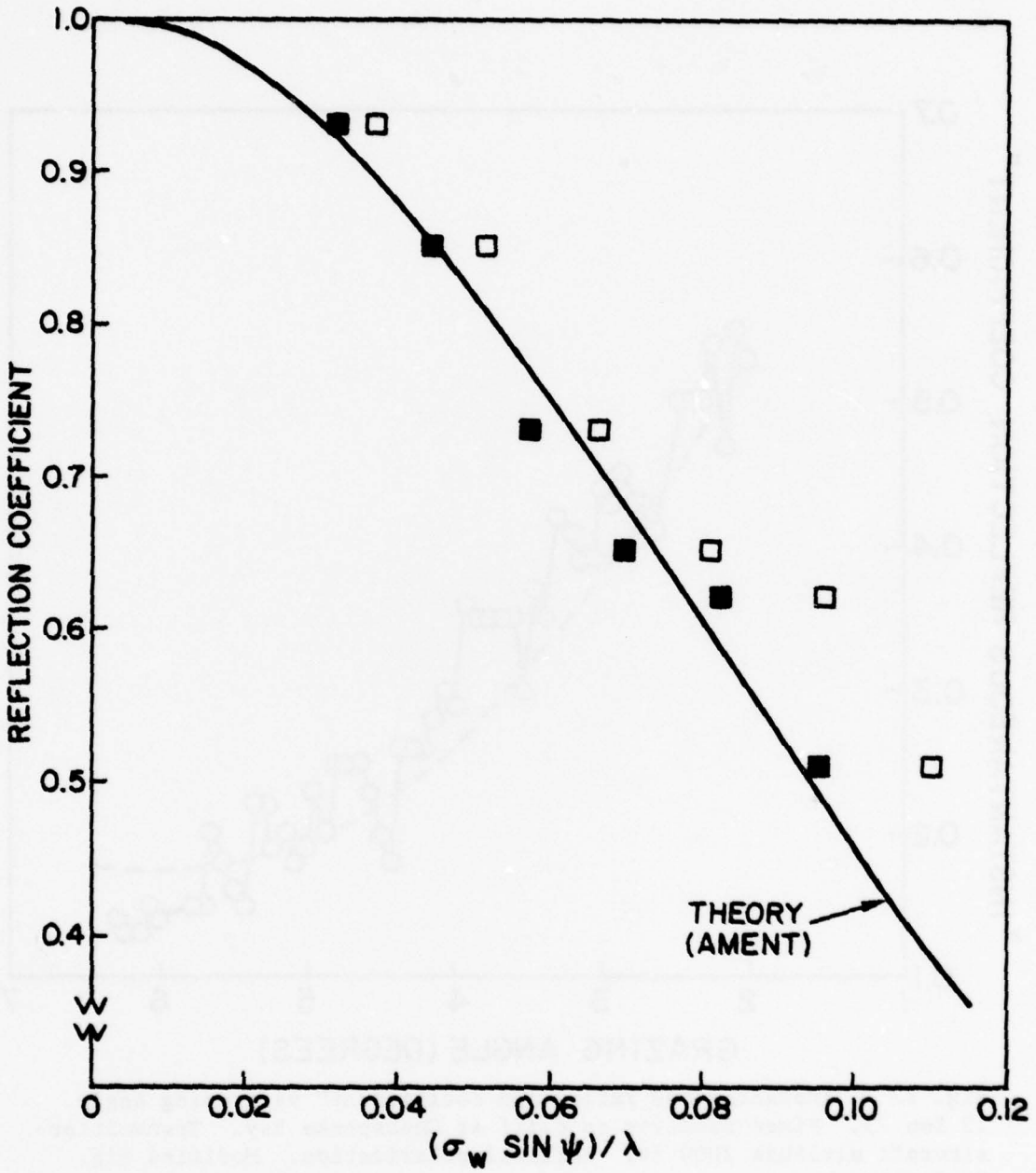

Fig. 13 - Smoothed reflection coefficient vs apparent surface roughness, $(\sigma_w \sin\psi)/\lambda$, compared to Ament's (1953) theory. Mission 15, Run 8 (4 Mar 74). Optical tracking.

□ Plotted with σ_w = 0.64 ft.

■ Plotted with σ_w = 0.55 ft.

Laser profilometer σ_w = 0.64 ft.

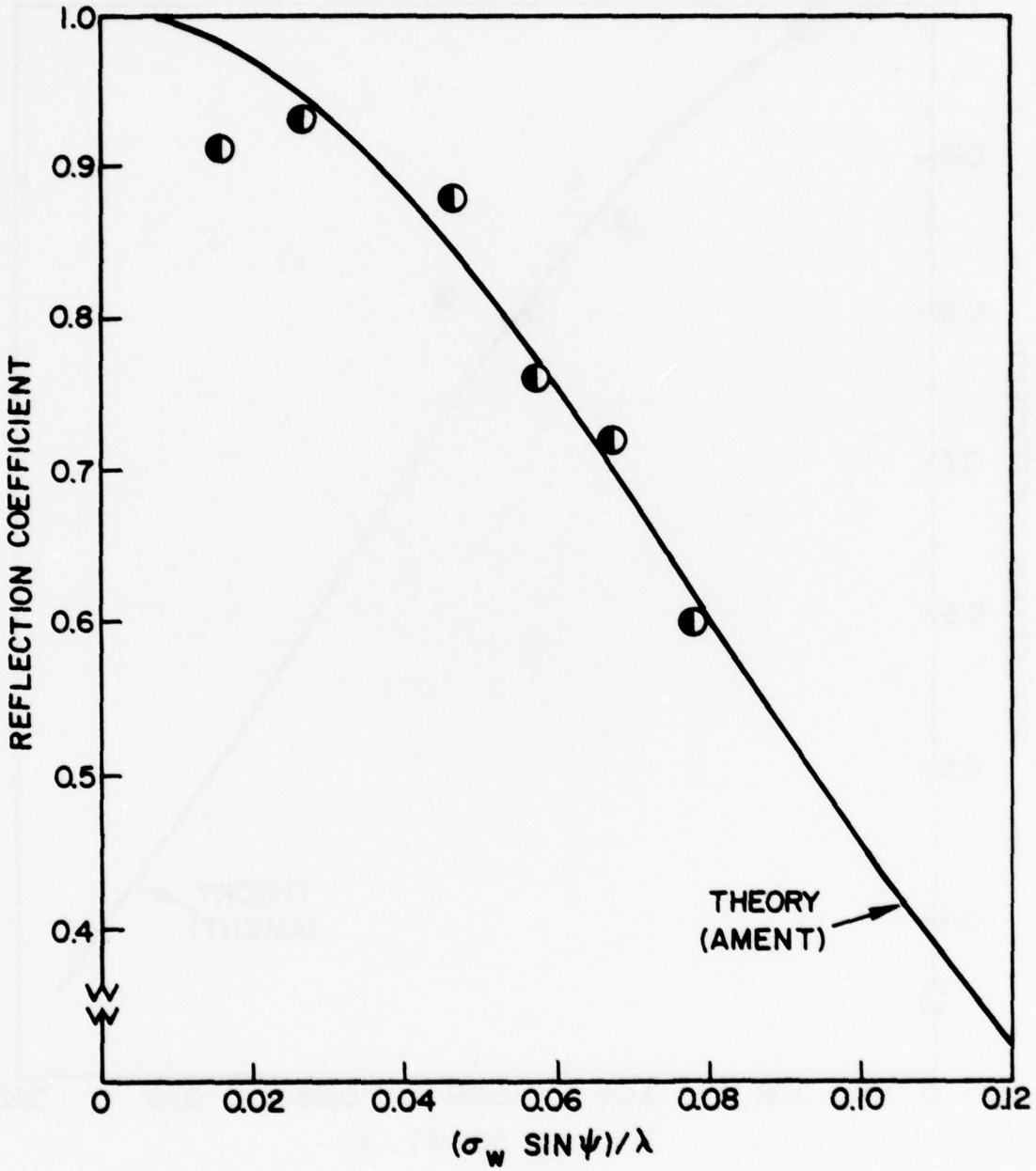

Fig. 14 - Smoothed reflection coefficient vs apparent surface roughness compared to Ament's theory. Mission 17, Run 11 (8 Mar 74). Radar tracking.
Data points plotted with σ_w = 0.45 ft.
Laser profilometer σ_w (extrapolated) $\simeq$ 0.45 ft.

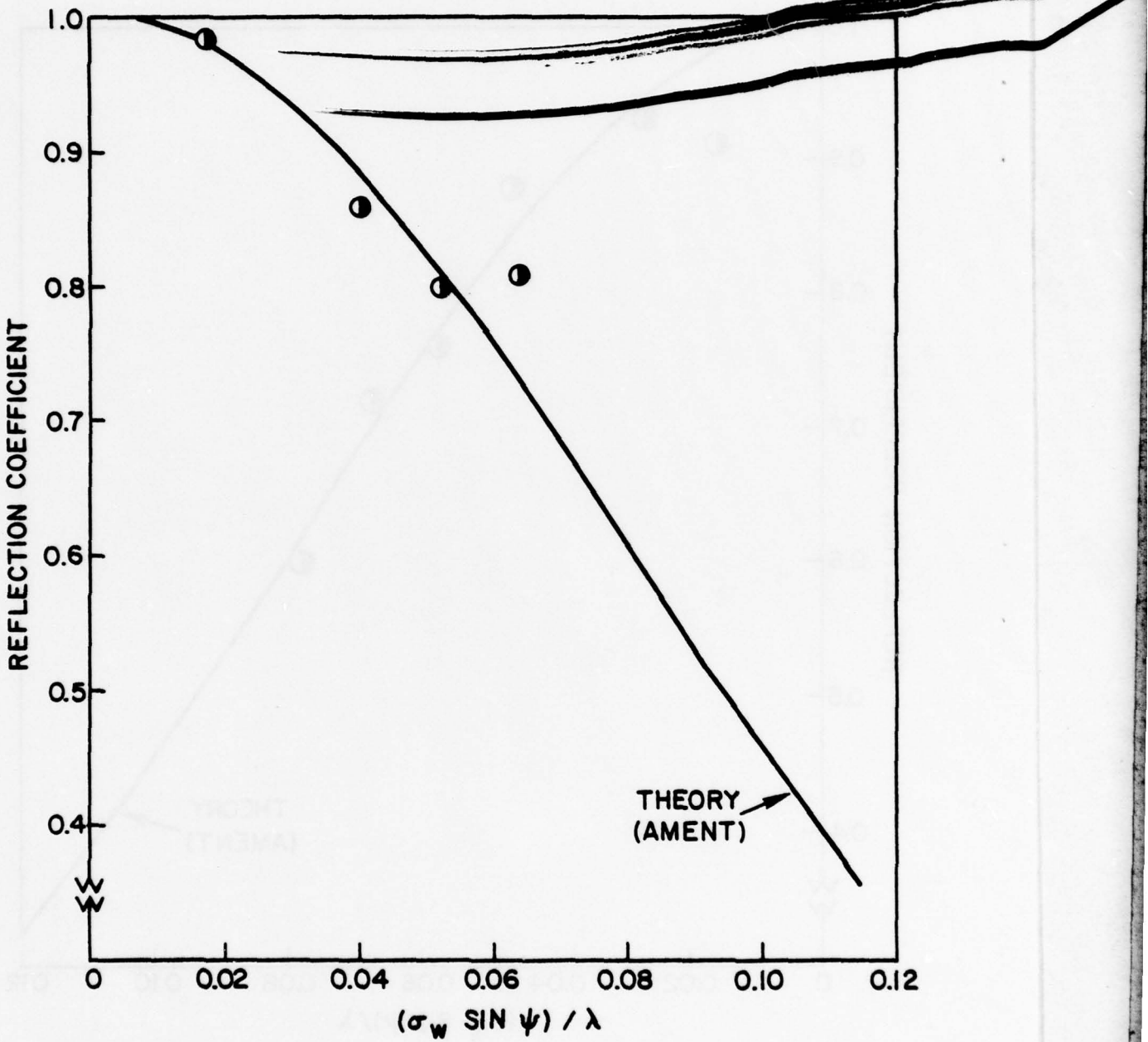

Fig. 15 - Smoothed reflection coefficient vs apparent surface roughness compared to Ament's theory. Mission 17, Run 12 (8 Mar 74).
Radar tracking.
Data points plotted with σ_w = 0.50 ft.
Laser profilometer σ_w (extrapolated) ≅ 0.40 ft.
Transmitter-aircraft altitude = 2500 ft.

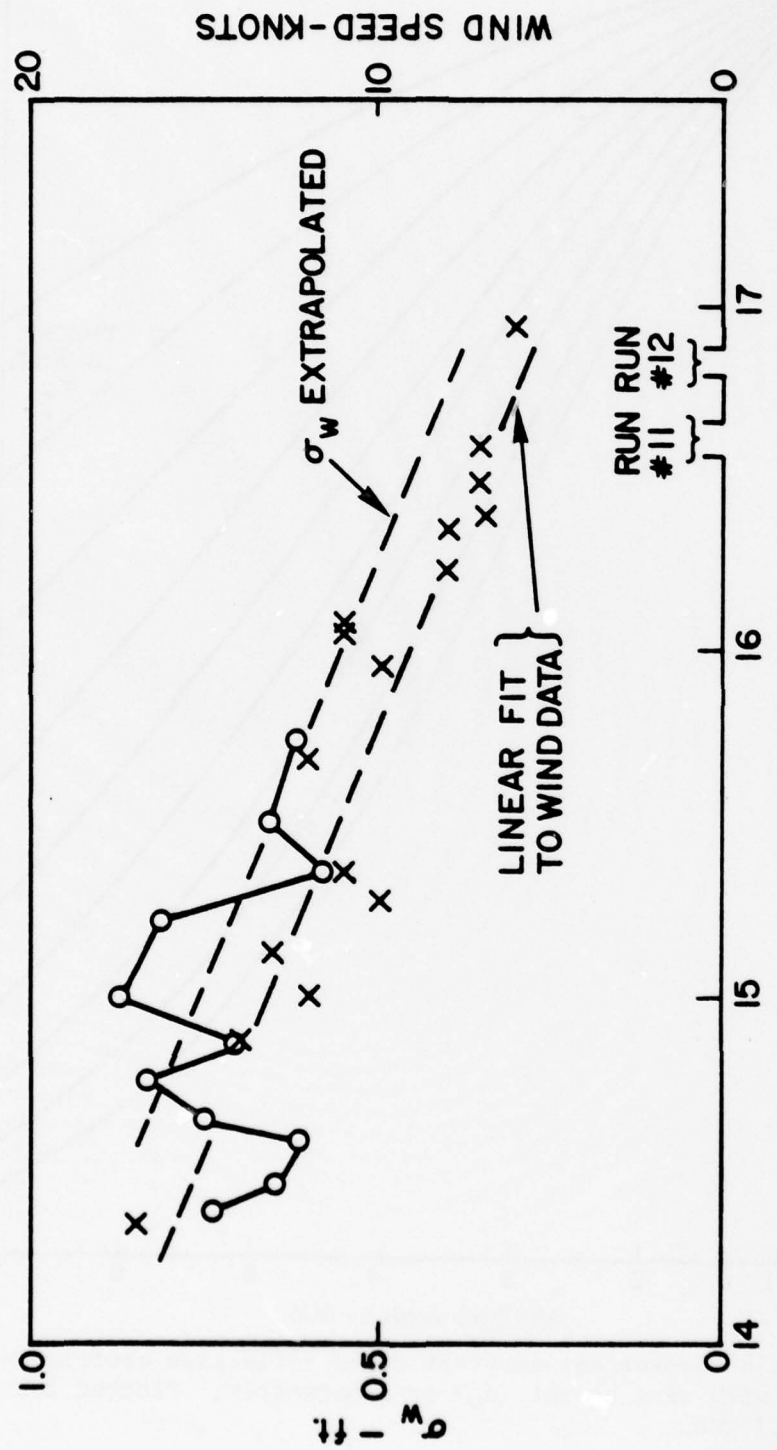

Fig. 16 - Wind and wave measurements. Mission 17 (8 Mar 74).
O Laser profilometer σ_w.
X Shipboard wind speed.

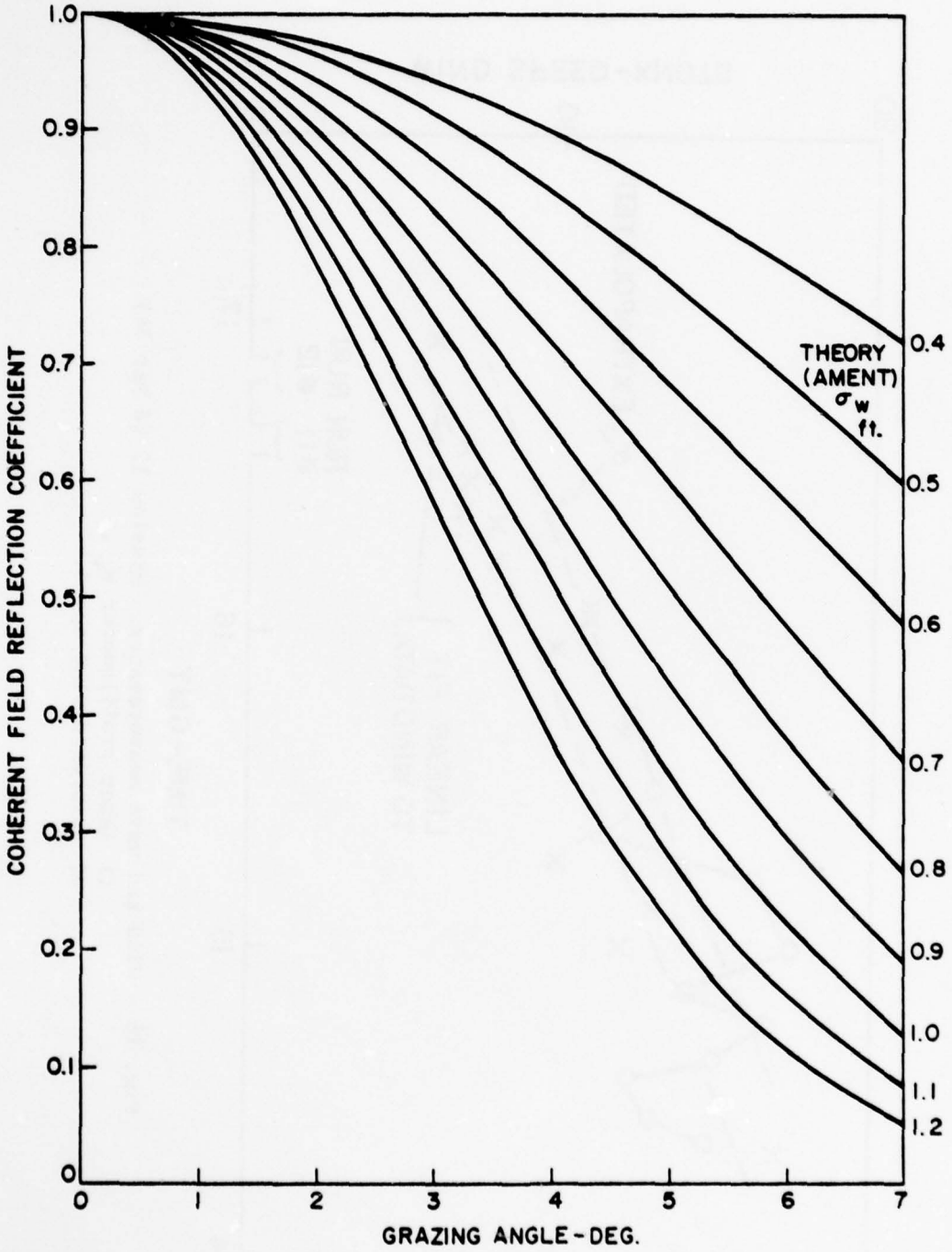

Fig. 17 - Ament's theoretical coherent field reflection coefficient vs grazing angle, with wave height (σ_w) as a parameter. Plotted for a frequency of 1.3 GHz.

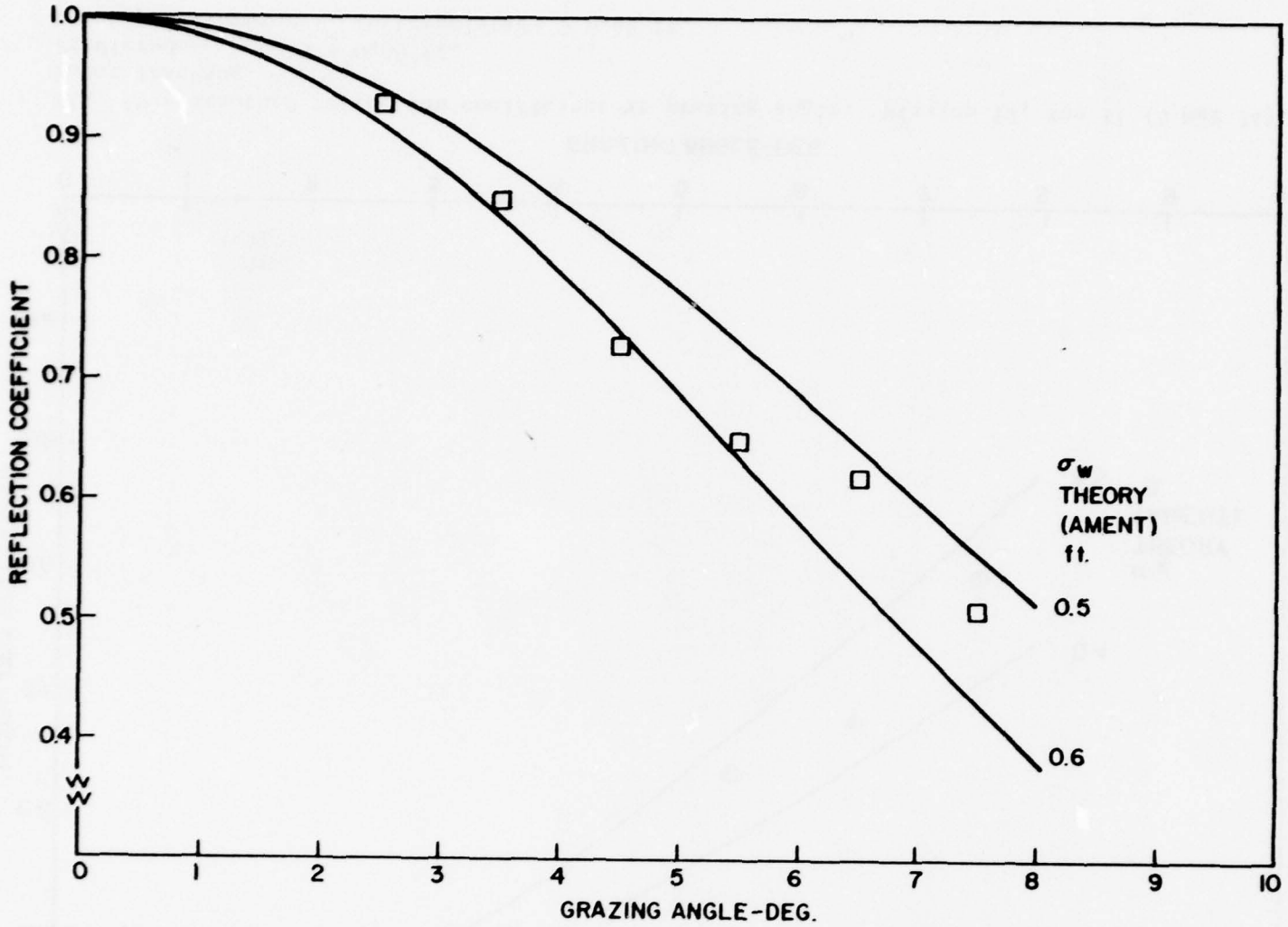

Fig. 18 - Smoothed reflection coefficient vs grazing angle. Mission 15, Run 8 (4 Mar 74). Optical tracking.
Predicted $\sigma_w = 0.55 \pm 0.05$ ft.
Laser profilometer $\sigma_w = 0.64$ ft.

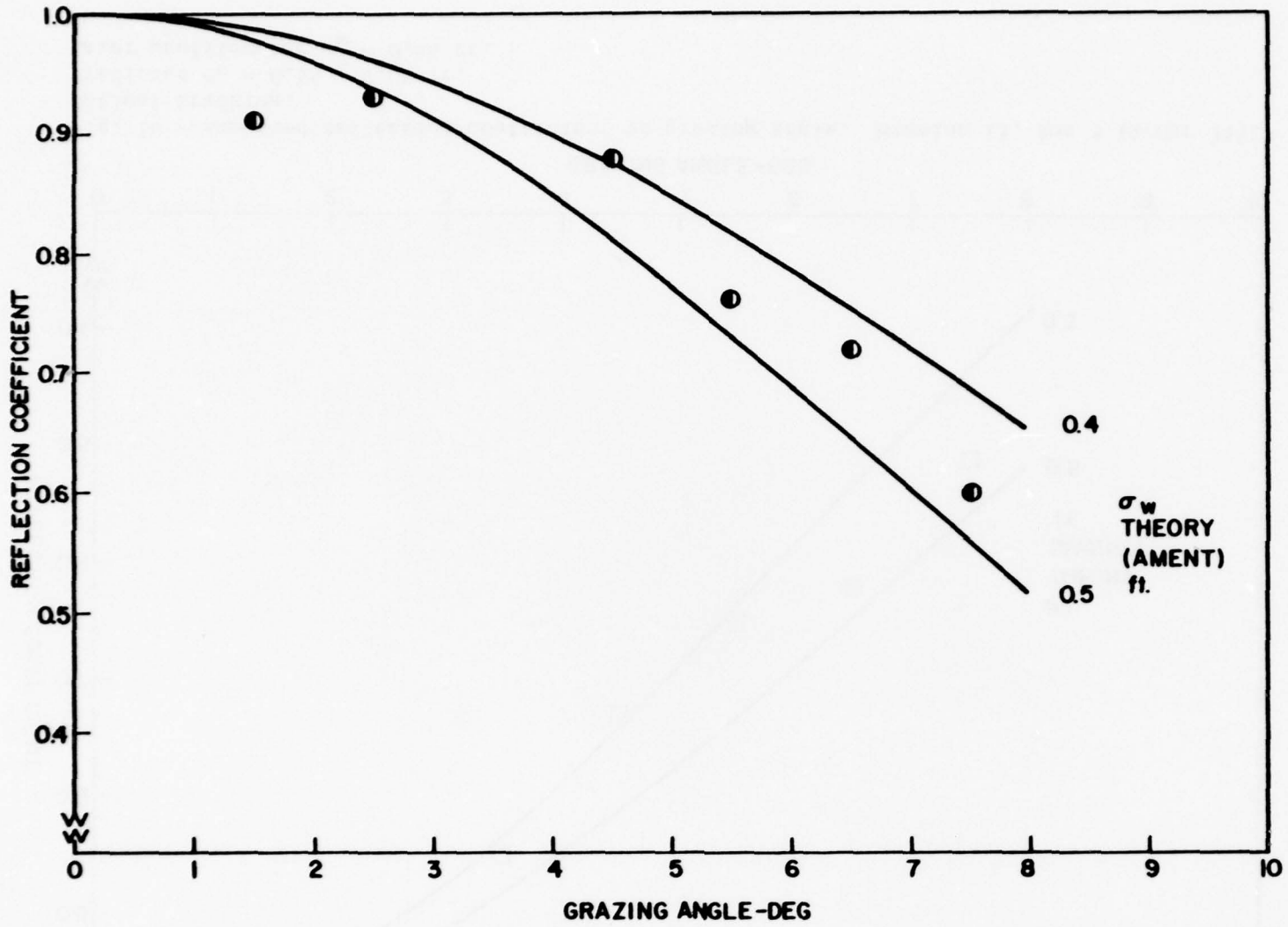

Fig. 19 - Smoothed reflection coefficient vs grazing angle. Mission 17, Run 11 (8 Mar 74). Radar Tracking.
Predicted $\sigma_w = 0.45 \pm 0.05$ ft.
Laser profilometer σ_w (extrapolated) $\cong 0.45$ ft.

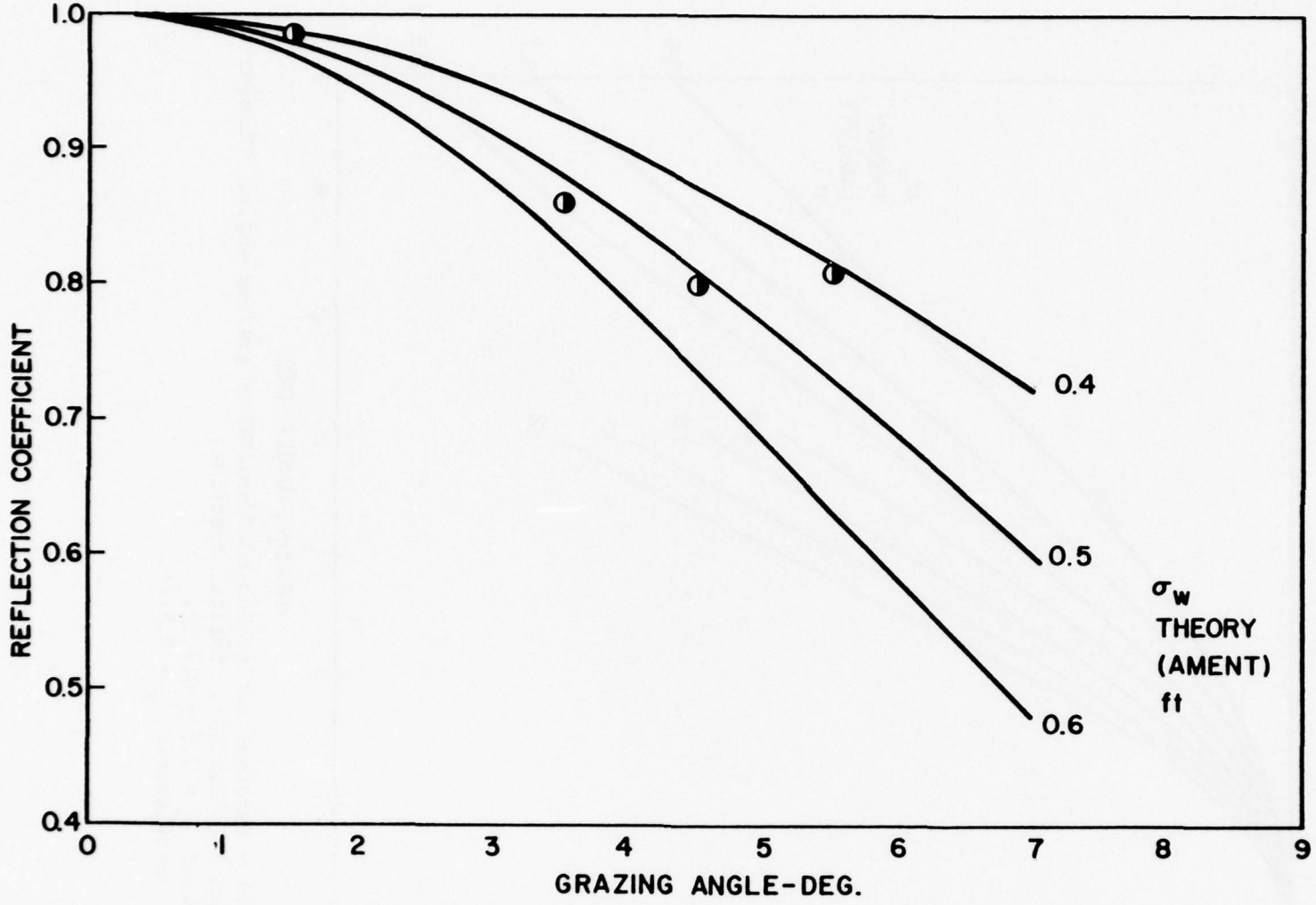

Fig. 20 - Smoothed reflection coefficient vs grazing angle. Mission 17, Run 12 (8 Mar 74).
Radar tracking.
Predicted $\sigma_w = 0.5 \pm 0.05$ ft.
Laser profilometer σ_w (extrapolated) $\cong$ 0.40 ft.

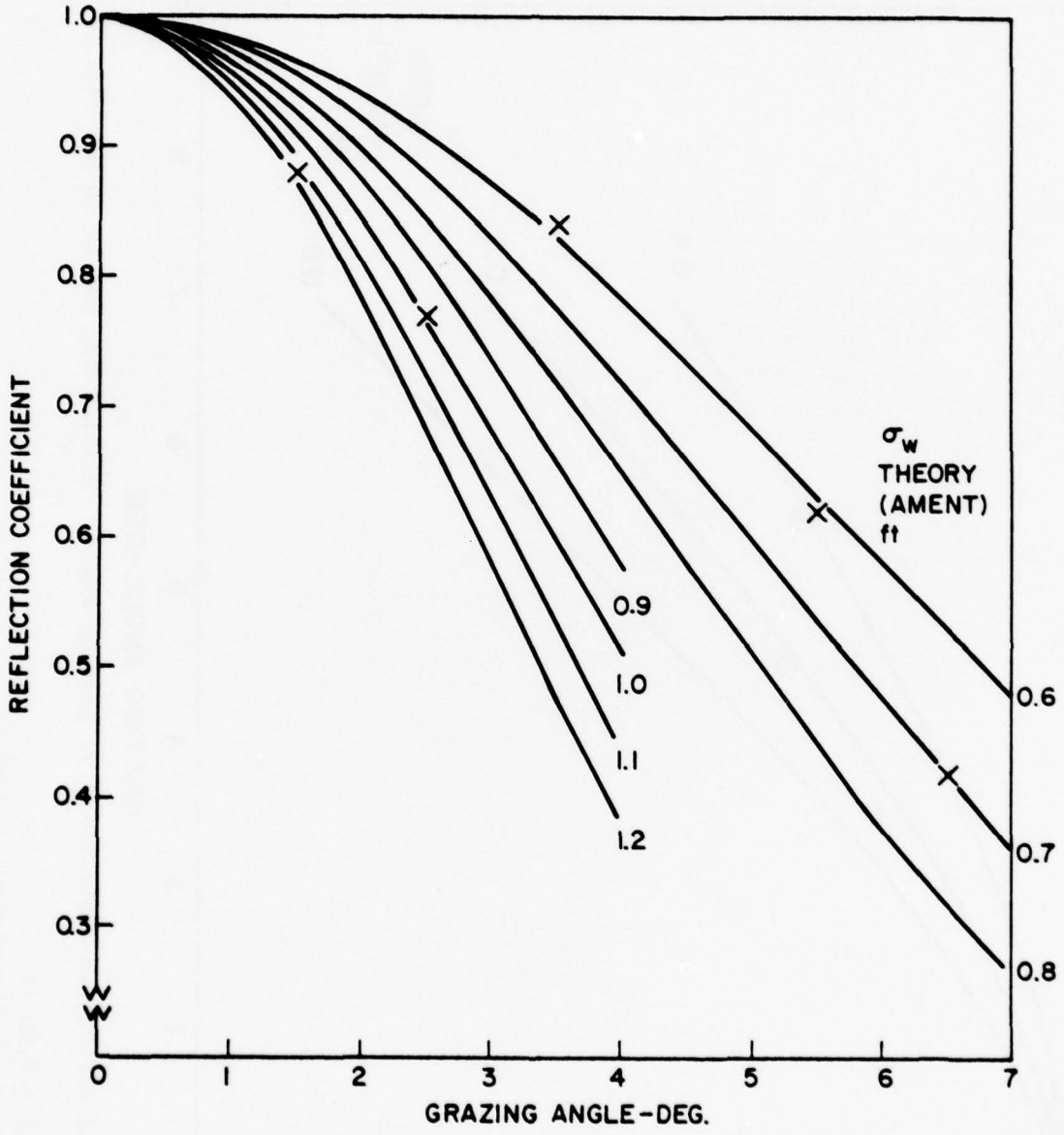

Fig. 21 - Smoothed reflection coefficient vs grazing angle. Mission 15, Run 5 (4 Mar 74). Optical tracking.
Predicted $\sigma_w = 0.8 \pm 0.3$ ft.
Laser profilometer $\sigma_w = 0.8$ ft.

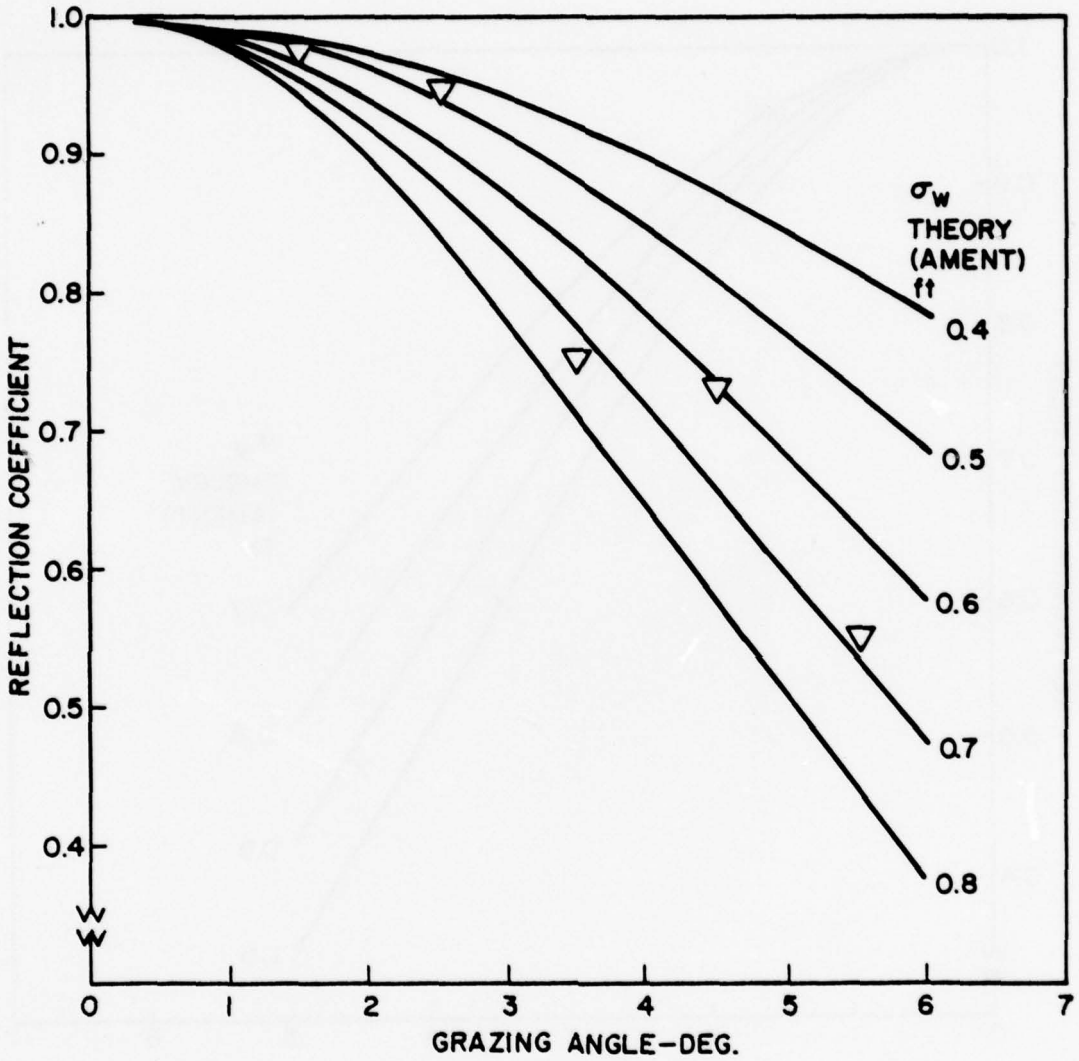

Fig. 22 - Smoothed reflection coefficient vs grazing angle.
Mission 16, Run 2 (6 Mar 74). Optical tracking.
Predicted $\sigma_w = 0.65 \pm 0.15$ ft.
Visual estimates of $\sigma_w = 0.75$ to 1.0 ft.

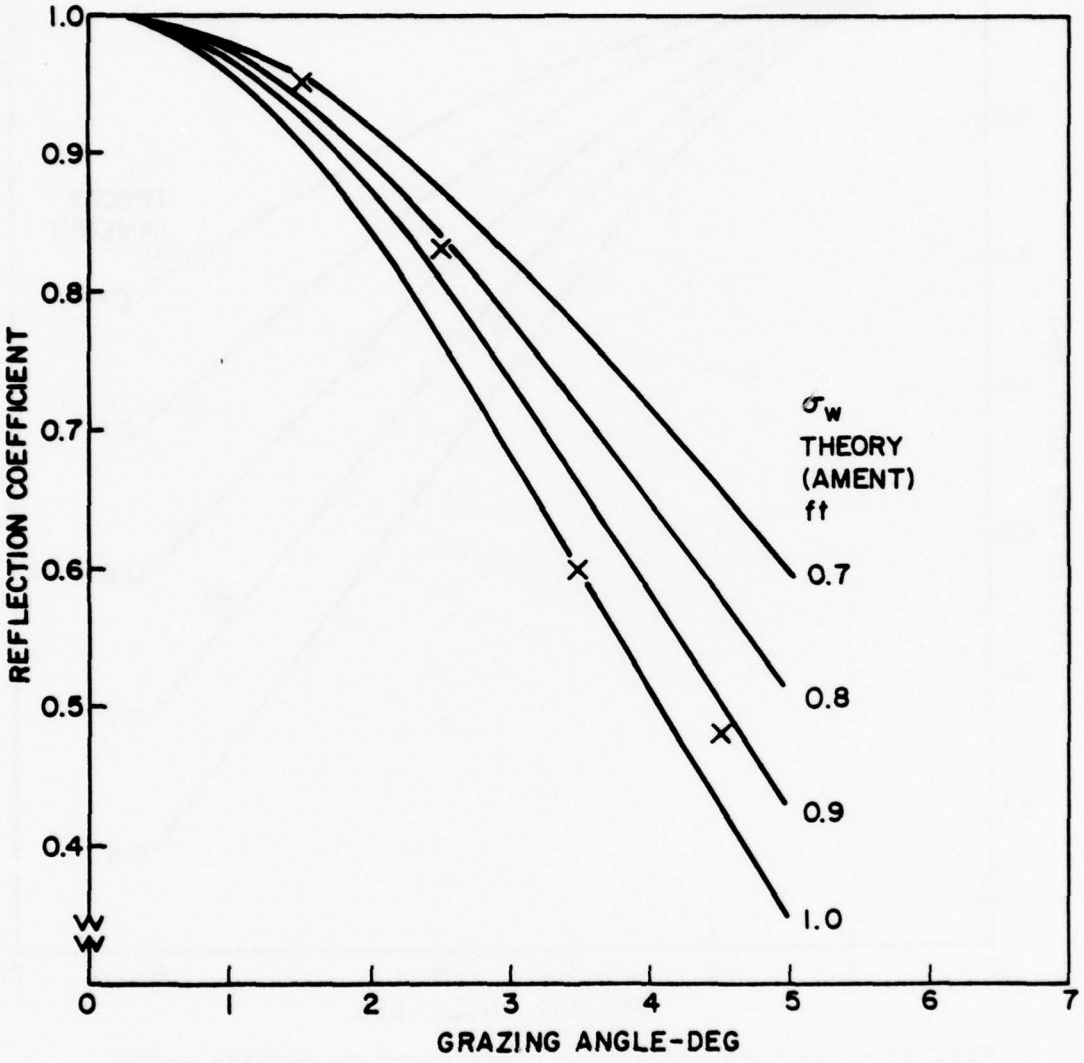

Fig. 23 - Smoothed reflection coefficient vs grazing angle.
Mission 16, Run 5 (6 Mar 74). Radar tracking.
Predicted $\sigma_w = 0.9 \pm 0.1$ ft.
Visual estimates of $\sigma_w = 0.75$ to 1.0 ft.

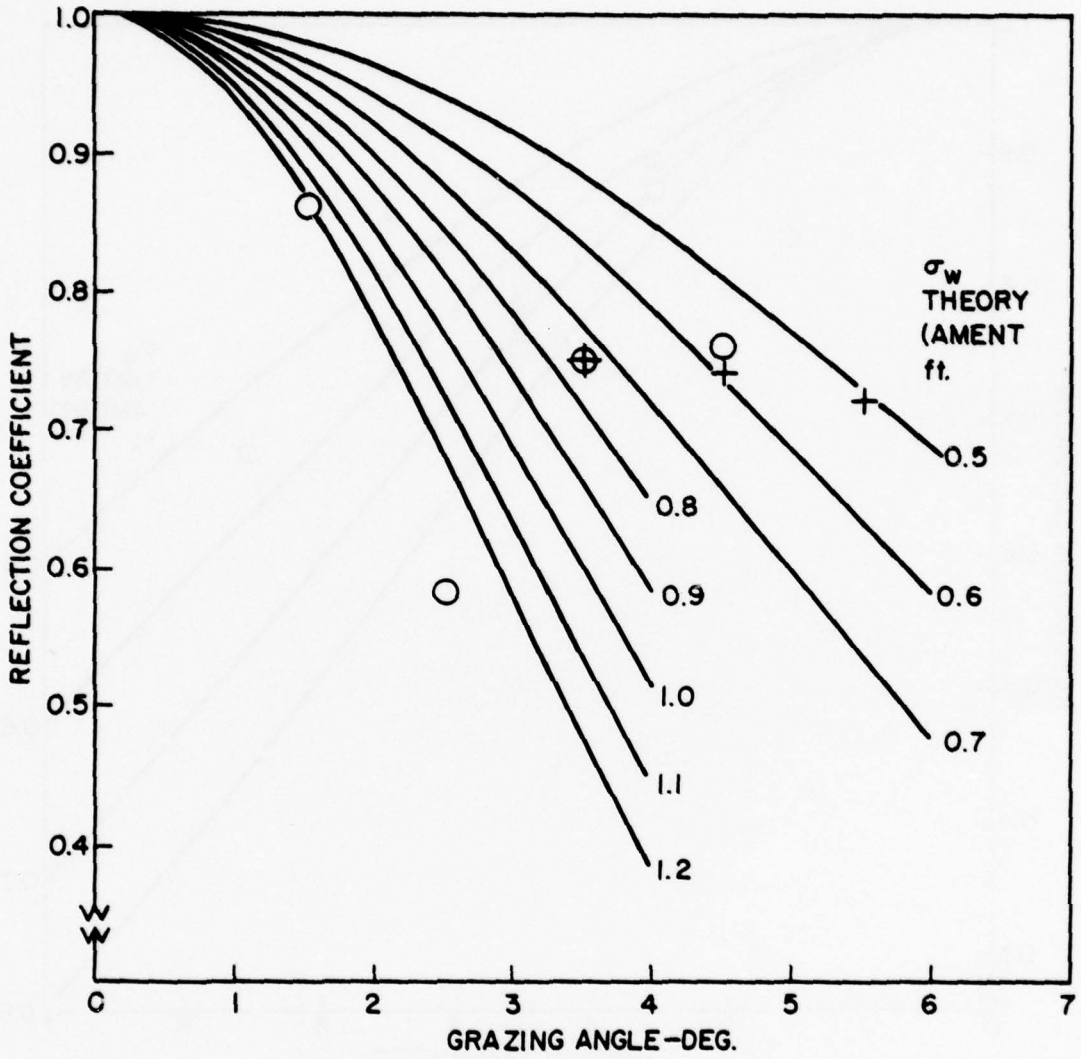

Fig. 24 - Smoothed reflection coefficient vs grazing angle.
Mission 16, Runs 3 and 4 (6 Mar 74). Radar tracking.
Predicted σ_w (avg. of all points) = 0.8 $\pm$ 0.2 ft.
Visual estimates of σ_w = 0.75 to 1.0 ft.

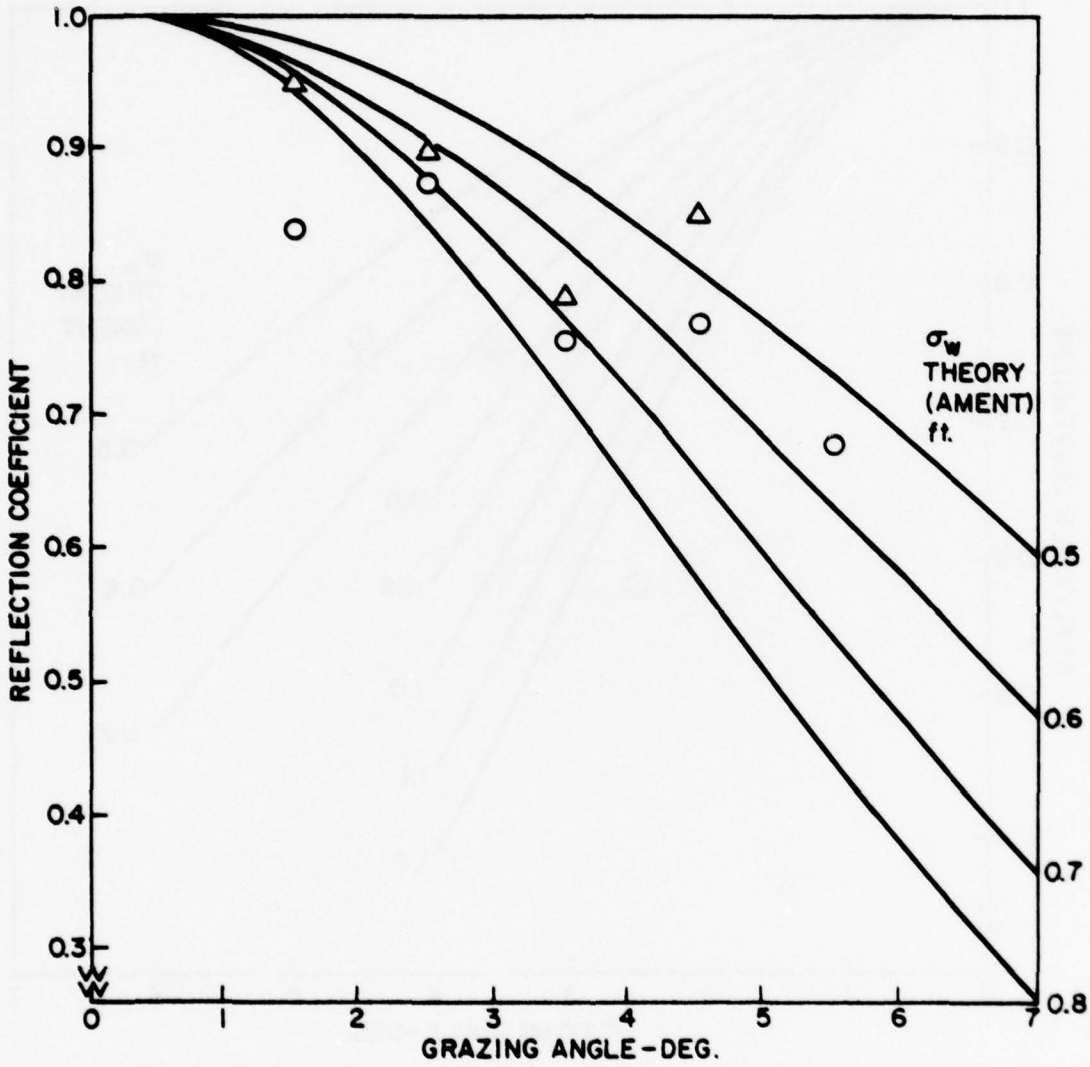

Fig. 25 - Smoothed reflection coefficient vs grazing angle.
Mission 18, Runs 1 and 3 (8 Apr 74). Radar Tracking.
Predicted σ_w (Run 1) = 0.60 $\pm$ 0.15 ft.
Predicted σ_w (Run 3, excluding the point at 1.5°) = 0.65 $\pm$ 0.1 ft.
Laser profilometer σ_w = 0.65 $\pm$ 0.07 ft.

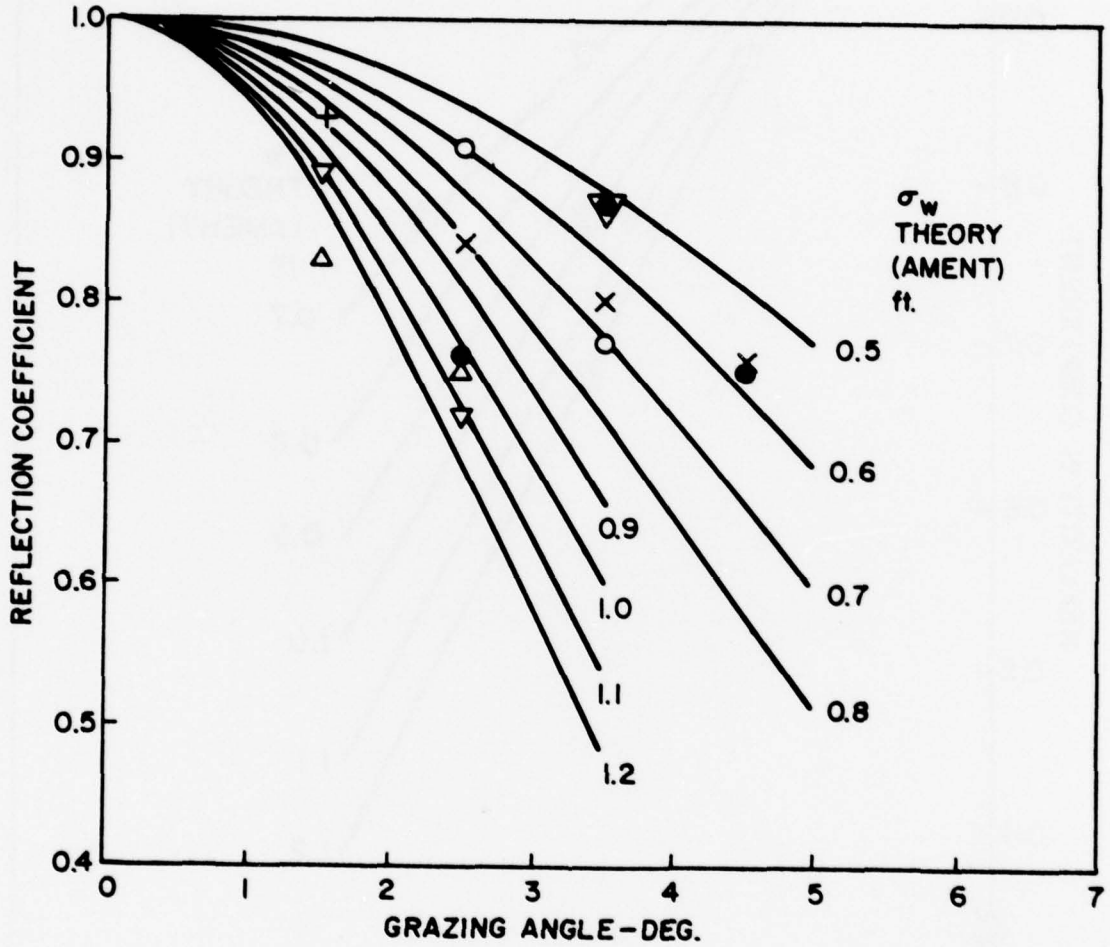

Fig. 26 - Smoothed reflection coefficient vs grazing angle.
Mission 14, Runs 1 to 6 (27 Feb 74). Optical tracking.
Predicted σ_w (avg. of all points) $\approx 0.8 \pm 0.5$ ft.
Laser profilometer σ_w (avg. of all points) = 1.15 ± 0.12 ft.

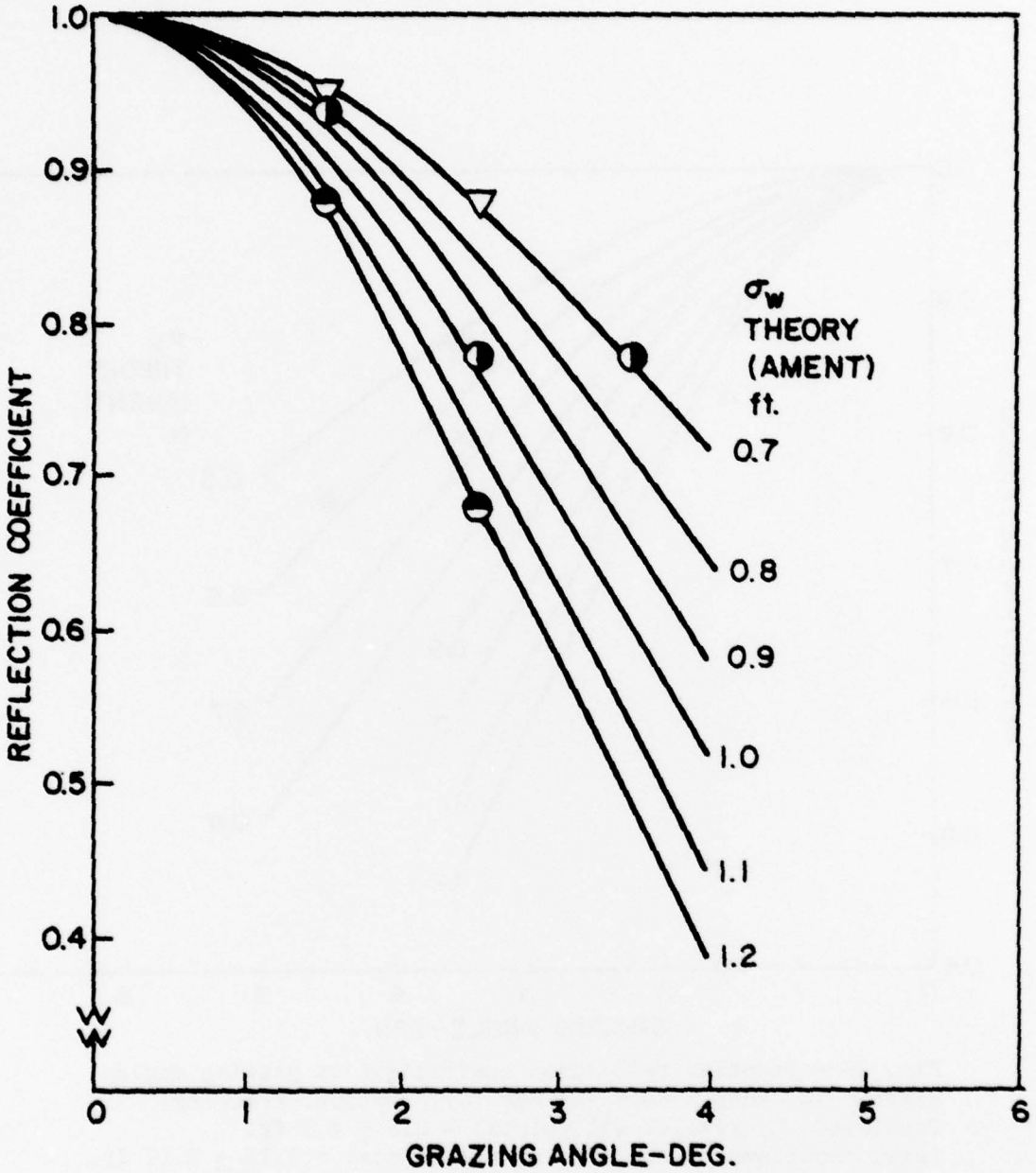

Fig. 27 - Smoothed reflection coefficient vs grazing angle.
Mission 13, Runs 2, 9, and 10 (25 Feb 74). Optical tracking.
Predicted σ_w (avg. of all points) $\approx 0.9 \pm 0.3$ ft.
Laser profilometer σ_w (avg.) = 1.33 ft.

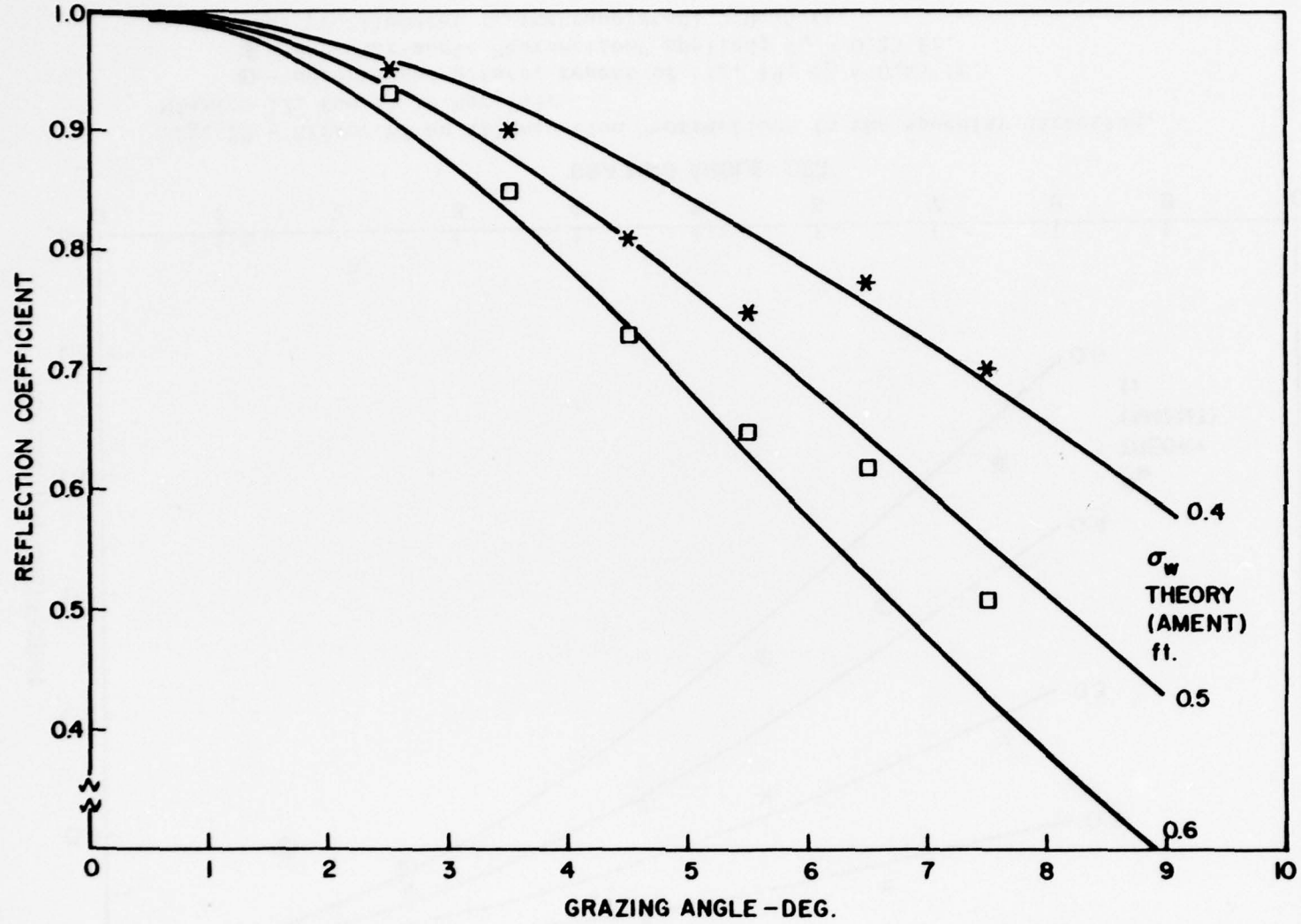

Fig. 28 - Effect of an illumination "correction" in the specular direction. Mission 15 Run 8 (4 Mar 74).
□ - uncorrected points, repeat of Fig. 18; $\sigma_w \approx 0.55$ ft.
✱ - specular-angle "correction" applied; $\sigma_w = 0.45$ ft.
Laser profilometer $\sigma_w = 0.64$ ft.

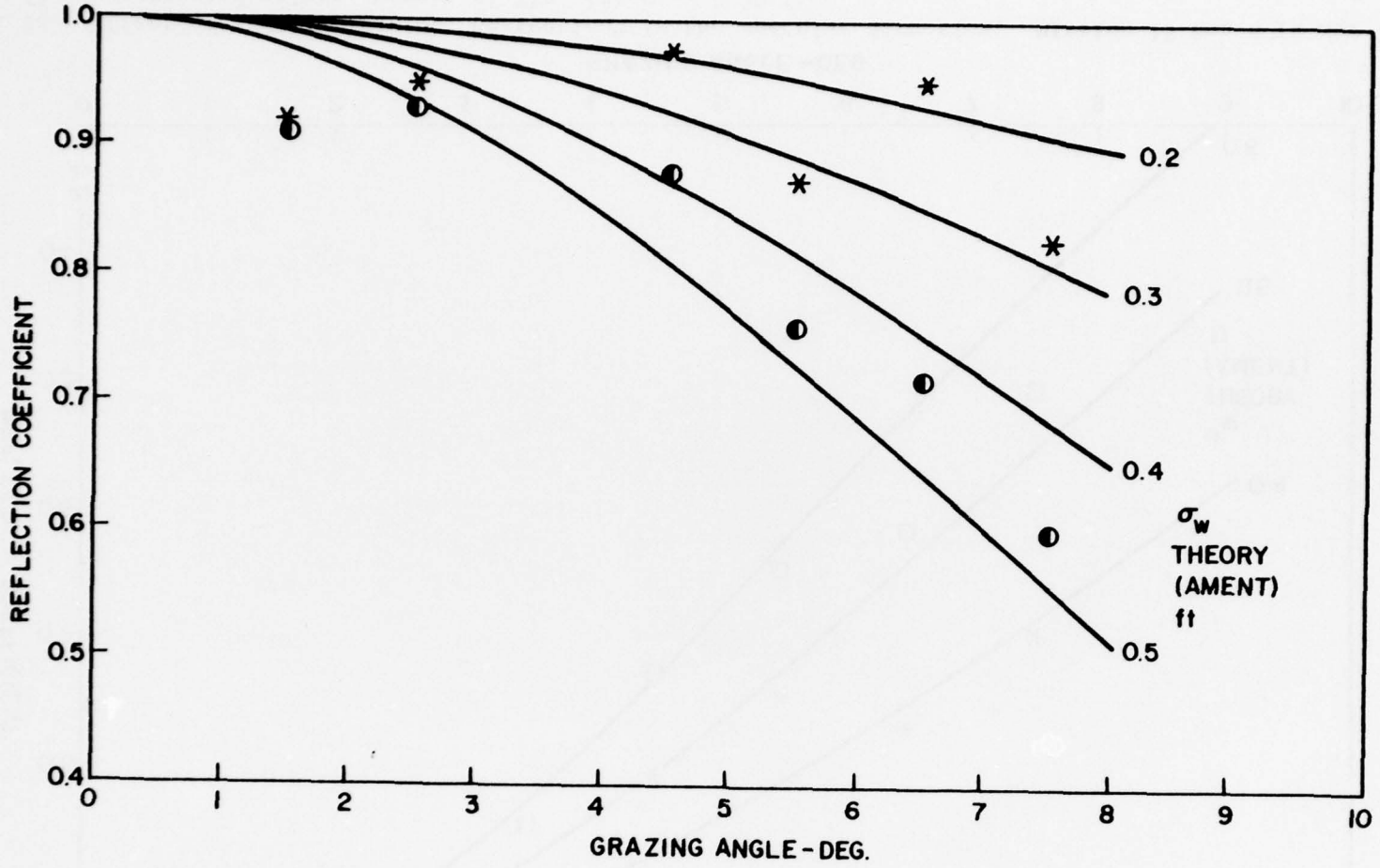

Fig. 29 - Effect of an illumination "correction" in the specular direction. Mission 17, Run 11 (8 Mar 74).

◐ - uncorrected points, repeat of Fig. 19; σ_w = 0.45 ft.

✱ - specular-angle "correction" applied; σ_w = 0.25 ft.

Laser profilometer σ_w (extrapolated) $\cong$ 0.45 ft.

Appendix A. Times of the 1974 Data Runs

Start and Stop Times of Each Run (GMT)												
Mission No.		13		14		15		16		17		18	
		Start	Stop	Start	Stop	Start	Stop	Start	Stop	Start	Stop	Start	Stop
Run No.	1	1708:50	1712:20	1754:20	1757:11	1617:30	1620:55	1236:40	1236:48	1420:50	1424-48	1532:10	1538:11
	2	1727:00	1728;50	1801:20	1804:25	1626:20	1628:49	1243:40	1247:05	1431:40	1435:44	1546:20	1550:27
	3	1737:00	1738:45	1809:40	1811:47	1633:30	1637:10	1252:00	1255:45	1433:10	1419:15	1559:50	1605:21
	4	1743:00	1746:30	1815:40	1817:52	1642:00	1644:30	1304:00	1305:25	1458:20	1503:47	1614:30	1619:42
	5	1751:00	1754:55	1822:40	1824:40	1648:40	1650:57	1313:00	1317:30	1511:10	1516:16	1630:10	1634:32
	6	1758:20	1801:25	1828:20	1831:10	1655:20	1657:15	1321:50	1326:05	1526:50	1533:25	1645:20	1650:31
	7	1805:20	1809:57			1702:30	1702:59	1331:00	1347:17	1543:00	1548:09		
	8	1815:00	1818:50			1707:40	1709:50	1335:00	1342:46	1554:20	1559:07		
	9	1823:00	1825:00			1713:10	1713:40	1348:40	1352:12	1606:10	1611:01		
	10	1832:40	1833:20			1714:20	1717:30	1358:50	1404:30	1619:20	1625:46		
	11	1837:20	1841:20					1412:00	1417:28	1634:01	1639:08		
	12	1846:00	1849:41					1424:10	1430:30	1647:50	1652:28		
	13									1657:50	1701:10		

Appendix B — Laser Profilometer Wave Heights (σ_w)

Mission No.	Date	Laser Profil. Run No.	Start Time GMT	Stop Time GMT	Laser Profil Aircraft Heading deg.	σ_w ft.
13	2/25/74	1	1710:10	1713:00	90	1.24
		2	1715:00	1717:00	240	≈1.3
		3	1718:10	1720:10	240	1.09
		4	1721:16	1724:16	350	1.44
		5	1726:20	1726:50	210	1.58
		6	1735:00	—	010	1.73
		7	1735:00	1737:00	010	1.57
		8	1737:30	1739:30	010	—
		9	1744:00	1744:30	200	—
		10	1810:00	1813:00	020	1.28
		11	1826:10	1827:40	020	1.28
		12	1834:00	1835:30	200	1.15
14	2/27/74	1	1735:00	1737:00	200	NG
		2	1753:00	1754:00	190	NG
		3	1756:10	1758:10	010	~1.08
		4	1800:10	1802:10	260	1.11
		5	1803:45	1804:45	080	1.26
		6	1805:30	1806:30	060	1.08
		7	1808:23	1810:23	220	1.23
		8	1811:45	1813:45	020	1.13
		9	1818:24	1820:24	110	1.22
		10	1822:11	1823:11	250	1.03
		11	1825:03	1826:03	040	1.22
		Avg.				1.15 ±0.12
15	3/4/74	1	1619:38	1621:38	290	0.52
		2	1623:25	1624:25	100	0.54
		3	1625:13	1626:13	130	—
		4	1627:14	1630:14	250	0.55
		5	1631:54	1632:54	080	—
		6	1633:32	1634:32	110	—
		8	1635:35	1637:35	240	—
		9	1639:45	1641:45	070	—
		10	1643:15	1645:12	270	—
		11	1646:38	1648:38	100	Noise

Appendix B — Laser Profilometer Wave Heights (σ_w) (Continued)

Mission No.	Date	Laser Profil. Run No.	Start Time GMT	Stop Time GMT	Laser Profil Aircraft Heading deg.	σ_w ft.
		12	1649:44	1650:50	260	Noise
			1652:55	1653-10	090	Noise
		13	1653:45	1654-43	130	Noise
		14	1656:10	1658:10	310	0.91
		15	1659:25	1701:25	150	Noise
		16	1702:55	1703:55	310	Noise
		17	1705:20	1707:20	155	Noise
		18	1708:30	1710:30	350	0.64
		19	1715:40	1718:40	350	0.66
16	3/6/74	No laser profilometer data.				
17	3/8/74	1	1422:50			0.74
		2	1427:28			0.65
		3	1435:15			0.61
		4	1438:35			0.75
		5	1445:50			0.84
		6	1451:15			0.60
		7	1459:55			0.77
		8	—			—
		9	1512:45			0.82
		10	1521:30			0.59
		11	—			—
		12	1530:00			0.66
		13	—			—
		14	—			—
		15	1544:40			0.62
18	4/8/74	1				0.65
		2				0.72
		3				0.59
		4				0.66
		Avg.				0.65 ±0.07

APPENDIX C

Shipboard Visual Observations of Sea State

Mission 13, 2/25/74.

Estimated sea state: 5
Estimated wave height*: 8-10 ft.
This was fairly consistent throughout the mission with some decrease at end of mission.
Shipboard photos: Available, but are not tied in with time except for sequence.
Aircraft photos: Available.

Mission 14, 2/27/74. No observations.

Mission 15, 3/4/74

Estimated sea state: 0-1. Winds: 1 to 2 kts.
Estimated wave height: On the order of 1 ft, maximum 2 ft.
Shipboard photos: None.
Aircraft photos: Available. No whitecaps on the photos.

Mission 16, 3/6/74.

Time: 13:04:30 GMT
Estimated sea state: Smooth, glassy seas; small localized cats paws.
Estimated wave height: Local wind waves less than 1 ft; swells ~3 ft, occasionally 5 ft.

Time: 14:06:30 GMT
Estimated sea state: Small wavelets on waves; seas still basically smooth (on top of the swell).
Shipboard photos: None.
Aircraft photos: Available.

---

* The observed wave height is approximately the "significant wave height" = $H_{1/3} = 4.0\sigma_w$, where σ_w is the standard deviation of height fluctuations.

Mission 17, 3/8/74.

Time GMT	Est. Sea State	Est. Wave Height ft	Wind kts	Description
14:37	2	2-3	14	Occasional whitecaps.
16:10:30	1-2	1-2	7	Occasional whitecaps; sea state borderline between 1-2.
17:05	-	1-2	<7	Only very occasional whitecaps.

Estimated sea state: steadily decreased during the mission.

Estimated wave height: towards end of mission the estimated wave height was still 1-2 ft. The wind dropped steadily during the mission. At the end of the mission, the waves were still decreasing and probably closer to 1 ft than 2 ft. By evening waves were less than 1 ft.

Shipboard photos: Available.

Aircraft photos: Available.

Mission 18, 4/8/74.

Time GMT	Est. Wave Height ft	Description
11:25	1	Only occasional whitecaps.
11:56	perhaps 1	No white caps.
12:39	1 to 1 1/2	Only occasional whitecaps.
13:41	1 to 1 1/2	Only occasional whitecaps.

Shipboard photos: Available.

Aircraft photos: Available.

APPENDIX D

Shipboard Wind Observations

Anemometer is approximately 113 ft above water.

Mission 13, 2/25/74.

Time GMT	Wind	
	Speed kts	direction true - deg.
1342	18	306°
1506	26	316°
1644	29	303°
1654	21	310°
1715	24	312°
1728	23	317°
1754	28	315°
1805	21	327°
1815	20	323°
1827	19	309°

Mission 14, 2/27/74.

Time GMT	Wind	
	Speed kts	direction true - deg.
1725	15	020°
1757	14	005°
1820	13	013°

Wind Data

Mission 15, 3/4/74.

Time GMT	Wind	
	Speed kts	Direction true - deg.
1611	2	081°
1619	3	104°
1627		
1635	3	097°
1650		
1656		
1709		180° (?)
1733		130°

Mission 16, 3/6/74.

Time GMT	Wind	
	Speed kts	Direction true - deg.
1141	6	163°
1202	6	168°
1230	8	164°
1245		(160°)*
1254		(154°)*
1304	8	156°
1315	(7)*	
1341	6	163°
1351	5	186°
1401	5	195°
1429	4	218°

* = interpolated.

Wind Data

Mission 17, 3/8/74.

Time GMT	Wind	
	Speed kts	Direction true - deg.
1355	15	286°
1420	17	290°
1433	(16)*	
1453	14	300°
1500	12	300°
1507	13	300°
1516	10	315°
1521	11	314°
1541	12	313°
1557	10	309°
1603	11	330°
1604	11	314°
1608	(9)*	
1614	8	313°
1621	8	310°
1623	7	318°
1629	7	321°
1635	7	320°
1638	-	320°
1650	(6)*	
1656	6	316°

Mission 18, 4/8/74.

1210 GMT	22 kts	039°

* = interpolated.

APPENDIX E

Forward-scatter remote sensing
15 April 1978

From further analysis, it now appears that forward scattering may be capable of determining several characteristics of ocean waves.

1. Wave height

Below an apparent roughness of 0.1, Ament's (1953) theoretical curve is recast as a family of curves vs grazing angle (ψ), with wave height (σ_w) as a parameter. Plotting the measured reflection coefficients of the L-band data on this graph then yields wave height directly.

2. Surface correlation length along line-of-sight

Above an apparent roughness of 0.1, two plane wave theories, one of acoustical scattering from a surface with exponential height statistics [Boyd and Deavenport, 1973], and the second of EM scattering from a particular non-Gaussian surface [Brown and Miller, 1974], both follow the over-ocean experimental data [Beard, 1961]. Boyd and Deavenport also pointed out the agreement. Assuming that the agreement is meaningful, even with non-Gaussian surfaces, led to the realization that shadowing of waves by other waves is a mechanism by which a non-Gaussian surface can be created from a Gaussian ocean. The probability distribution of the non-shadowed (i.e., illuminated) portion of the ocean surface has been derived by Wagner [1967], and is non-Gaussian. In addition, the effective wave height of the non-shadowed surface is less than the physical wave height of the ocean surface. Both these factors would raise Ament's curve upward towards the ocean data "experimental curve."

Wagner's shadowing theory is a function of σ_w, $\tan\psi$, and L_x, where L_x is the surface correlation length along the direction of the propagation path (from transmitter to receiver). The unknown σ_w can be found as above, leaving only L_x as the one unknown to be solved for. Wagner's expression needs to be tested for its region of applicability where values of L_x produce best agreement with experimental data.

3. Surface correlation length transverse to line-of-sight

The fact that Beckmann's [1967] spherical wave theory, evaluated for wave tank conditions [Beard, 1967], follows the over-ocean data also seemed remarkable. Calculations made of the sphericity parameters of the wave tank conditions indicate that the wave height (in the vertical plane) is insufficient to produce the observed sphericity effects.

However, if one looks down on the ocean at scattering in azimuth, or in the horizontal plane, the ocean correlation length transverse to the line-of-sight path (L_y) is sufficient to produce the observed sphericity effects. (L_y can be thought of approximately as the wave-crest lengths.)

Beckmann's theory is an explicit function of σ_w, ψ, L_x, R, and λ, where R is the range, or distance between trnasmitter and receiver. It also seems to be an implicit function of L_y, and thus has the capability of determining L_y.

4. Proposed remote sensing experiment

A millimeter wave experiment at David Taylor Model Basin is proposed for FY-79 to exploit the different functional dependencies of these theories to determine the wave characteristics σ_w, L_x, and L_y. The region of applicability of each theory has first to be determined.

All of these measurements for different functional dependence must be made under controlled conditions and with adjustable water wave directions (to vary L_x and L_y with constant σ_w, etc.). Consequently, a wave basin, as at David Taylor Model Basin, is required. The two-dimensional surface correlation function must be measured.

In order to achieve apparent surface roughnesses between 0.1 and 0.3, where the various theories differ, it is necessary to use a short wavelength, 3.3 mm (90 GHz).

C. I. Beard

DEPARTMENT OF THE NAVY

NAVAL RESEARCH LABORATORY
Washington, D.C. 20375

OFFICIAL BUSINESS
PENALTY FOR PRIVATE USE, $300

POSTAGE AND FEES PAID
DEPARTMENT OF THE NAVY
DoD-316
THIRD CLASS MAIL